SINGLE QUANTUM DOT APPROACH FOR MOLECULAR DISSECTION OF SEROTONIN TRANSPORTER REGULATION IN LIVING CELLS

By
CHIA HUA CHANG

Dissertation
Submitted to the Faculty of the
Graduate School of Vanderbilt University
in partial fulfillment of the requirements
for the degree of
DOCTOR OF PHILOSOPHY
in
Chemistry
May, 2013
Nashville, Tennessee

Approved:

Professor Sandra J. Rosenthal

Professor David W. Wright

Professor Ned A. Porter

Professor Randy D. Blakely

Copyright © 2013 by Chia Hua Chang

All Rights Reserved

Dedicated to my beloved grandfather.

May you rest in peace in heaven.

ACKNOWLEDGEMENTS

Thank you to my family for your love and support throughout my life. Thank you to my thesis advisor, Sandy, for your encouragement and investment in my research and my future as a scientist. Thank you to my thesis co-advisor, Randy, for bringing me to the field of neuroscience and consistently pushing me to become a better scientist. Thank you to Dr. Louis De Felice, Dr. Dave Piston, Dr. Sam Wells, Dr. David Wright, and Dr. Ned Porter for your advice and input at numerous points along the way.

A good support group is important to surviving in graduate school. I am very fortunate to have been surrounded by sub-group members we like to call "bio-side" and refer to Michael (Warnement), Oleg, Emily and myself. I would have been lost in graduate school without your countless discussions, support, and companionship. Best wishes to you, Oleg, as you finish up. Thank you to other present and past members of the Rosenthal group, including Amy, James, Noah, Sarah, Scott, Joe, Toshia, Melissa, Danielle, Albert, Michael (Schreuder), Michael (Bowers), Ian, Shawn, Teresa, Jessica, Kevin, and Nat. The past seven years have not been an easy ride for me, both academically and personally. Each and everyone of you have supported and/or helped me in many ways. I am very fortunate to join such a loving and down to earth group. Additionally, I also like to thank the members of the Piston and Blakely group, in particular Alessandro Ustione and Dr. Hideki Iwamoto, for helping important part of my experiments. Finally, I would like to thank the Department of Chemistry at the Vanderbilt University, the Vanderbilt Institute of Nanoscale Science and Engineering (VINSE), and the National Institutes of Health (NIH) for funding.

ABSTRACT

The presynaptic serotonin (5-HT) transporter (SERT) is targeted by widely prescribed antidepressant medications. Altered SERT expression or regulation has been implicated in multiple neuropsychiatric disorders, including anxiety, depression and autism. It has been previous reported that SERT is regulated by lipid raft, a cholesterol-enriched subdomain in the plasma membrane that has been frequently reported a platform to facilitate neuronal signaling.

To better understand the membrane diffusion dynamics of SERT, I developed a single quantum dot (QDot) tracking approach that exploits antagonist-conjugated single QDots to monitor, for the first time, single SERT proteins on the surface of serotonergic cells. We document two pools of SERT proteins defined by lateral mobility, one that exhibits relatively free diffusion, and a second, localized to cholesterol and GM1 ganglioside-enriched microdomains, that displays restricted mobility. Receptor-linked signaling pathways that enhance SERT activity mobilize transporters that, nonetheless, remain confined to membrane microdomains. Mobilization of transporters arises from a p38 MAPK-dependent untethering of the SERT C terminus from the juxtamembrane actin cytoskeleton. Our studies establish the utility of single QDot tracking approach for analysis of the behavior of single membrane proteins and reveal a physical basis for signaling-mediated SERT regulation.

In line with the single QDot-SERT analysis, single QDot-labeled ganglioside GM1 was incorporated in this dissertation that aimed to quantitatively measure the diffusion dynamics and membrane compartmentalization of lipid raft in living RN46A cells. Diffusion measurements revealed that single QDot-labeled GM1 ganglioside complexes undergo slow, confined lateral diffusion with a diffusion coefficient of 7.87×10^{-2} $\mu m^2/s$

and a confinement domain about 200 nm in size. Further analysis of their trajectories showed lateral confinement persisting on the order of tens of seconds, comparable to the time scales of the majority of cellular signaling and biological reactions. Hence, our results provide further evidence in support of the putative function of lipid rafts as signaling platforms.

Finally, I discussed the recent progress of single-QDot techniques, with emphasis on their applications in exploring membrane dynamics and intracellular trafficking. In recent years, single QDot imaging approach has been introduced as a sub-category of single molecule fluorescent techniques for revealing the single protein/vehicle dynamics in real-time. One of the major advantages of using single QDots is the high signal-to-noise ratio, which is beneficial due to the unique photophysical properties of QDot such as extraordinarily high molar extinction coefficients and large Stokes shifts. Although there are some limitations due to the physical nature of the QDots, advances in QDot synthesis and surface chemistry show significant potential to eliminate these pitfalls. Considering the applications of a single QDot approach in the past few years, I am optimistic that the use of single QDots in bioimaging will largely advance our understanding in the biological research field in the near future.

TABLE OF CONTENTS

LIST OF TABLES

LIST OF FIGURES

The majority part of chapter 1 was published as a review (Chang, J.C., Kovtun, O., Blakely, R.D. & Rosenthal S.J. (2012) Labeling of neuronal receptors and transporters with quantum dots. *WIREs: Nanomedicine and Nanobiotechnology*, 4, 605–619*)* by Wiley Periodicals, Inc., and some part of this chapter was published by Cell Press (Rosenthal, S.J., Chang, J.C., Kovtun, O., McBride, J.R. & Tomlinson, I.D. (2011) Biocompatible quantum dots for biological applications. *Chemistry & Biology*, 18, 10-24). Permission is granted for the author's request for the dissertation use and for the benefit of the author's institution.

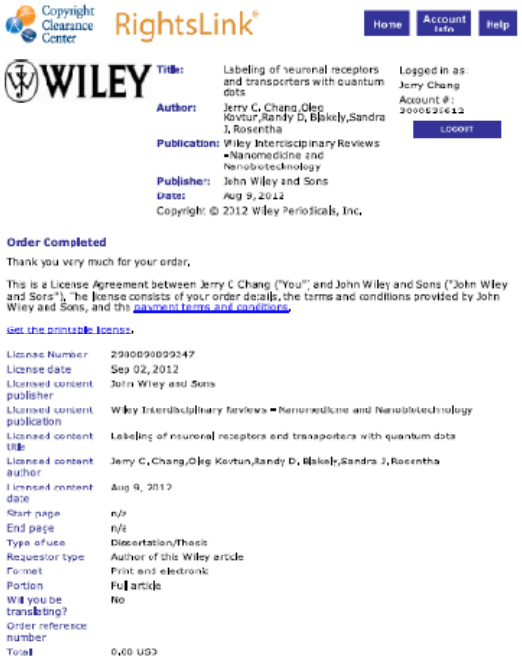

Copyright Clearance Center RightsLink®

Home | Account Info | Help

WILEY

Title: Labeling of neuronal receptors and transporters with quantum dots
Author: Jerry C. Chang,Oleg Kovtur,Randy D. Blakely,Sandra J. Rosentha
Publication: Wiley Interdisciplinary Reviews -Nanomedicine and Nanobiotechnology
Publisher: John Wiley and Sons
Date: Aug 9, 2012
Copyright © 2012 Wiley Periodicals, Inc.

Logged in as: Jerry Chang
Account #: 3000926612
LOGOUT

Order Completed

Thank you very much for your order.

This is a License Agreement between Jerry C Chang ("You") and John Wiley and Sons ("John Wiley and Sons"). The license consists of your order details, the terms and conditions provided by John Wiley and Sons, and the payment terms and conditions.

Get the printable license.

License Number	2900890099247
License date	Sep 02, 2012
Licensed content publisher	John Wiley and Sons
Licensed content publication	Wiley Interdisciplinary Reviews - Nanomedicine and Nanobiotechnology
Licensed content title	Labeling of neuronal receptors and transporters with quantum dots
Licensed content author	Jerry C,Chang,Oleg Kovtun,Randy D, Blakely,Sandra J,Rosentha
Licensed content date	Aug 9, 2012
Start page	n/a
End page	n/a
Type of use	Dissertation/Thesis
Requestor type	Author of this Wiley article
Format	Print and electronic
Portion	Full article
Will you be translating?	No
Order reference number	
Total	0.00 USD

Copyright Clearance Center RightsLink®

Home | Account Info | Help

Title: Biocompatible Quantum Dots for Biological Applications
Author: Sandra J. Rosenthal,Jerry C. Chang,Oleg Kovtun,James R. McBride,Ian D. Tomlinson
Publication: Chemistry & Biology
Publisher: Elsevier
Date: 28 January 2011
Copyright © 2011, Elsevier

Logged in as: Jerry Chang
Account #: 3000535612
LOGOUT

Order Completed

Thank you very much for your order.

This is a License Agreement between Jerry C Chang ("You") and Elsevier ("Elsevier"). The license consists of your order details, the terms and conditions provided by Elsevier, and the payment terms and conditions.

Get the printable license.

License Number	2913780814710
License date	May 21, 2012
Licensed content publisher	Elsevier
Licensed content publication	Chemistry & Biology
Licensed content title	Biocompatible Quantum Dots for Biological Applications
Licensed content author	Sandra J. Rosenthal,Jerry C. Chang,Oleg Kovtun,James R. McBride,Ian D. Tomlinson
Licensed content date	28 January 2011
Licensed content volume number	18
Licensed content issue number	1
Number of pages	15
Type of Use	reuse in a thesis/dissertation
Portion	full article
Format	both print and electronic
Are you the author of this Elsevier article?	Yes
Will you be translating?	No
Order reference number	
Title of your thesis/dissertation	Single Quantum Qdot approach for Molecular Dissection of Serotonin Transporter Regulation in Living Cells
Expected completion date	Jun 2012
Estimated size (number of pages)	200
Elsevier VAT number	GB 494 6272 12
Permissions price	0.00 USD
VAT/Local Sales Tax	0.0 USD / 0.0 GBP
Total	0.00 USD

All other uses, reproduction and distribution, including without limitation commercial reprints, selling or licensing copies or access, or posting on open internet sites, your personal or institution's website or repository, without permission from the publisher are prohibited.

CHAPTER 1

SINGLE-QUANTUM DOT IMAGING FOR MOLECULAR NEUROSCIENCE

1.1 Introduction

Since the pioneering neuroanatomical work of Santiago Ramón y Cajal in the early 20th century, the need to visualize dynamic communication within neuronal networks has been a challenge for modern neuroscience.[1] Synaptic transmission, and hence central nervous system (CNS) excitability, are modulated in a tightly regulated manner by a myriad of neuronal membrane receptors and transporters that rely on specific ligand binding and transport and the initiation of intracellular signaling cascades. Despite extensive biochemical and genetic analyses, mechanisms that regulate synaptic receptor and transporter activity, trafficking, and localization continue to challenge neuroscientists.[2, 3] These considerations have driven our desire to combine recently developed receptor and transporter labeling methods with the tools of advanced fluorescence imaging that can permit single molecule visualization to dissect mechanisms of synaptic protein trafficking and signaling.

Fluorescent labeling techniques commonly used to interrogate cellular processes can be classified into two broad categories: (1) the construction and expression of fluorescent fusion proteins such as GFP[4, 5] and (2) chemical methods of fluorescent labeling.[6] With the rapid evolution of fluorescent protein technology and the elaboration of readily available, multicolor GFP expression vectors, GFP-based labeling methods have quickly found widespread use as the proteins produced bypass many time-consuming probe preparation steps and assure that labeling is restricted to specifically-tagged proteins. However, certain limitations are associated with the GFP fusion approach: (1) The inability of GFP construct transfection to provide for the study

endogenously expressed proteins; (2) The failure of GFP-tagged proteins to, in some cases, localize properly; (3) Differences in the activity and signaling of GFP-tagged proteins compared to their wild-type counterparts. As a result, fluorescence labeling strategies have emerged as important alternatives for the visualization of cellular proteins, particularly those that prove incompatible with GFP-based methods. However, since chemical labeling techniques typically utilize conventional fluorescent dyes, live-cell imaging is often hampered by the low photostability and brightness, narrow Stoke's shift, and relatively broad emission spectra of these labels. To address these shortcomings, researchers have developed fluorescent nanomaterials with significantly improved optical properties for biological imaging.

Semiconductor nanocrystals, also known as quantum dots (QDots) are one such class of fluorescent nanomaterials that overcome instability issues associated with conventional fluorescent dyes.[7-9] Over the past decade, QDots have shown tremendous potential for *in vitro* and *in vivo* biological imaging.[8-12] Among the capabilities QDots offer to the life science research,serving as a bright and stable fluorescent tag for singlemolecule imaging is perhaps the most exciting one. No this note, an interesting property associated with QDots is the fluorescent intermittency, known as blinking,whereby a time trace of fluorescent intensity from a single QDot can switch between two distinct on/off states.[13] This blinking phenomenon is sometimes considered a minor drawback since it might cause temporary trajectory data loss in single-molecule tracking.[14] On the other hand, blinking is often used to identify single molecules, providing a practical benefit.[15, 16] Details of single QDot tracking and its recent advances in the neuroscience field are discussed later in this chapter.

1.2 Water-Soluble Quantum Dot for Biological Labeling

As crystalline inorganic nanoparticles, QDots are typically composed by semiconductor materials, such as CdSe or CdTe. Because of their inherent quantum confinement effect with discrete atomic-like energy levels, QDots are often described as 'artificial atoms'. By adjusting their size, the emission spectra of QDots can be tuned to cover the entire visible range (Fig. 2). The quantum yield of QDots can be significantly improved after capping the "core" with a wider bandgap semiconductor "shell". Until now, the most commonly used and most well-known QDot architecture is the CdSe/ZnS core/shell QDot.[17, 18] Typically, QDots are synthesized in organic solvents at high temperatures and passivated with hydrophobic surfactants such as trioctylphosphine oxide (TOPO) and trioctylphosphine (TOP) to yield monodisperse and stable particles.[7] However, these surfactant-passivated QDots require hydrophilic functionalization prior to any further biological application. In 1998, two groups simultaneously reported different procedures for designing water-soluble QDots which lead to a new era of QDots in biological applications. The first approach, originally demonstrated by Alivisatos and coworkers,[9] involves a hydrophilic silica shell around quantum dot. In this procedure, functional organosilicone molecules are directly absorbed onto the QDot surface. As QDots are embedded into a highly cross-linked silica shell, these coated CdSe QDots are extremely stable with 6-15% quantum yield. The second approach, initially reported by Chen and Nie,[8] employs a ligand exchange strategy to displace the hydrophobic surfactant on the QDot surface with thiol (−SH) functionalized hydrophilic ligand. However, water-soluble QDots produced by the above approaches tend to cause aggregation, absorb nonspecifically, and yield lower quantum efficiency.[19] In order to overcome these shortcomings, a breakthrough approach reported by Dubertret *et al.* utilizes bifunctional hydrophobic/hydrophilic phospholipids to self-assemble onto the hydrophobic QDot surface, forming a water-soluble micelle while retaining the organic

surfactants on the QDot surface.[20] This elegant approach was subsequently improved by several groups using ampiphilic copolymer.[21, 22] As the organic surfactant is retained, the inherent photophysical properties are preserved to the highest extent. The micelle encapsulation strategy is generally superior to surface silanisation or ligand exchange approach in generating water-soluble QDots with better photostability and lower toxicity.[22] The schematic of common methodologies used in water-soluble QDot preparation is shown in Figure 1.2.Notably, two major commercial QDot suppliers, Evident Technologies and Invitrogen®, have all adapted micelle encapsulation approach for their water-soluble QDot product line.

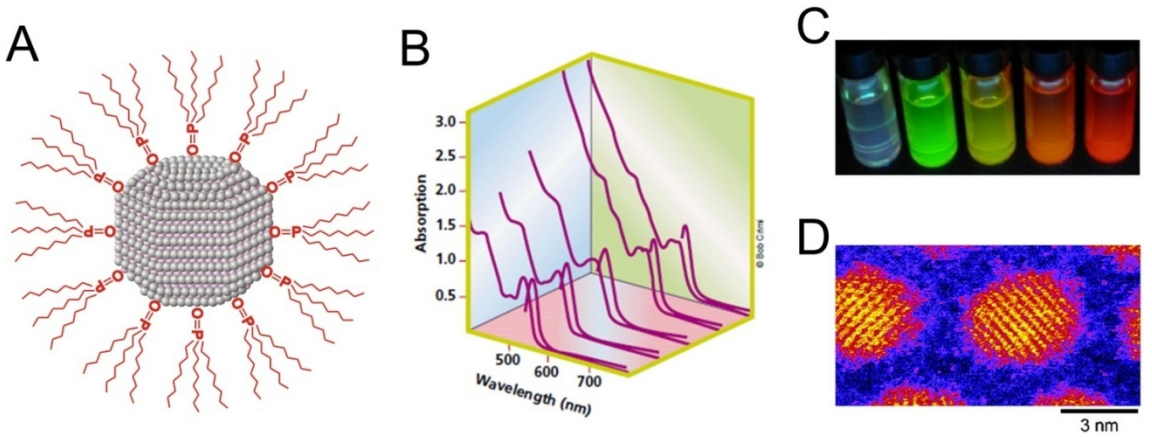

Figure 1.1 Basic properties of fluorescent quantum dot. (A) Diagram of surfactant-passivated quantum dot. (B) Absorption and emission spectra of CdSe quantum dots with different core sizes. (C) Photograph of CdSe QDots under UV illumination illustrates that QDot emission can be tuned across the visible spectrum. (D) High resolution atomic number contrast scanning transmission electron (Z-STEM) micrograph shows the atomic structure of individual CdSe QDots.

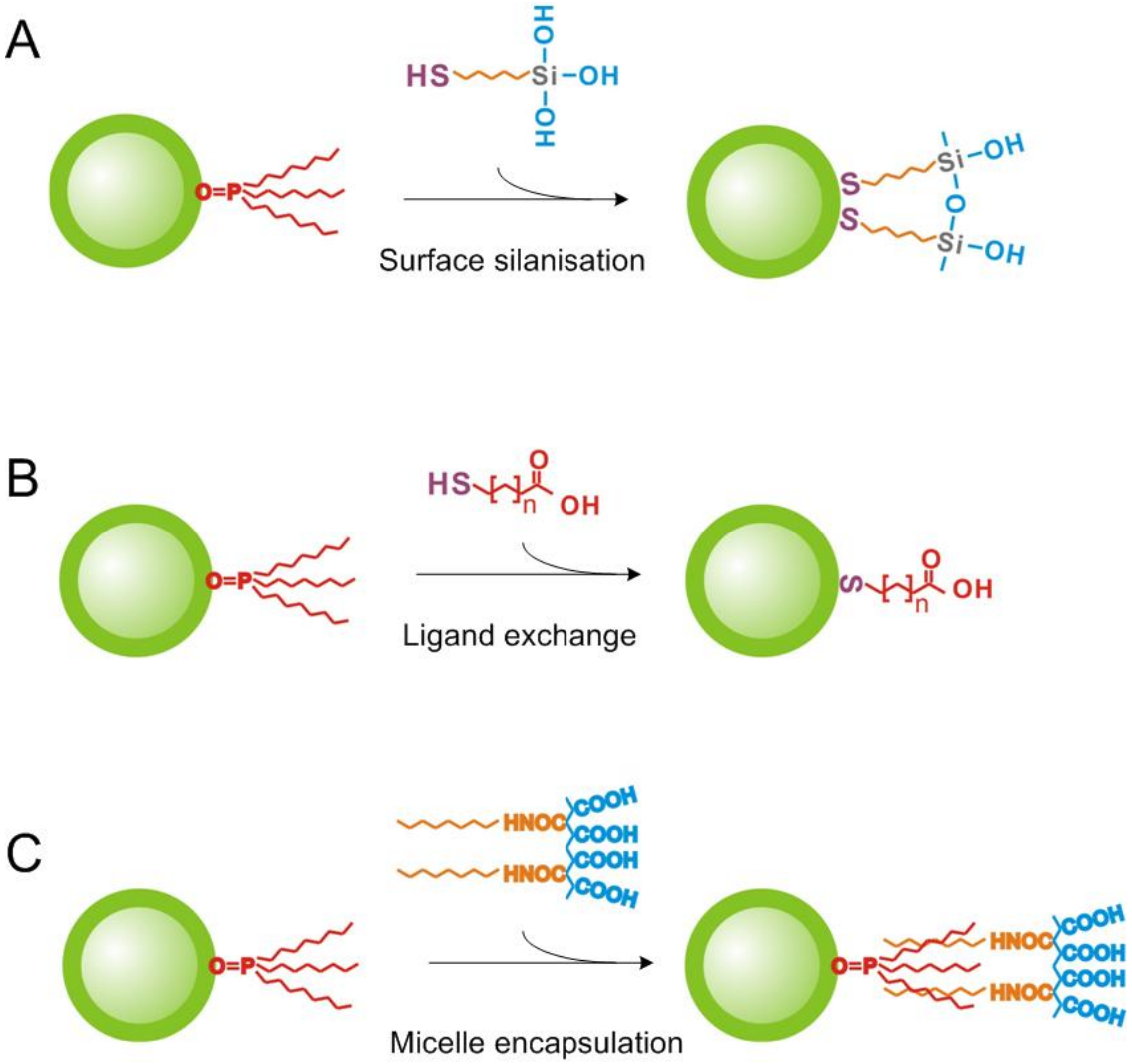

Figure 1.2 Three general strategies to yield water-soluble QDots. (A) Silica-shelled water-soluble QDots is generated by replacing TOPO ligand with functional organosilicone molecules containing thiol group. (A) TOPO ligand on QDot surface is replaced by wate-soluble mercaptocarbonic acids via ligand-exchange approach. (C) A water-soluble QDot micelle is formed by encapsulating a TOPO QDot with amphilphilic polymer.

Although the ampiphilic copolymer-encapsulated QDots (AMP QDots) are disperse and remain stable in an aqueous solution, the polymershells easily cause non-specific binding to the cell membrane,[23] most likely due to the hydrophobic interaciton between the polymer and the lipid bilayer.[24]In a pioneer work reported by Bentzen et al., six different cell types, HEp-2, LLC, HEK, COS7, 3T3, and CHO were tested to verify the nonspecifically staining of unconjugated AMP QDots to these cell lines. Importantly, the authors concluded that the degree of nonspecific staining of AMP QDots to different cell lines are not uniform, in which the HEK cells was the highest among the list. To resolved this shortcoming, the author functionalized AMP QDots with poly(ethylene glycol) (PEG)and the non-specific labeling was significantly reduced.[23]

The ability to detect specific targets in biological studies relies on linking QDots to bioaffinity ligands, such as antibodies, peptides, oligonucleotides, saccharides, or small-molecule drugs. Three general types of strategies used in attaching bioaffinity ligands onto the QDot surface are: (1) covalent conjugation, (2) streptavidin-biotin assembly, and (3) electrostatic interaction. In the first approach, water-soluble QDots synthesized with carboxyl functionalized surface enable the conjugation of amino terminated ligands via EDC coupling strategy (1-ethyl-3-(3-dimethylaminopropyl)-carbodiimide; EDC)[23] (Fig. 1.3A). However, in certain cases where (*i*) site-specific controlled coupling is required, or (*ii*) to avoid random polymerization of QDot-ligand complexes if the chosen ligand contains multiple amines, an alternative method for site-specific conjugation can be achieved for coupling thiol terminated bioaffinity ligands with amino surface functionalized QDots via SMCC heterobifunctional crosslinker (Succinimidyl-4-(N-maleimidomethyl) cyclohexane-1-carboxylate: SMCC) (Fig. 1.3B). Both amine and carboxyl terminated water-soluble QDots are commercially available from Invitrogen®.

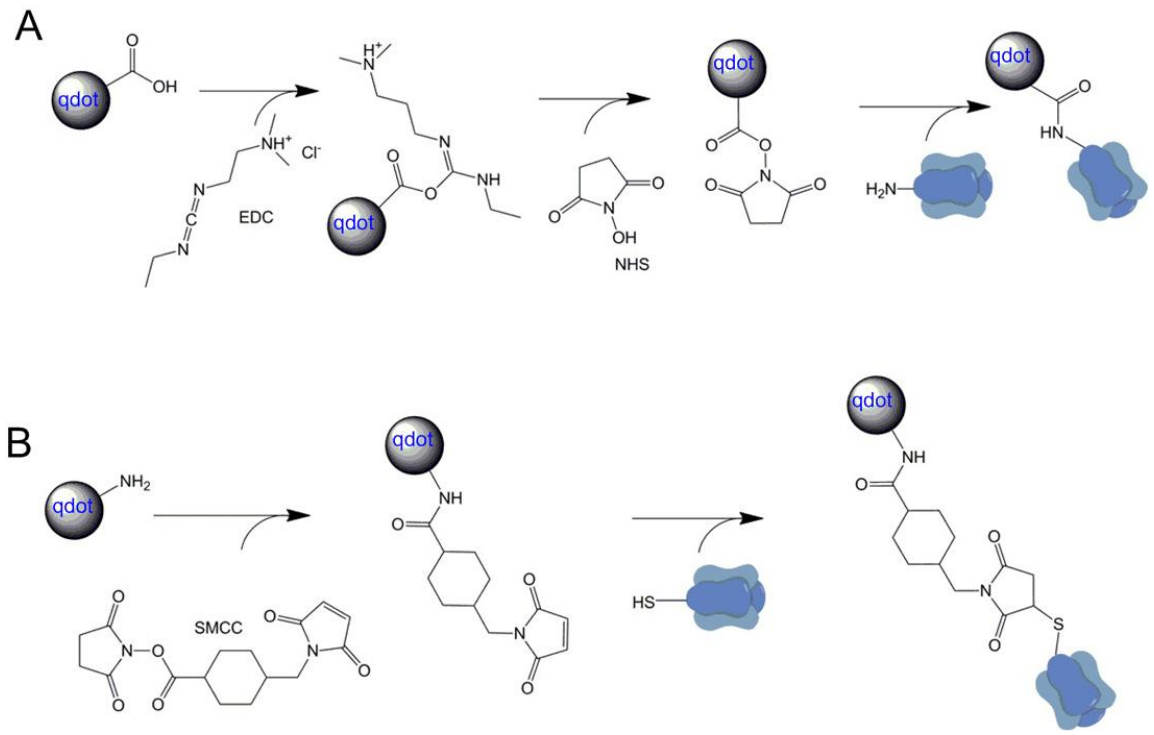

Figure 1.3 Covalent coupling strategies of amino and carboxyl functionalized QDots. (A) EDC coupling of ligand with free amine group to carboxyl terminated water-soulble QDot. (B) Covalent coupling of thiol terminated ligand to amino terminated water-soluble QDot via SMCC bi-functional cross-linker.

In addition to covalent coupling methodology, non-covalent binding approaches such as streptavidin-biotin assembly strategy are also commonly used in QDot nanoprobe design. Streptavidin- functionalized QDots (SA-QDots), which take advantage of the strong streptavidin-biotin non-covalent interaction (K_d: ~10^{-14}), were initially designed for immunofluorescent labeling with a biotinylated antibody.[25] Since their introduction, SA-QDots are commonly used due to the fact that a wide variety of commercially available biotinylated molecules, such as peptides, proteins, and antibodies, have already been routinely applied in various biological experiments.[26, 27] Additionally, SA-QDots appear to have no effect on random association of endogenous proteins, permitting target-specific labeling in living cells.[28]

An alternative non-covalent coupling strategy involves electrostatic interaction, where the biomolecules are engineered with positively charged domains that can self-assemble onto the negatively charged, functionalized QDot surface. Such an approach was pioneered by Mattoussi et al.[29] which showed that electrostatic forces can be used to drive self-assembly between the dihydrolipoic acid (DHLA) capped CdSe/ZnS QDots and engineered maltose binding proteins (MBP) bearing a positively charged binding domain. Recently, Clapp et al.[30] provided a detailed protocol which allows the electrostatic coupling method to be applied to any protein appended with either an electrostatic attachment domain (namely, the basic leucine zipper) or a polyhistidine (poly-His) tag.

1.3 Overview of Single-QuantumDotTracking

Single-molecule fluorescent microscopy, derived from high-speed fluorescence microscopy, is probably the most accessible method for cell biologists to investigate single-molecule dynamics in living cells.[31] The basis of this method is to follow the real-time movement of individual molecules by using fluorescent microscope, resulting in a map of the dynamics upon observing many individual events. Based on the above definition, a high sensitivity is required that allows *individual single molecules* to be monitored in a picoliter to femtoliter-sized microscope sampling volume. However, even if performed on an optimally designed microscope, equipped with a camera offering single photon sensitivity per frame, optical detection of a single molecule is still diffraction-limited. The diffraction pattern of a point object viewed through a microscope, known as the Airy disk, is illustrated in Figure 1.4 and can be modeled by an appropriate point-spread function (PSF). The theoretical 2D paraxial PSF of the wide field fluorescence microscope can be calculated as:[32]

$$PSF = [2 \times \frac{J_1(k_{em} \cdot NA \cdot r)}{k_{em} \cdot NA \cdot r}]^2 \quad [1]$$

where *r* is the radial distance to the optical axis, *NA* is the numerical aperture, J_1 is the first-order Bessel function, $k_{em} = \frac{2\pi}{\lambda}$ defines the emission wavenumber, and λ is the wavelength of light. The smallest resolvable distance between two points of the 2D plane corresponds to the first root of the PSF and is given by the Rayleigh distances [33],

$$d_{xy}^R = 0.61\frac{\lambda}{NA} \quad [2]$$

As can be seen from the eq. [1] & [2], under the important prerequisite in which single emitters are placed in extremely low concentration to be spatially separated greater than the diffraction-limited region, it is possible to identify the localization (x, y) of a single molecule from an optical microscope image by fitting the PSF. Indeed, the fundamental idea of the modern single-molecule microscopy is reliant on PSF fitting to localize the centroid position of single point emitters. As a result, the achievable accuracy and precision of the fitted position is highly dependent upon the signal-to-noise ratio (SNR).It is important to note that organic fluorescent dyes suffer from limited photon yield and narrow Stokes shift (difference in excitation and emission wavelength). These drawbacks make them difficult to produce a sufficient SNR and can increase background signals which further reduce SNR. Hence, the shortcomings associated with organic fluorophores places a high demand for advanced materials such as QDots for single-molecule tracking.

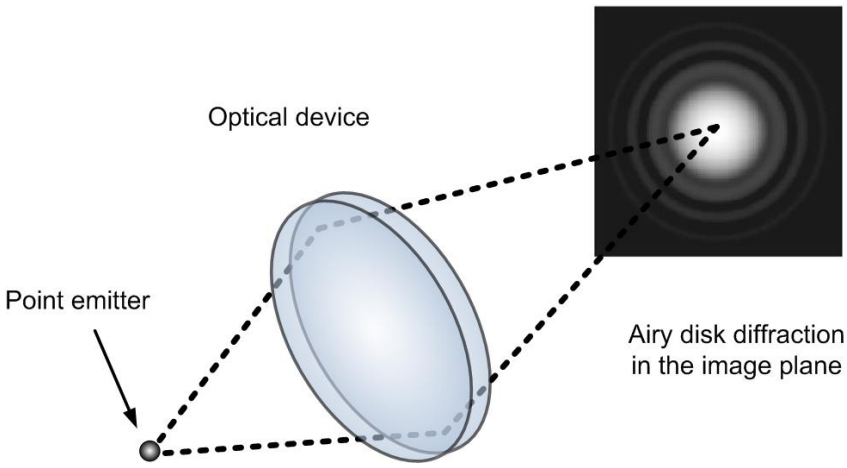

Figure 1.4 Schematic representation of the diffraction pattern from a point emitter passed through an optical device. Owing to diffraction, the smallest distance to which an imaging system can optically resolve separate light sources at is limited by the size of the Airy disk.

The process of QDot-based single-molecule microscopy is typically divided into three steps (Fig. 1.5). The first step is to acquire time-lapse imaging after single target-specific labeling has been made. Single fluorescent molecules should be able to produce diffraction-limited blurred spots in each flame. The second step involves imaging data processing and single-molecule localization from time-lapse images and is therefore normally anticipated as a computationally demanding step. In the third step, the diffusion dynamics can be analyzed from the trajectories of individual molecules, *e.g.* Brownian motion. Each step will be discussed in detail in Chapter 2.

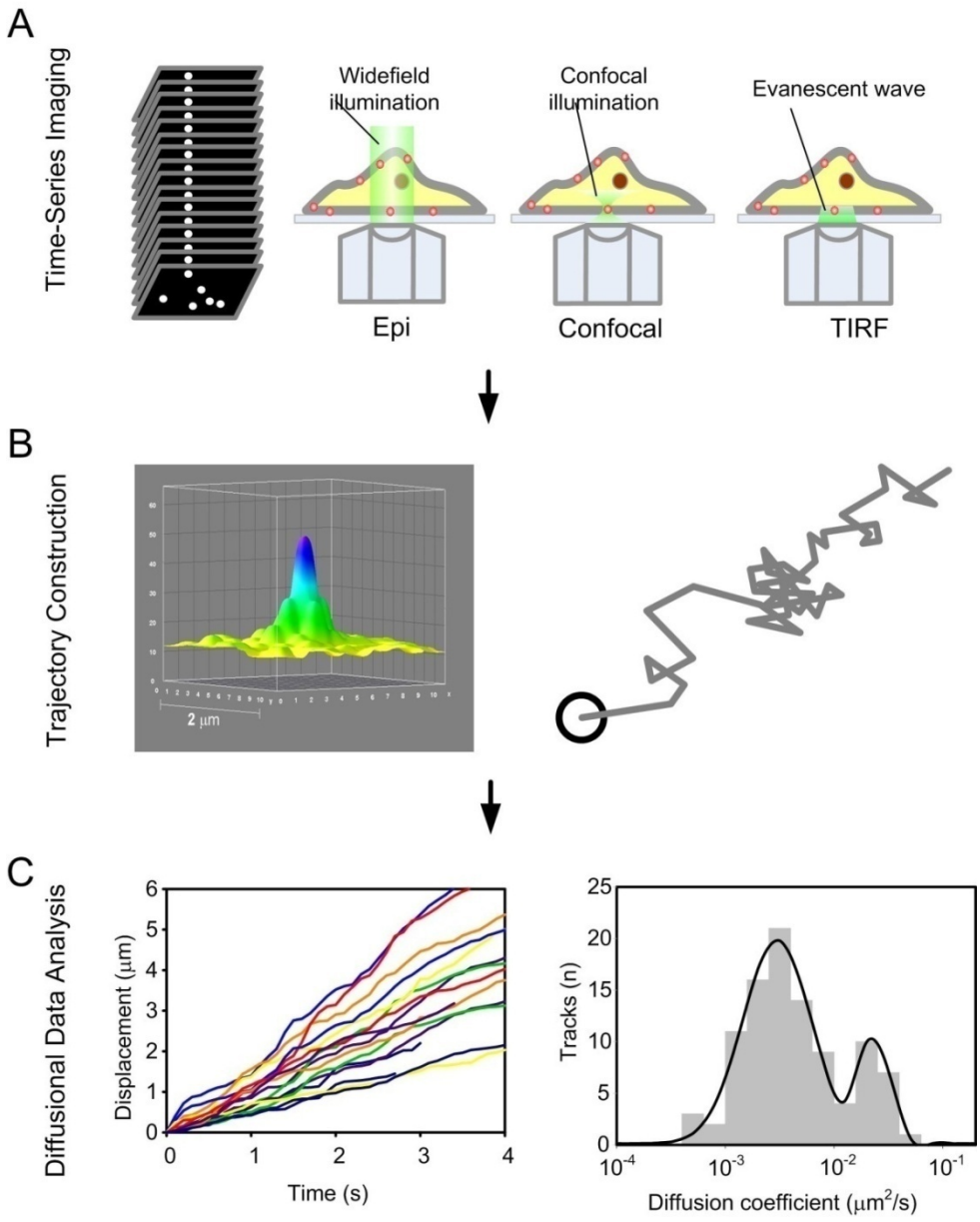

Figure 1.5 Approach to single-QDot microscopy. (A) Time-lapse images of single QDot-tagged biomolecules in living cells acquired from an optical fluorescent microscope system. (B) Estimation of the positions of single QDots with sub-pixel accuracy and trajectory generation. (C) Analysis of diffusional properties (displacement, velocity, and diffusion coefficient) from single-QDot trajectories.

1.4 Recent Advances of Single-Quantum Dot Tracking in Neuroscience Research

Dahan and coworkers first reported the diffusion dynamics of endogenous glycine receptor (GlyR) in living neurons using single QDot tacking technique.[34] The specific detection of GlyR α1 subunits was achieved through the use of a primary monoclonal antibody, a biotinylated Fab fragment of the secondary antibody, and Sav-QDots. This pioneering study made it possible to reveal multiple diffusion domains of glycine receptors in synaptic, perisynaptic, and extrasynaptic locations.

In 2008, Lévi et al. established that Ca^{2+}-driven excitatory synaptic transmission significantly restricted GlyR lateral diffusion and led to an increased subsequent clustering of GlyRs within the synaptic domain.[35] A following experiment reported by Charrier et al. in 2010 demonstrated that such a regulation of GlyR lateral diffusion at the excitatory synapses is mediated by β1 and β3 integrins, cell adhesion molecules and signaling receptors that interact via calcium/calmodulin-dependent protein kinase II.[36] This progression is an impressive example of the evolution of QDots as fluorescent probes aimed at unraveling the molecular aspects of neuronal receptor regulation.

A similar “sandwich” approach was also employed by Bouzigues et al.[37] to label $GABA_A$Rs in the tips of growing axons, the growth cones (GCs), of the rat spinal cord neurons. In the presence of an extracellular GABA gradient, the authors showed that single QDot-labeled $GABA_A$ receptors redistribute asymmetrically across the growth cone, located at the axon tip, toward the gradient source in a microtubule- and calcium-dependent manner. In 2009, Bannai et al.[38] relied on a modified approach for $GABA_A$R labeling, in which a biotinylated secondary Fab fragment was used in conjunction with primary antibody and Sav-QDots. In this study, the authors demonstrated that $GABA_A$R diffusion coefficient and confinement domain size increase in response to enhanced excitatory synaptic activity.

A distinct labeling approach based on Streptavidin-biotin assembly was developed in the Ting Lab, where the authors adapted an enzymatic reaction to specifically biotinylate their proteins of interest.[39] In their design, a fifteen amino acid acceptor peptide sequence (AP) is genetically fused to a C- or N-terminus of the protein, and a bacterial enzyme biotin ligase (BirA) is used to biotinylate a lysine side chain within the AP sequence. Howarth et al. applied this approach to label AP-fused α-amino-3-hydroxy-5-methyl-4-isoxazolepropionate (AMPA) receptors in hippocampal neurons and then study AMPA receptor synaptic localization.[40]

Cui and colleagues also used the biotin-Streptavidin approach to prepare QDot nanoconjugates to label nerve growth factor (NGF) receptors in live PC12 and rat dorsal root ganglion (DRG) neurons.[26] In their study, biotinylated NGF peptides were pre-conjugated to Sav-QDots with a stoichiometric ratio of NGF to QDot of 1 to 1.2 to achieve a monovalent presentation of NGF dimer on the QDot surface. In a clever setup, NGF-QDot conjugates were first added to the microfluidic chamber containing distal axons of DRG neurons and allowed to bind and form complexes with NGF receptors and undergo subsequent internalization into early endosomes. Endosomes containing NGF-QDots were then demonstrated to exhibit “stop-and-go” retrograde transport toward the neuronal cell body with an average speed of 1.31 ± 0.03 μm/s. Similarly to Cui et al.,[26] Fichter and coworkers employed the preconjugation strategy to link a biotinylated anti-hemagglutinin (HA) antibody to SA-QDot. The resulting QDot conjugates were used to label HA-fused serotonin receptor subtype 1A (5-HT_{1A}) and investigate the kinetics of receptor-mediated internalization of QDots.[41]

1.5 Summary

In the past two decades, technological advances in QDot synthesis have advanced opportunities for fluorescence-based biological imaging.[42] Currently available QDot probes are characterized by minimal cytoxicity, improved stability in biological environments, and ultra-low non-specific binding. Most importantly, advances in surface chemistry have allowed for the preservation of key QDot optical properties, including high quantum yield, large Stokes shift, and narrow fluorescence emission spectra. These advances have prompted a significant increase in the use of QDots by molecular and cellular neuroscientists. An exhaustive list of the recent instances of QDots used to target neuronal receptors and receptors is given in Table 1.1.

The most important achievement of QDot nanotechnology for molecular neuroscience is likely to be the single QDot tracking approach to investigate diffusion dynamics of membrane proteins at the single-molecule level. We mentioned previously that Dahan and coworkers were first to utilize this tool to interrogate the lateral diffusion of individual glycine receptors.[34] Similar approaches were subsequently employed to investigate various neuronal signaling related targets including nerve growth factor (NGF),[26] glial fibrillary acidic protein,[43] and gamma-aminobutyric acid A receptor ($GABA_AR$).[38] To fully explore the tremendous potential that QDots offer to the field of neuroscience, interdisciplinary collaborations of researchers representing a diverse range of disciplines, including chemistry, material science, neuroscience, pharmacology, and medicine, are required. With the continuous advances in QDot synthesis in parallel with the improvements in the QDot bioconjugation protocols, hopefully it will not be long before QDot-based biological labeling technique is considered as a routine method in a standard neuroscience laboratory.

Protein of interest	Targeting probe	QDot conjugation strategy	Cellular expression model	Reference
Serotonin transporter	Organic ligand	Ligand exchange	Transfected HEK293 cells	11
Serotonin transporter	Organic ligand	Biotin-Sav binding	mRNA-microinjected *Xenopus*	44
Serotonin transporter	Organic ligand	Biotin-Sav binding	Serotonergic RN46A cells	45
Dopamine transporter	Organic ligand	Biotin-Sav binding	Transfected flp-In 293 cells	46,47
GABAc receptor	Organic ligand	EDC coupling	mRNA-microinjected *Xenopus* oocytes	48
$GABA_A$ receptor (with GFP tag)	Anti-GFP antibody	2^{nd} antibody coupled to QDot	Hippocampal neurons	49
Glycine receptor	Antibody	Biotin-Sav binding	Primary rat spinal cord neurons	34, 35
Glycine receptor	Antibody	SPDP/SMCC coupling	Transfected HeLa cells, primary neurons	50
Glial fibrillary acidic protein	Antibody	Biotin-Sav binding	Primary neurons and glia	43
TrkA and and P75 NGF receptors	NGF peptide	Biotin-Sav binding	PC12 cells	51, 52
$5\text{-}HT_{1A}$ receptor (with HA tag)	Anti-HA antibody	Biotin-Sav binding	N2a cells	41
AMPA receptor	Antibody	2^{nd} antibody coupled to QDot	Primary rat cortical neurons	36, 53
AMPA receptor	Peptide	2^{nd} antibody coupled to QDot	Primary rat hippocampal neurons	40
Cannabinoid type 1 receptor	Antibody	2^{nd} antibody coupled to QDot	Primary rat hippocampal neurons	54
NMDA receptor	Antibody	2^{nd} antibody coupled to QDot	Primary rat hippocampal neurons	55
metabotropic glutamate receptors (mGluR5)	Antibody	Biotin-Sav binding	Primary rat hippocampal neurons	56
Nicotinic acetylcholine receptor (nAChR)	Protein/toxin	Biotin-Sav binding	Neuromuscular synapses in the mouse diaphragm	57
Nicotinic acetylcholine receptor (nAChR)	Antibody; Protein/toxin	Biotin-Sav binding	Chick CG neurons	58
Angiotensin II receptor type 1	Peptide	EDC coupling	Transfected CHO cells	59
Presynaptic L-type calcium channel	Antibody	Biotin-Sav binding	Synapses of the tiger salamander retina	60
P2 purinergic receptors	Organic ligand	EDC coupling	PC12 cells	61
D2 dopamine receptor	Organic ligand	EDC coupling	Transfected A9 cells	62

Table 1.1 Recent quantum dot applications in the studies of neuronal receptors and transporters

1.6 References

(1) Rozental, R.; Giaume, C.; Spray, D. C., Gap junctions in the nervous system. *Brain Res. Rev.* **2000,***32*, 11-15.

(2) Collingridge, G. L.; Isaac, J. T.; Wang, Y. T., Receptor trafficking and synaptic plasticity. *Nat. Rev. Neurosci.* **2004,***5*, 952-62.

(3) Blakely, R. D.; Defelice, L. J.; Galli, A., Biogenic amine neurotransmitter transporters: just when you thought you knew them. *Physiology* **2005,***20*, 225-31.

(4) Tsien, R. Y., The green fluorescent protein. *Annu. Rev. Biochem.* **1998,***67*, 509-544.

(5) Bastiaens, P. I. H.; Pepperkok, R., Observing proteins in their natural habitat: the living cell. *Trends Biochem.Sci.* **2000,***25*, 631-637.

(6) Marks, K. M.; Nolan, G. P., Chemical labeling strategies for cell biology. *Nat. Methods* **2006,***3*, 591-596.

(7) Rosenthal, S. J.; McBride, J.; Pennycook, S. J.; Feldman, L. C., Synthesis, surface studies, composition and structural characterization of CdSe, core/shell and biologically active nanocrystals. *Surf. Sci. Rep.* **2007,***62*, 111-157.

(8) Chan, W. C.; Nie, S., Quantum dot bioconjugates for ultrasensitive nonisotopic detection. *Science* **1998,***281*, 2016-8.

(9) Bruchez, M.; Moronne, M.; Gin, P.; Weiss, S.; Alivisatos, A. P., Semiconductor nanocrystals as fluorescent biological labels. *Science* **1998,***281*, 2013-2016.

(10) Alivisatos, P., The use of nanocrystals in biological detection. *Nat. Biotechnol.* **2004,***22*, 47-52.

(11) Rosenthal, S. J.; Tomlinson, I.; Adkins, E. M.; Schroeter, S.; Adams, S.; Swafford, L.; McBride, J.; Wang, Y.; DeFelice, L. J.; Blakely, R. D., Targeting cell surface receptors with ligand-conjugated nanocrystals. *J. Am. Chem. Soc.* **2002,***124*, 4586-94.

(12) Kim, S.; Lim, Y. T.; Soltesz, E. G.; De Grand, A. M.; Lee, J.; Nakayama, A.; Parker, J. A.; Mihaljevic, T.; Laurence, R. G.; Dor, D. M.; Cohn, L. H.; Bawendi, M. G.; Frangioni, J. V., Near-infrared fluorescent type II quantum dots for sentinel lymph node mapping. *Nat. Biotechnol.* **2004,***22*, 93-7.

(13) Nirmal, M.; Dabbousi, B. O.; Bawendi, M. G.; Macklin, J. J.; Trautman, J. K.; Harris, T. D.; Brus, L. E., Fluorescence intermittency in single cadmium selenide nanocrystals. *Nature* **1996,***383*, 802-804.

(14) Wang, X.; Ren, X.; Kahen, K.; Hahn, M. A.; Rajeswaran, M.; Maccagnano-Zacher, S.; Silcox, J.; Cragg, G. E.; Efros, A. L.; Krauss, T. D., Non-blinking semiconductor nanocrystals. *Nature* **2009,***459*, 686-689.

(15) Zhang, Q.; Li, Y.; Tsien, R. W., The dynamic control of kiss-and-run and vesicular reuse probed with single nanoparticles. *Science* **2009,***323*, 1448-53.

(16) Thompson, M. A.; Lew, M. D.; Badieirostami, M.; Moerner, W. E., Localizing and Tracking Single Nanoscale Emitters in Three Dimensions with High Spatiotemporal Resolution Using a Double-Helix Point Spread Function. *Nano Lett.* **2009,***10*, 211-218.

(17) Dabbousi, B. O.; Rodriguez-Viejo, J.; Mikulec, F. V.; Heine, J. R.; Mattoussi, H.; Ober, R.; Jensen, K. F.; Bawendi, M. G., (CdSe)ZnS core−shell quantum dots: synthesis and characterization of a size series of highly luminescent nanocrystallites. *J. Phys. Chem. B* **1997,***101*, 9463-9475.

(18) McBride, J.; Treadway, J.; Feldman, L. C.; Pennycook, S. J.; Rosenthal, S. J., Structural basis for near unity quantum yield core/shell nanostructures. *Nano Lett.* **2006,***6*, 1496-1501.

(19) Kim, S.; Bawendi, M. G., Oligomeric Ligands for Luminescent and Stable Nanocrystal Quantum Dots. *J. Am. Chem. Soc.* **2003,***125*, 14652-14653.
(20) Dubertret, B.; Skourides, P.; Norris, D. J.; Noireaux, V.; Brivanlou, A. H.; Libchaber, A., In vivo imaging of quantum dots encapsulated in phospholipid micelles. *Science* **2002,***298*, 1759-62.
(21) Pellegrino, T.; Manna, L.; Kudera, S.; Liedl, T.; Koktysh, D.; Rogach, A. L.; Keller, S.; Radler, J.; Natile, G.; Parak, W. J., Hydrophobic nanocrystals coated with an amphiphilic polymer shell: A general route to water soluble nanocrystals. *Nano Lett.* **2004,***4*, 703-707.
(22) Gao, X. H.; Cui, Y. Y.; Levenson, R. M.; Chung, L. W. K.; Nie, S. M., In vivo cancer targeting and imaging with semiconductor quantum dots. *Nat. Biotechnol.* **2004,***22*, 969-976.
(23) Bentzen, E. L.; Tomlinson, I. D.; Mason, J.; Gresch, P.; Warnement, M. R.; Wright, D.; Sanders-Bush, E.; Blakely, R.; Rosenthal, S. J., Surface modification to reduce nonspecific binding of quantum dots in live cell assays. *Bioconjug. Chem.* **2005,***16*, 1488-94.
(24) Warnement, M. R.; Tomlinson, I. D.; Chang, J. C.; Schreuder, M. A.; Luckabaugh, C. M.; Rosenthal, S. J., Controlling the Reactivity of Ampiphilic Quantum Dots in Biological Assays through Hydrophobic Assembly of Custom PEG Derivatives. *Bioconjug. Chem.* **2008,***19*, 1404-1413.
(25) Goldman, E. R.; Balighian, E. D.; Mattoussi, H.; Kuno, M. K.; Mauro, J. M.; Tran, P. T.; Anderson, G. P., Avidin: a natural bridge for quantum dot-antibody conjugates. *J. Am. Chem. Soc.* **2002,***124*, 6378-82.
(26) Cui, B.; Wu, C.; Chen, L.; Ramirez, A.; Bearer, E. L.; Li, W.-P.; Mobley, W. C.; Chu, S., One at a time, live tracking of NGF axonal transport using quantum dots. *Proc. Natl. Acad. Sci. U.S.A.* **2007,***104*, 13666-13671.
(27) Rozenzhak, S. M.; Kadakia, M. P.; Caserta, T. M.; Westbrook, T. R.; Stone, M. O.; Naik, R. R., Cellular internalization and targeting of semiconductor quantum dots. *Chem. Commun.* **2005**, 2217-9.
(28) Howarth, M.; Takao, K.; Hayashi, Y.; Ting, A. Y., Targeting quantum dots to surface proteins in living cells with biotin ligase. *Proc. Natl. Acad. Sci. USA* **2005,***102*, 7583-7588.
(29) Mattoussi, H.; Mauro, J. M.; Goldman, E. R.; Anderson, G. P.; Sundar, V. C.; Mikulec, F. V.; Bawendi, M. G., Self-assembly of CdSe-ZnS quantum dot bioconjugates using an engineered recombinant protein. *J. Am. Chem. Soc.* **2000,***122*, 12142-12150.
(30) Clapp, A. R.; Goldman, E. R.; Mattoussi, H., Capping of CdSe-ZnS quantum dots with DHLA and subsequent conjugation with proteins. *Nat. Protoc.* **2006,***1*, 1258-1266.
(31) Joo, C.; Balci, H.; Ishitsuka, Y.; Buranachai, C.; Ha, T., Advances in single-molecule fluorescence methods for molecular biology. In *Annu. Rev. Biochem.*, **2008**; Vol. 77, pp 51-76.
(32) Zhang, B.; Zerubia, J.; Olivo-Marin, J. C., Gaussian approximations of fluorescence microscope point-spread function models. *Appl. Opt.* **2007,***46*, 1819-29.
(33) Thomann, D.; Rines, D. R.; Sorger, P. K.; Danuser, G., Automatic fluorescent tag detection in 3D with super-resolution: application to the analysis of chromosome movement. *J. Microsc.* **2002,***208*, 49-64.
(34) Dahan, M.; Levi, S.; Luccardini, C.; Rostaing, P.; Riveau, B.; Triller, A., Diffusion dynamics of glycine receptors revealed by single-quantum dot tracking. *Science* **2003,***302*, 442-445.

(35) Levi, S.; Schweizer, C.; Bannai, H.; Pascual, O.; Charrier, C.; Triller, A., Homeostatic regulation of synaptic GlyR numbers driven by lateral diffusion. *Neuron* **2008,***59*, 261-73.
(36) Charrier, C.; Machado, P.; Tweedie-Cullen, R. Y.; Rutishauser, D.; Mansuy, I. M.; Triller, A., A crosstalk between b1 and b3 integrins controls glycine receptor and gephyrin trafficking at synapses. *Nat. Neurosci.* **2010,***13*, 1388-95.
(37) Bouzigues, C.; Morel, M.; Triller, A.; Dahan, M., Asymmetric redistribution of GABA receptors during GABA gradient sensing by nerve growth cones analyzed by single quantum dot imaging. *Proc. Natl. Acad. Sci. U.S.A.* **2007,***104*, 11251-6.
(38) Bannai, H.; Levi, S.; Schweizer, C.; Inoue, T.; Launey, T.; Racine, V.; Sibarita, J. B.; Mikoshiba, K.; Triller, A., Activity-dependent tuning of inhibitory neurotransmission based on $GABA_AR$ diffusion dynamics. *Neuron* **2009,***62*, 670-82.
(39) Chen, I.; Howarth, M.; Lin, W.; Ting, A. Y., Site-specific labeling of cell surface proteins with biophysical probes using biotin ligase. *Nat. Methods* **2005,***2*, 99-104.
(40) Howarth, M.; Takao, K.; Hayashi, Y.; Ting, A. Y., Targeting quantum dots to surface proteins in living cells with biotin ligase. *Proc. Natl. Acad. Sci. U.S.A.* **2005,***102*, 7583-7588.
(41) Fichter, K. M.; Flajolet, M.; Greengard, P.; Vu, T. Q., Kinetics of G-protein-coupled receptor endosomal trafficking pathways revealed by single quantum dots. *Proc. Natl. Acad. Sci. U.S.A.* **2010,***107*, 18658-63.
(42) Rosenthal, S. J.; Chang, J. C.; Kovtun, O.; McBride, J. R.; Tomlinson, I. D., Biocompatible quantum dots for biological applications. *Chem. Biol.* **2011,***18*, 10-24.
(43) Pathak, S.; Cao, E.; Davidson, M. C.; Jin, S.; Silva, G. A., Quantum dot applications to neuroscience: new tools for probing neurons and glia. *J. Neurosci.* **2006,***26*, 1893-5.
(44) Chang, J. C.; Tomlinson, I. D.; Warnement, M. R.; Iwamoto, H.; DeFelice, L. J.; Blakely, R. D.; Rosenthal, S. J., A fluorescence displacement assay for antidepressant drug discovery based on ligand-conjugated quantum dots. *J. Am. Chem. Soc.* **2011,***133*, 17528-17531.
(45) Chang, J. C.; Tomlinson, I. D.; Warnement, M. R.; Ustione, A.; Carneiro, A. M. D.; Piston, D. W.; Blakely, R. D.; Rosenthal, S. J., Single molecule analysis of serotonin transporter regulation using antagonist-conjugated quantum dots reveals restricted, p38 MAPK-dependent mobilization underlying uptake activation. *J. Neurosci.* **2012,***32*, 8919-8929.
(46) Kovtun, O.; Tomlinson, I. D.; Sakrikar, D. S.; Chang, J. C.; Blakely, R. D.; Rosenthal, S. J., Visualization of the cocaine-sensitive dopamine transporter with ligand-conjugated quantum dots. *ACS Chem. Neurosci.* **2011,***2*, 370-378.
(47) Kovtun, O.; Ross, E. J.; Tomlinson, I. D.; Rosenthal, S. J., A flow cytometry-based dopamine transporter binding assay using antagonist-conjugated quantum dots. *Chem. Commun.* **2012**.
(48) Gussin, H. A.; Tomlinson, I. D.; Little, D. M.; Warnement, M. R.; Qian, H. H.; Rosenthal, S. J.; Pepperberg, D. R., Binding of muscimol-conjugated quantum dots to GABA(c) receptors. *J. Am. Chem. Soc.* **2006,***128*, 15701-15713.
(49) Muir, J.; Arancibia-Carcamo, I. L.; MacAskill, A. F.; Smith, K. R.; Griffin, L. D.; Kittler, J. T., NMDA receptors regulate $GABA_A$ receptor lateral mobility and clustering at inhibitory synapses through serine 327 on the gamma2 subunit. *Proc. Natl. Acad. Sci. U.S.A.* **2010,***107*, 16679-84.

(50) Yeow, E. K. L.; Clayton, A. H. A., Enumeration of oligomerization states of membrane proteins in living cells by homo-FRET spectroscopy and microscopy: Theory and application. *Biophys. J.* **2007,***92*, 3098-3104.
(51) Sundara Rajan, S.; Vu, T. Q., Quantum dots monitor TrkA receptor dynamics in the interior of neural PC12 cells. *Nano Lett.* **2006,***6*, 2049-59.
(52) Rajan, S. S.; Liu, H. Y.; Vu, T. Q., Ligand-bound quantum dot probes for studying the molecular scale dynamics of receptor endocytic trafficking in live cells. *ACS Nano* **2008,***2*, 1153-1166.
(53) Bats, C.; Groc, L.; Choquet, D., The interaction between Stargazin and PSD-95 regulates AMPA receptor surface trafficking. *Neuron* **2007,***53*, 719-34.
(54) Mikasova, L.; Groc, L.; Choquet, D.; Manzoni, O. J., Altered surface trafficking of presynaptic cannabinoid type 1 receptor in and out synaptic terminals parallels receptor desensitization. *Proc. Natl. Acad. Sci. U.S.A.* **2008,***105*, 18596-601.
(55) Michaluk, P.; Mikasova, L.; Groc, L.; Frischknecht, R.; Choquet, D.; Kaczmarek, L., Matrix metalloproteinase-9 controls NMDA receptor surface diffusion through integrin b1 signaling. *J. Neurosci.* **2009,***29*, 6007-12.
(56) Renner, M.; Lacor, P. N.; Velasco, P. T.; Xu, J.; Contractor, A.; Klein, W. L.; Triller, A., Deleterious effects of amyloid beta oligomers acting as an extracellular scaffold for mGluR5. *Neuron* **2010,***66*, 739-54.
(57) Orndorff, R. L.; Warnement, M. R.; Mason, J. N.; Blakely, R. D.; Rosenthal, S. J., Quantum dot ex vivo labeling of neuromuscular synapses. *Nano Lett.* **2008,***8*, 780-785.
(58) Fernandes, C. C.; Berg, D. K.; Gomez-Varela, D., Lateral mobility of nicotinic acetylcholine receptors on neurons is determined by receptor composition, local domain, and cell type. *J. Neurosci.* **2010,***30*, 8841-51.
(59) Tomlinson, I. D.; Mason, J. N.; Blakely, R. D.; Rosenthal, S. J., Peptide-conjugated quantum dots: imaging the angiotensin type 1 receptor in living cells. *Methods Mol. Biol.* **2005,***303*, 51-60.
(60) Mercer, A. J.; Chen, M.; Thoreson, W. B., Lateral mobility of presynaptic L-type calcium channels at photoreceptor ribbon synapses. *J. Neurosci.* **2011,***31*, 4397-406.
(61) Jiang, S.; Liu, A. P.; Duan, H. W.; Soo, J.; Chen, P., Labeling and tracking P2 purinergic receptors in living cells using ATP-conjugated quantum dots. *Adv. Funct. Mater.* **2011,***21*, 2776-2780.
(62) Clarke, S. J.; Hollmann, C. A.; Zhang, Z.; Suffern, D.; Bradforth, S. E.; Dimitrijevic, N. M.; Minarik, W. G.; Nadeau, J. L., Photophysics of dopamine-modified quantum dots and effects on biological systems. *Nat. Mater.* **2006,***5*, 409-17.

The majority part of chapter 2 is going to be published in the book by Humana Press (Chang, J.C.& Rosenthal, S.J. (2013) Single quantum dot imaging in living cells, in Cellular and Subcellular Nanotechnology: Methods and Protocols, of Springer Series Methods in Molecular Biology, eds. Weissig, V., Elbayoumi, T., & Olsen, M., Springer Press) and some part of this chapter has been published by Humana Press (Chang, J.C.& Rosenthal, S.J. (2011) Real-time quantum dot tracking of single proteins, in Biomedical Nanotechnology: Methods and Protocols, of Methods in Molecular Biology Ser. ed. Hurst, S., Humana Press. vol. 726, 51-62), New Jersey. Permission is granted for the author's request for the dissertation use and for the benefit of the author's institution.

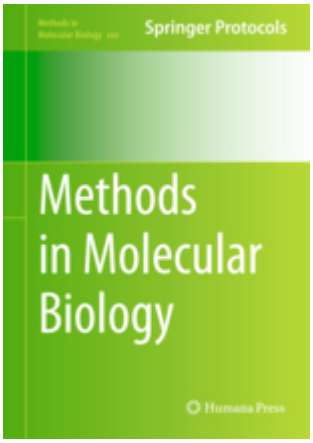

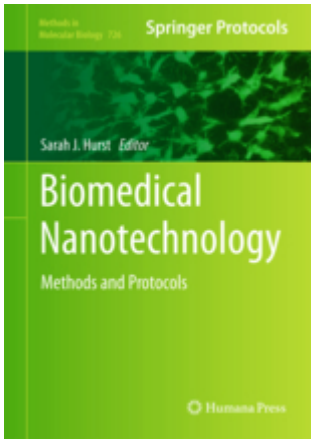


Springer
the language of science

Title: Real-Time Quantum Dot Tracking of Single Proteins
Author: Jerry C. Chang
Publication: Springer eBook
Publisher: Springer
Date: Jan 1, 2011
Copyright © 2011, Humana Press

Logged in as: Jerry Chang
LOGOUT

Order Completed

Thank you very much for your order.

This is a License Agreement between Jerry C Chang ("You") and Springer ("Springer"). The license consists of your order details, the terms and conditions provided by Springer, and the payment terms and conditions.

Get the printable license.

License Number	2913700187811
License date	May 21, 2012
Licensed content publisher	Springer
Licensed content publication	Springer eBook
Licensed content title	Real-Time Quantum Dot Tracking of Single Proteins
Licensed content author	Jerry C. Chang
Licensed content date	Jan 1, 2011
Type of Use	Thesis/Dissertation
Portion	Full text
Number of copies	1
Author of this Springer article	Yes and you are a contributor of the new work
Title of your thesis / dissertation	Single Quantum Qdot approach for Molecular Dissection of Serotonin Transporter Regulation in Living Cells
Expected completion date	Jun 2012

All other uses, reproduction and distribution, including without limitation commercialreprints, selling or licensing copies or access, or posting on open internet sites, yourpersonal or institution's website or repository, without permission from the publisher are prohibited.

CHAPTER 2

SINGLE QUANTUM DOT IMAGING TECHNIQUES (METHODS)

2.1 Microscopy Setup for QDot-Based Single-Molecule Observation

Driven from high-speed video microscopy, single-molecule tracking has been demonstrated in various configurations of fluorescent microscopes, including wide-field epifluorescence, confocal, and total internal reflection fluorescence (TIRF) microscope. The basic requirements for single-molecule microscopy are: a high numerical aperture (NA) objective, dichroic and emission filters, a stable monochromatic excitation source, and an ultrasensitive photon detector, combined with appropriate software for imaging acquisition and data processing. However, real-time visualization of fluorescent signal from a single-molecule is not an easy task. In principle, the microscope system needs to be optimized to maximize the number of detected photons while still guaranteeing minimizing any background noise.

A standard wide-field epifluorescence microscope equipped with an ultrasensitive photon detector is by far the simplest microscopy setup for single-molecule tracking. Taking advantage of high quantum yield of core/shell QDots, common excitation light source, such as a mercury or a xenon arc lamp, may be sufficient;[1] however, laser illumination, which provides higher power and narrower excitation wavelength, is a better (although more expensive) choice. As noted in Chapter 1, single-molecule microscopy is a technique highly dependent on SNR. To achieve ultra-sensitivity with high temporal resolution, detector for fluorescent imaging is required to obtain high quantum efficiency with minimum shot-noise. A commonly used detector for single-molecule imaging is the electron-multiplying charge-coupled device (EMCCD). Back-illuminated type EMCCD

cameras are preferred due to their better quantum efficiency (~90%) in the visible region (Fig. 2.1).[1, 2]

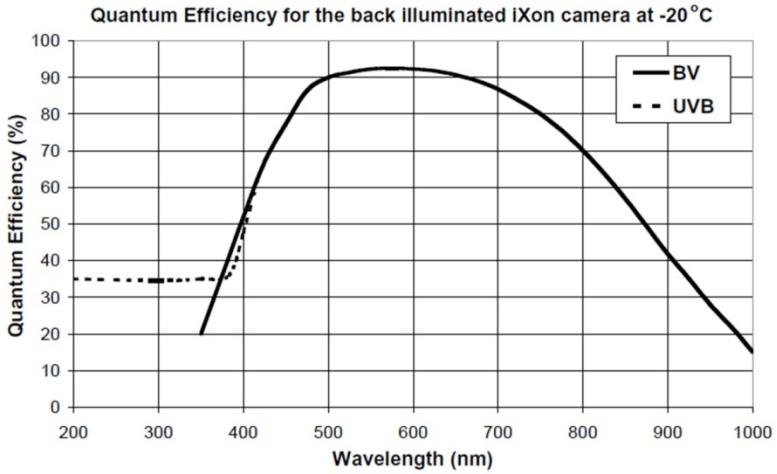

Figure 2.1 Quantumefficiency of a Back-Illuminated EMCCD camera. (iXon DV 887 EMCCD; Andor Technology, Belfast, Northern Ireland) (adapted from AndorCCD specification documents at http://www.andor.com). Noted the high quantumefficiency(Evolve > 90% across the 500 – 650 nm visible spectrum), this can serve to reduce the exposure time for greater temporal resolution for single molecule imaging.

In addition to the detector, there are other factors that impact the SNR. In a wide-field epifluorescence microscope, the excitation bean passes through the entire specimen and may excite any fluorophores in the illumination path, including molecules outside the focal plane, which increases background noise. A solution to overcome this drawback is TIRF microscopy.[3] For a typical biological sample in aqueous buffer, TIRF is particularly useful since the difference in refractive index, *n*, between water and a glass cover-slip is large enough to generate total internal reflection for TIRF microscopy imaging (water n=1.33; cover-slip n=1.52). Currently, TIRF microscopy is the most popular setup for QDot-based single-molecule tracking.[2, 4, 5]

Conventional point scanning confocal microscopy, which effectively excludes the out-of-focus fluorescence by adding an additional pinhole, is capable of generating an image with high positional accuracy. However, this approach suffers from low temporal

resolution and is seldom used in single-molecule tracking, even though it provides an advantage without the restriction of imaging close to the proximity of an interface like TIRF. For example, the Zeiss LSM 510 META is a popular point-scanning confocal microscope. In a high noise fast scanning setup, data collection takes about 1-2 seconds to acquire a 512 $\times$ 512 pixels image. As a result, the acquisition of a single frame with high SNR may take more than 5 seconds. Recently, two advanced confocal microscope configurations, distinguished by their scanning approaches, have been introduced for their rapid scanning speeds. The first approach named as the spinning-disk confocal method (SDCM) uses a disc with a series of pinhole apertures to process simultaneous multi-spot scanning.[6] The second method is often referred to as the line scanning confocal method (LSCM), which uses an oscillating mirror to simultaneously illuminate an entire line of the specimen and focus the fluorescence into a linear detector.[7] Currently, confocal systems based on these fast scanning concepts to achieve video frame rates suitable for single-molecule imaging are commercially available, which include the LSCM microscope by Carl Zeiss (LSM 7 Live: 120 frames/sec @ 512x512 pixels), SDCM microscope by Leica (SD6000: multipoint scanning at 1000 Hz), and SDCM microscope by Andor (custom-made system: 30 frames/sec @ 512x512 pixels).

2.2 Imaging Data Processing and Subpixel Localization

As we described in the introduction, fluorescent intensity distribution from a single emitter can be fit with a 2D Gaussian.[8, 9] To calculate a subpixel estimate of single QDot position, the general method is to fit the single QDot intensity distribution with a 2D Gaussian function and then calculate the local maximum intensity (Fig. 2.2):

$$I_{xy} = A_0 + A \cdot e^{-\frac{(x-x_0)^2+(y-y_0)^2}{w^2}} \quad [3]$$

where I_{xy} is the intensity of the pixel, x_0 and y_0 is the designated local maximum coordinates of the Gaussian, A is the amplitude of the signal with local background A_0, and w is the width of the Gaussian curve. The smallest distance at which two emitters can be recognized and separated is roughly equal to the full width at half maximum (FWHM) of the w :

$$w_{FWHM} = w \cdot \sqrt{\ln(4)} = 1.177w \quad [4]$$

It is important to note that the coordinate (x_0 , y_0) acquired by fitting function [3] using chi-squared minimization is not a true position, but only an estimate. The accuracy, as we mentioned in the introduction, is strongly dependent upon the respective SNR, which is defined as:[9]

$$SNR = \frac{I_0}{\sqrt{\sigma_{bg}^2 + \sigma_{I_0}^2}} \quad [5]$$

where I_0 is the maximum signal intensity above background, σ_{bg}^2 is the variance of the background intensity values, and $\sigma_{I_0}^2$ is the true variance of the maximum signal intensity above the background. Since w width is approximately equal to the wide-field diffraction limit (for visible light is about 250 nm), the uncertainty of the fitted coordinate ($\Delta\sigma$) is approximately given by:

$$\Delta\sigma \approx \frac{250}{SNR}(nm) \quad [6]$$

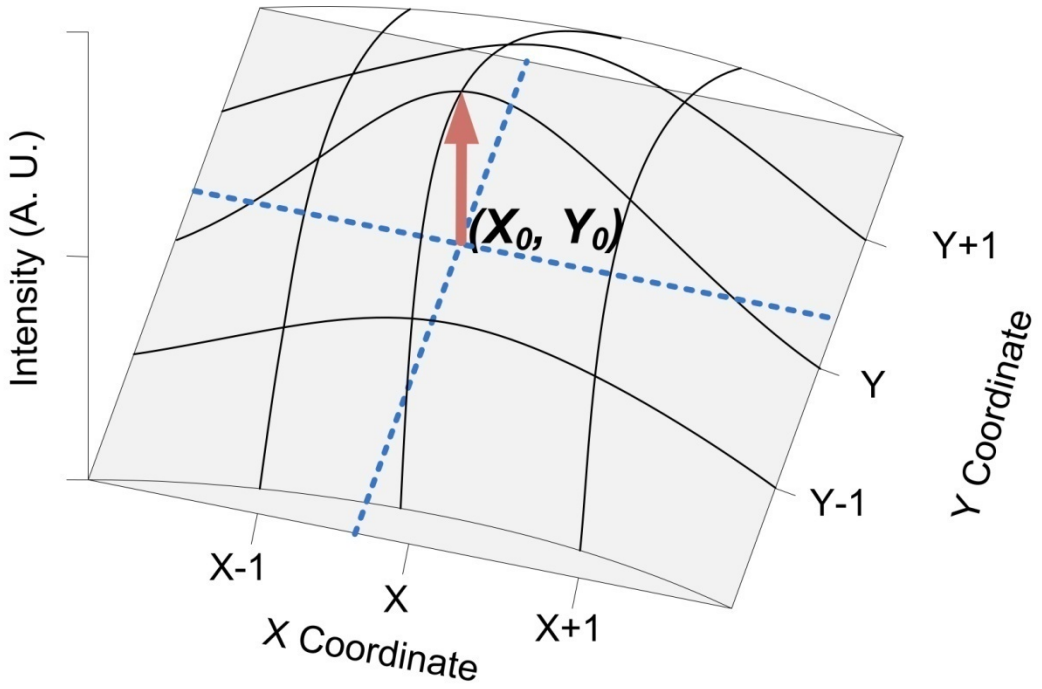

Figure 2.2 Schematic of 2D Gaussian regression of a single QDot fluorescent image. Note that a much more accurate localization in the center can be obtained by fitting the 2D Gaussian function to the experimental intensity data

After x and y coordinates of the targeted single-molecules are determined in each frame, cumulative displacement of each single targets can be generated to reflect the rate of movement (Fig. 2.3). The timecourse of the corresponding moment is determined by the following formula:

$$\Delta d_n = \left\{ [x(n+1) - x(n)]^2 + [y(n+1) - y(n)]^2 \right\}^{(1/2)} \quad [7]$$

where $x(n)$, $y(n)$ denotes the position in frame (n), Δd_n indicates that a single step takes place during a single lag time Δt from time point $\Delta t \times (n)$ to $\Delta t \times (n+1)$.

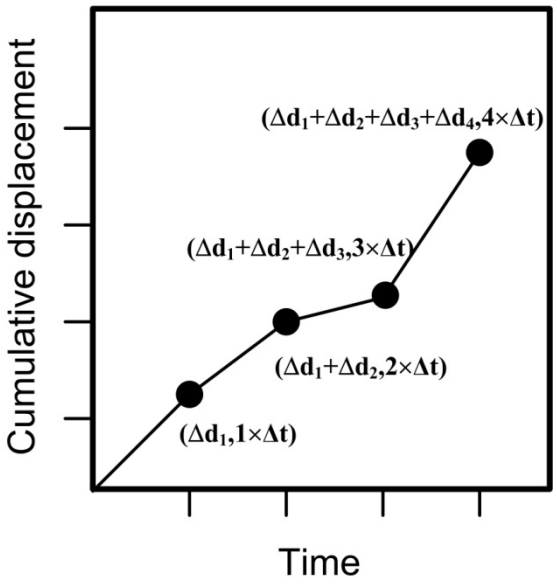

Figure 2.3 Schematic of a step displacement plot of single-molecule tracking.

2.3 Diffusion Theory and Calculation

Simple diffusion caused by the random movement of molecules is known as Brownian motion. The general diffusion theory of Brownian motion was developed by Einstein in 1905[10] and is still suitable to describe single-molecule protein dynamics. Importantly, according to Einstein's theory, the diffusion coefficient, *D*, is not dependent on the velocity, but is essentially determined by the mean square displacement (MSD). In his paper entitled "On the movement of small particles suspended in stationary liquids required by the molecular-kinetic theory of heat",[10] Einstein started with a 1D random walk. Assuming that a total of n Brownian particles move only along a given axis, x, in a time interval, τ, where the displacement of individual particle is Δ, the equations Einstein obtained reads:

$$dn = n\varphi(\Delta)d\Delta \qquad [8]$$

where $\int_{-\infty}^{+\infty} \varphi(\Delta)d\Delta = 1$, and φ satisfies the condition $\varphi(\Delta) = \varphi(-\Delta)$

From the condition of the function $\varphi(\Delta)$, he then calculated the distributions of the particle at ($t + \tau$) from their distribution at time t:

$$f(x, t+\tau)dx = dx\int_{\Delta=-\infty}^{\Delta=+\infty} f(x+\Delta)\varphi(\Delta)d\Delta \qquad [9]$$

Based on the equation [7] and [8], an equation for the diffusion coefficient Dcan be derived from the MSD $\langle\Delta^2\rangle$:

$$D = \frac{1}{\tau}\int_{-\infty}^{+\infty}\frac{\Delta^2}{2}\varphi(\Delta)d\Delta = \frac{1}{2\tau}\langle\Delta^2\rangle \qquad [10]$$

In a 2D and 3D random walk case, equation [10] can be rewritten as:

2D: $\langle\Delta^2\rangle = 4\Delta\tau$ [11]

3D: $\langle\Delta^2\rangle = 6\Delta\tau$ [12]

From the equation [10], Einstein shows how the diffusion coefficient can be related to the MSD in single-molecule dynamics. However, the diffusion process may not follow Brownian motion in many biological systems. Common causes include diffusion barriers in the cellular structures, active transport along intracellular networks, or membrane-facilitated exocytotic and endocytotic processes. For the cases of non-Brownian motion in the biological systems, it is very difficult to obtain an explicit solution. Methods for connecting MSD estimates with motion modes can roughly be classified into "itemized" and "unified". The former type of method classifies the diffusion modes into several categories. Each mode has a distinct $\left\langle \Delta^2 \right\rangle$ vs. time dependence, such as that studied by the Saxton and Jacobson [11] for the lateral diffusion modeling of individual proteins or lipids in the plasma membrane. Listed below are the models proposed by Saxton used for predicting diffusion processes in biological systems (Fig. 2.2).

$$\left\langle \Delta^2 \right\rangle = 4\Delta\tau \qquad \textit{---normal diffusion} \qquad [13]$$

$$\left\langle \Delta^2 \right\rangle = 4\Delta\tau^{\alpha} \qquad \textit{---anomalous diffusion} \qquad [14]$$

$$\left\langle \Delta^2 \right\rangle = 4\Delta\tau + (v\tau)^2 \qquad \textit{---directed motion with diffusion} \qquad [15]$$

$$\left\langle \Delta^2 \right\rangle \approx \left\langle r_c^2 \right\rangle [1 - A_1 e^{-\frac{4A_2 D\tau}{\left\langle r_c^2 \right\rangle}}] \qquad \textit{---corralled motion} \qquad [16]$$

, where D denotes the diffusion coefficient, $\tau$is the time-resolution, α is the anomalous diffusion exponent, v is the velocity, $\left\langle r_c^2 \right\rangle$ indicates the corral size, and A_1 and A_2 are constants determined by the corral geometry.

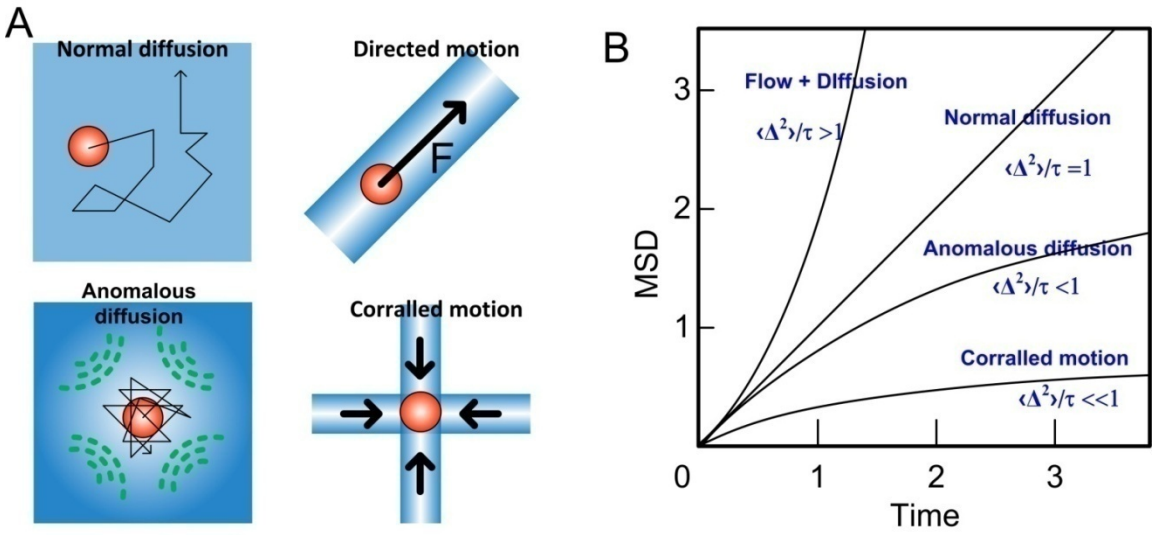

Figure 2.4 Schematics of different modes of diffusive behavior. (A) and their corresponding MSD plot (B). When MSD is plotted as a function of time, the linear plot of MSD versus time represents normal diffusion. When the change in MSD is nonlinear with time, an increasing slope indicates directed diffusion, and confined diffusion (anomalous diffusion or corralled motion) produces an MSD plot with a decreasing slope.

Due to its simplicity and ability to produce rapid results, the random walk model (normal diffusion) is commonly used to estimate the diffusion coefficient. However, in biological interpretation, anomalous diffusion was reported as the dominant model of diffusion dynamics in the plasma membrane.[12, 13] The standard method to obtain the diffusion coefficient from anomalous diffusion model is through a linear fit, as indicated below, since this fit converges more consistently than the variable power-law fit:[12]

$$\log\left\langle \Delta^2 \right\rangle = \alpha \log\left(\Delta\tau\right) + \log\left(4D\right) \qquad [17]$$

In a complicated biological environment, diffusion mode of the same biological target may vary at different time scales. For example, it has been reported that G-protein coupled receptor (GPCR) shows a confined diffusion mode at the short time scale, indicating entrapment at certain membrane compartment. However, at the longer time scale GPCRs can move from onecompartment to another, undergoing free diffusion.[14] This phenomenon is often referred to as “hop diffusion”. In complicated cases like this

one, using a “unified” method in which only one simple equation is used to fit the MSD data over the entire time scale seems to be a better approach. Therefore, Destainville and Salomé proposed to use a simple law to fit MSD data.[15] A single equation is provided with two time-correlation functions: a short-term diffusion coefficient D_μ describes a rapid, “microscopic” diffusion behavior, and a long-term diffusion coefficient D_M indicates a slower, “macroscopic” movement:

$$\left\langle \Delta^2 \right\rangle = \frac{L}{3}\left[1 - \exp(-\frac{\tau}{T})\right] + 4D_M\tau \text{ , and } T = \frac{L^2}{12D_\mu}, \qquad [18]$$

where$L$ is the typical size of the short-term confining domains and T is the so-called “equilibration” or “relaxation” time. As a result, the size of the shot-term confinement zone (L^2) can be estimated.

2.4 Imaging System Calibration Using Spin-Cast Single Quantum Dots

A general strategy to identify whether the optical system is able to detect individual QDots is to carry out time-lapse imaging of a very dilute QDot solution to avoid multiple QDots overlapping within diffraction limited distance. Individual QDots are characterized by their blinking properties. The emission intensity of a single QDot is shown in Figure2.3, where a single QDot blinks completely on and off during a time-lapse sequence of 80 sec at a 10 Hz frame rate. When the fluorescence is produced by an aggregate structure consisting of several QDots, such blinking effects are completely cancelled out. The protocol described below is based on a custom-built Zeiss Axiovert 200M inverted fluorescence microscope coupled with a charge-coupled device (CCD) camera (Cool-Snap$_{HQ2}$, Roper Scientific, Trenton, NJ). To track single QDots in real-time, the acquisition rate should be set at 10 Hz or higher. However, the imaging rate is usually limited by the frame readout time of the camera. This particular CCD is chosen due to its adequate 60 % quantum efficiency (QE) throughout the entire visible spectrum range (450 - 650 mm) with a frame rate > 20 at 512 × 512 pixels (*see* Photometrics CCD specification document at http://www.photomet.com). And again, as introduced in the section 2.1, a more advanced back-illuminated Electron Multiplying CCD (EMCCD) with sub-msec temporal resolution will be a much better choice. Imaging should be performed with a high-resolution (63× or 100×) oil-immersion objective lens with numerical aperture of 1.30 or greater.

The sample preparation steps are:

1. Prepare a clean microscope glass slide coverslip or 35 mm culture dish with a coverslip at the bottom (e.g. MatTek dish).
2. Add 1 drop (20 µL) of 100 pM QDot® 605 ITK™ carboxyl quantum dots solution onto the coverslip.

3. Spin cast the QDot solution on the coverslip for 30 sec at 2000 rpm or less. *(Note*: The spinning force is not critical in this step. In most cases, a rotational speed as low as 500 rpm is sufficient to achieve a uniform spread when using common compact spin coater.)
4. Mount the coverslip on the microscope stage.
5. QDots are excited using a xenon arc lamp (excitation filter 480/40 BP) and detected with CCD camera thorough appropriate emission filter (600/40 BP for QDot 605). Acquire time-lapse images (100 msec per frame, 60 sec).

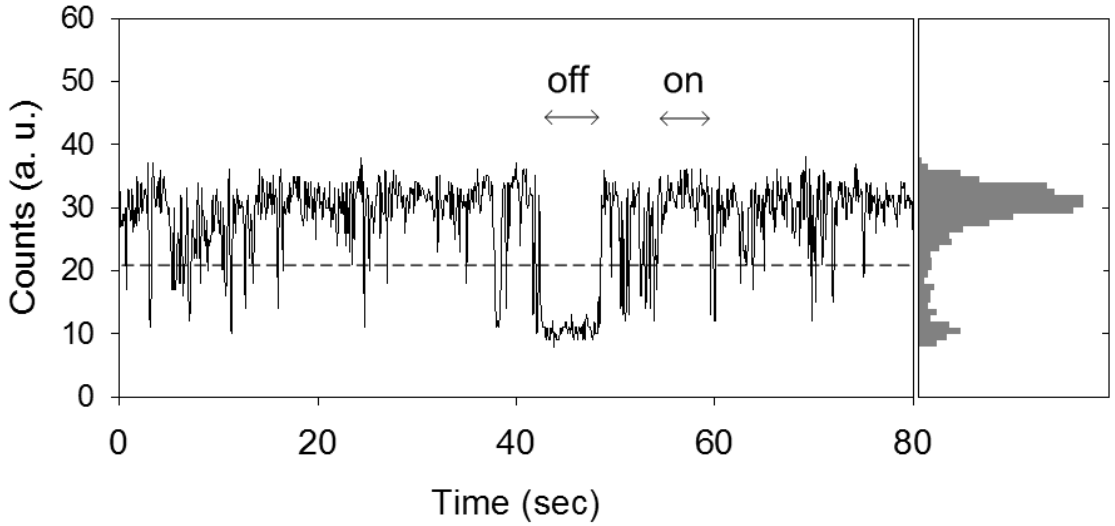

Figure 2.5 A typical intensity over time plot from a single blinking QDot. As displayed in the left panel, the intensity trajectory of a single QDot displays two dominant states: an "on" state and an "off" state, termed blinking. A predefined intensity threshold is shown by the dashed line. Right panel displays the probability density distribution.

2.5 Single Quantum Dot Labeling in Living Cells

Single quantum dot labeling can be prepared through either a direct labeling (one step) procedure or an indirect (two step) protocol. In the direct labeling procedure, the target-specific probe (small molecule organic ligand, peptide, or antibody) is directly conjugated to the QDots surface to make ligand-QDot nanoconjugates. Therefore, the cellular labeling strategy could be performed in one step in which the live cell sample is incubated with a target-specific nanoconjugate prior to fluorescent imaging. In the two step procedure, the cell sample is first incubated with biotinylated ligand to yield the desired specific ligand-protein binding. After an appropriate washing step, strep-QDots are added as the fluorescent tag of the biotinylated ligand-protein complex for the single-molecule imaging.

A general protocol for single QDot labeling of adherent cells is given here, which is applicable to most mammalian cell lines. The standard protocol given below should be followed:

1. Prepare a 35 mm coverslip-buttoned culture dish with cells that have reached about 50 % confluence.
2. Wash the cells gently 3 times with Phenol red-free culture medium by repeatedly pipetting out.
3. Incubate cells with a biotinylated small molecule probe (0.5 nM- 0.5 μM dependent upon the biological affinity) or antibody (1-10 μg/mL) in red-free DMEM for 20 min at 37 ˚C. (For one step labeling protocol, incubate cells with 10-50 pM ligand-QDot nanoconjugates and skip step 4-5)

   Note: The labeling concentration/cell type relationship should be adjusted for the surface protein expression level. In our experiments, we choose low concentrations for transfected cells. For labeling endogenously expressing membrane proteins in living cells, higher concentrations may be needed.

4. Wash cells gently 3 times with Phenol red-free culture medium.

5. Incubate the cells with QDot Streptavidin conjugate (0.1 nM - 0.5 nM) in Phenol red-free culture medium for 5 min at 37 °C.

6. Wash the cells at least 3 times with Phenol red-free culture medium.

7. Place the culture dish on the microscope stage with mounted heating chamber and heat to 37 °C.

8. The labeling quality can be observed under fluorescent microscope. Punctate QDot staining should be visible through the eye piece or CCD detector (Fig. 9). Single QDots can be identified by their blinking property.

9. Acquire time-lapse images at 37 °C. In our experiments, acquisition procedure typically lasts for 60 seconds at 10 Hz rate.

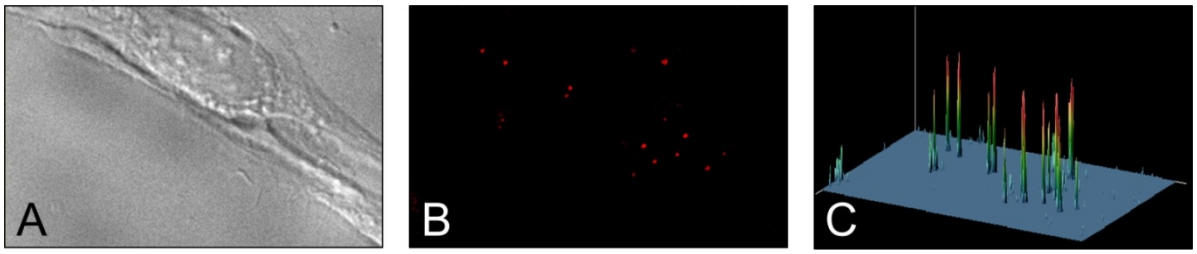

Figure 2.6 Example live HeLacell imaging of membrane SERT proteins labeled with single QDots. (A: bright field, B: fluorescence, and C: surface intensity plot of B).

2.6 Tracking Programs for Single-Molecule Analysis

Tracking and trajectory construction is a computationally demanding step of following single QDot-labeled biological targets through successive images. One of the most important determinants of modern single-molecule tracking techniques is the nanometer accuracy, which is heavily weighted by the PSF fitting to localize the centroid position for sub-pixel resolution, normally demonstrated as a fitting of a 2D Gaussian function to a PSF (see Section 2.2). For practical application, estimated background-corrected intensities of an image are normally filtered out, a necessary step for the calculation of centroid position (x_0, y_0). After locations of single molecules are identified in each frame, the next step is to link the detected single-molecule positions. However, single QDot blinking brings additional difficulties for the trajectory generation, as the spots can temporarily disappear. A practical and most frequently used approach is to define a tolerance limit of blinking frames (usually $\leq$ 10 frames) and process an additional association step in the trajectory generation algorithm to merge multiple trajectories into one.[16] This procedure allows tracking to continue and thus compensates for the transient data loss caused by QDot blinking. In addition, QDot blinking frequency is dependent on the excitation power; hence, it is generally recommended to perform single QDot tracking experiments with low power excitation if signal intensity is sufficiently high.

As the popularity of the single molecule/particle technique expands, computational algorithms for tracking have become more widely available. For example, *particle tracking using IDL,*[17] developed by Crocker and Grier, provides a total solution including 2D Gaussian fit for spot localization, trajectory generation, as well as MSD calculation (Fig. 2.7). The algorithms with detailed tutorial are available at http://www.physics.emory.edu/~weeks/idl/index.html. Matlab version of these routines can be found at http://physics.georgetown.edu/matlab/. In addition, with recent advances

in computing power and numerical software, the development of tracking algorithms has evolved rapidly during the past few years in supporting better correspondence for motion detection,[18] high computational efficiency,[19] or 3D motion segmentation and localization.[20] All the tracking algorithms mentioned above may, however, require technical training to operate since they all established under technical computing environments such as Matlab, IDL, or C^{++}.

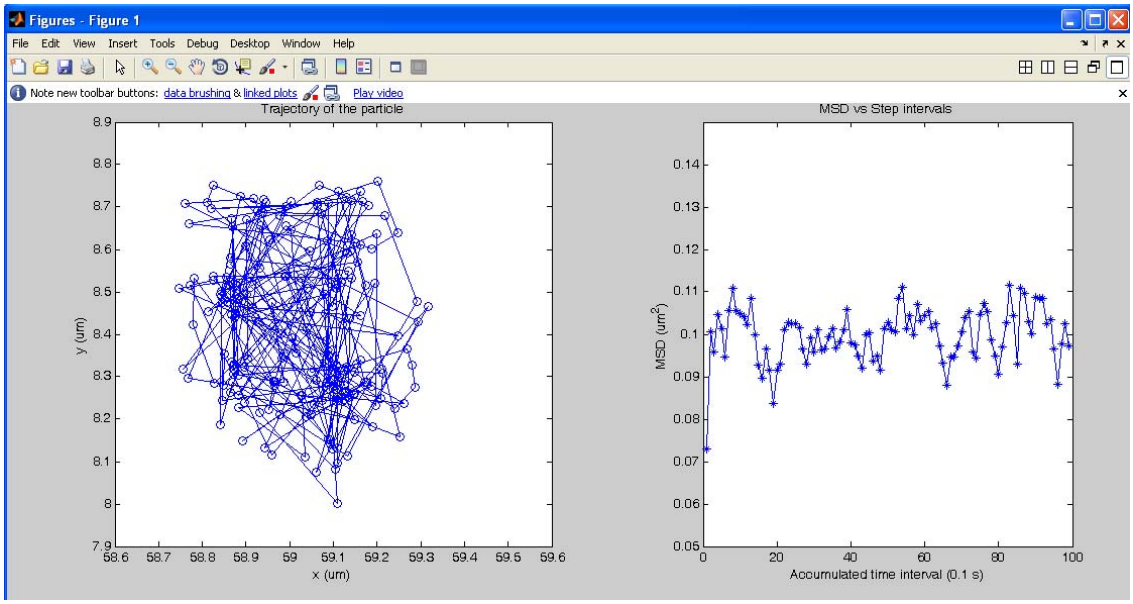

Figure 2.7 Snapshot of the interface of Matlab-based particle tracking program originally developed from *particle tracking using IDL* algorithm. Data obtained from 600 frames of single QDot imaging. Left panel indicates the 2D trajectory and right panel shows the MSD over time.

In addition to the tracking algorithms requiring technical computing environments, ParticleTracker,[21] an ImageJ plugin for single molecule/particle tracking, offers several user-friendly features including an easily understandable interface, free on-line tutorial, and computationally efficient process. The program is free to download at ImageJ website: http://rsbweb.nih.gov/ij/plugins/index.html. Given below is a general tracking procedure using ParticleTracker:

1. Use the *File/Open* commend in the ImageJ to import the pre-recorded TIF stack or uncompressed avi file (Fig 2.11A). If the avi file contains multi channel imaging data, use the *Image/Color/RGB Split* to QDot data channel extraction.
2. Next, click the *Plugins/Particle Detector & Tracker* commend. If RGB images or images with greater then 8-bits are loaded for tracking, a checkable menu item will show up to ask whether the images are converted to 8-bits. If running on a computer with fewer than 2GB of memory installed, it is strongly recommended to convert to 8-bits to reduce the memory consumption.
3. As indicated in Fig. 11 B, three basic parameters for particle detection are given. *Radius*: Approximate radius of the particles in the images in units of pixels. *Cutoff*: The score cut-off for the non-particle discrimination. *Percentile*: The percentile (r) that determines which bright pixels are accepted as Particles. Click on preview detected and then the successfully detected spots will be circulated. Here we recommend to use *Radius = 3*, *Cutoff = 0*, and *Percentile = 0.1* as initial guess, but these values might vary based on the images. Start with our recommended parameter and change these values until most of the visible particles are detected after clicking the preview button.
4. After setting the parameters for the detection, set up the particle linking parameters (*Displacement* & *Link Range*) in the bottom of the dialog window (Fig. 2.11B). Here the *Displacement* parameter means the maximum number of

pixels a particle is allowed to move between two succeeding frames. The *Link Range* parameter is used to specify the number of subsequent frames that is taken into account to determine the optimal correspondence matching. We recommend to use *Displacement = 2* and *Link Range = 10* as initial guess, and again, these parameters can also be modified after viewing the initial results.

5. Next push the OK button and the result window will then be displayed (Fig. 2.11C) after seconds to minutes computational calculation (for 600 frames of 128x128 pixel images takes less than one minute on a regular dual core PC). With the *Filter Options* button given on the dialog window, you can filter out trajectories under a given length. Particular trajectory of interest can be selected by clicking it once with the mouse left button (as indicated in yellow box of Fig. 2.11C).
6. The selected trajectory can be displayed in a separate window by clicking on the *Focus on Selected Trajectory* button. The visualization of the selected trajectory can then be saved individually in .gif format (Fig. 2.11D). Detected time-series trajectory coordinates can also be exported in a single .txt file for further analyses.
7. After exporting trajectory coordinates, MSD of a specific trajectory can be obtained according to the formula below:

$$MSD(n\Delta t) = (N-n)^{-1}\sum_{i=1}^{N-n}[(x_{i+n}-x_i)^2 + (y_{i+n}-y_i)^2] \qquad [17]$$

, where x_i and y_i are the position of particle on the frame i, Δt is the-time resolution, N is total number of frames, $n\Delta t$is the time interval over which the MSD is calculated.

It is important to note that we have tested hundreds of single QDot trajectories and found that the algorithm used in the ParticleTracker program can easily cause false linking of different molecules/particles between frames. This could lead to incorrect trajectory construction. It may be improved by manual re-linking with visual inspection. However, potential problems and limitations can still be associated with such manual re-linking. Due to its respectable efficiency, ParticleTracker program is suitable for preliminary screening tests. However, for serious and in-depth analysis, we recommend use of *particle tracking using IDL* or the Matlab-based tracking routines mentioned earlier.

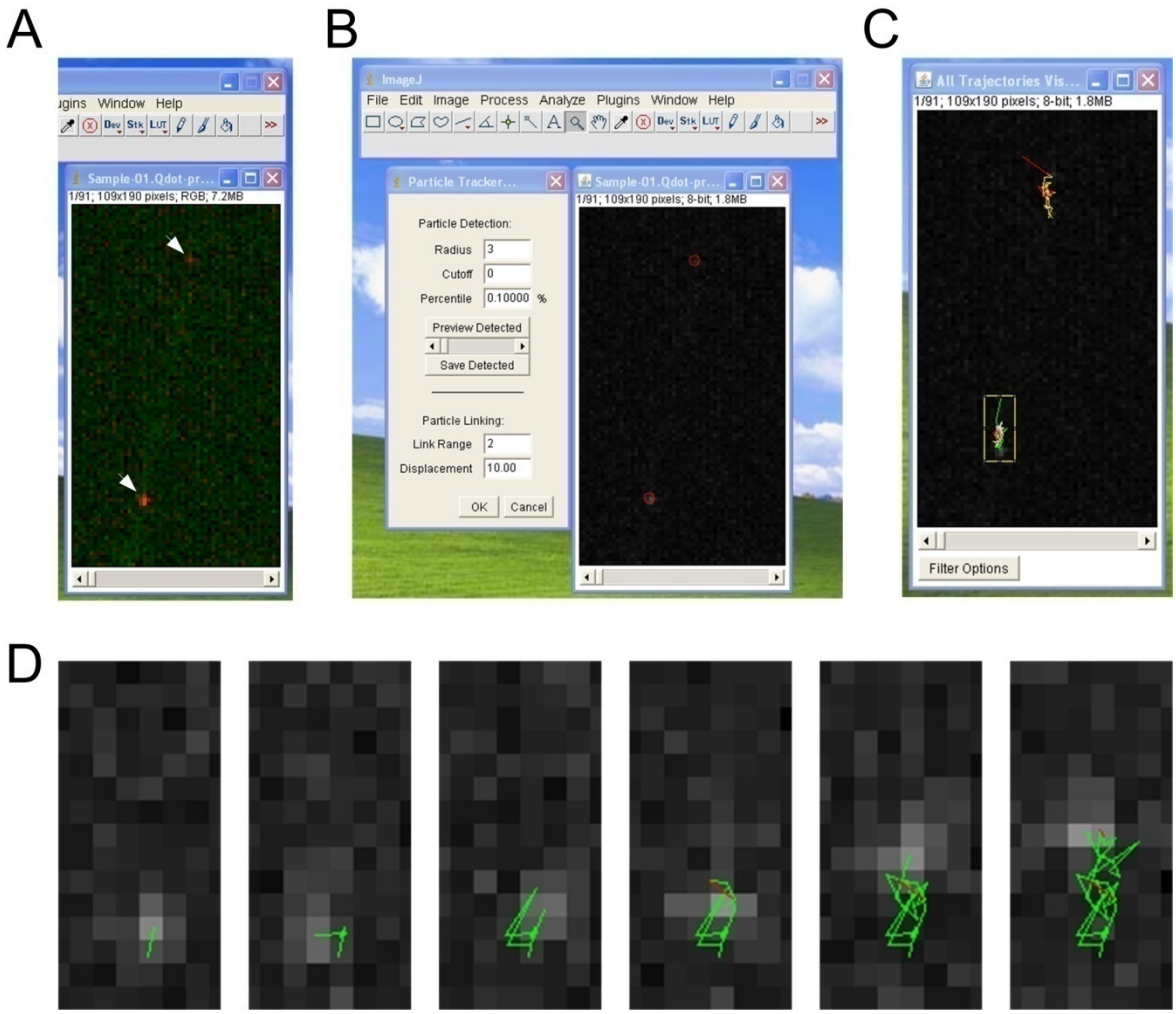

Figure 2.8 Steps of single QDot tracking using ParticleTracker - an ImageJ plugin. (A) A typical raw frame from a time-lapse single-QDot labeling movie. White arrows indicate the QDot-labeled target proteins. (B) Image conversion and preview detection from the raw frame. Image conversion to Gray 8 is preferred to increase computational efficiency. Red circle masks the successfully targeted spots for tracking after executing the Preview Detected function. (C) Visualization of all trajectories after executing the Show Detected function. Particular area of interest can be selected and zoomed in as indicated in yellow box. (D) Time-lapse trajectory from the selected area of interest. Red line drawn indicates the "Gaps" in the trajectory.

2.7 References

(1) Dahan, M.; Levi, S.; Luccardini, C.; Rostaing, P.; Riveau, B.; Triller, A., Diffusion dynamics of glycine receptors revealed by single-quantum dot tracking. *Science* **2003,***302*, 442-445.

(2) Cui, B.; Wu, C.; Chen, L.; Ramirez, A.; Bearer, E. L.; Li, W.-P.; Mobley, W. C.; Chu, S., One at a time, live tracking of NGF axonal transport using quantum dots. *Proc. Natl. Acad. Sci. U.S.A.* **2007,***104*, 13666-13671.

(3) Alcor, D.; Gouzer, G.; Triller, A., Single-particle tracking methods for the study of membrane receptors dynamics. *Eur. J. Neurosci.* **2009,***30*, 987-997.

(4) Bouzigues, C.; Morel, M.; Triller, A.; Dahan, M., Asymmetric redistribution of GABA receptors during GABA gradient sensing by nerve growth cones analyzed by single quantum dot imaging. *Proc. Natl. Acad. Sci. U.S.A.* **2007,***104*, 11251-6.

(5) Pinaud, F.; Michalet, X.; Iyer, G.; Margeat, E.; Moore, H.-P.; Weiss, S., Dynamic partitioning of a glycosyl-phosphatidylinositol-anchored protein in glycosphingolipid-rich microdomains imaged by single-quantum dot tracking. *Traffic* **2009,***10*, 691-712.

(6) Nakano, A., Spinning-disk confocal microscopy - a cutting-edge tool for imaging of membrane traffic. *Cell Struct. Funct.* **2002,***27*, 349-355.

(7) Ralf, W.; Bernhard, Z.; Michael, K., High-speed confocal fluorescence imaging with a novel line scanning microscope. *J. Biomed. Opt.* **2006,***11*, 064011.

(8) Cheezum, M. K.; Walker, W. F.; Guilford, W. H., Quantitative comparison of algorithms for tracking single fluorescent particles. *Biophys. J.* **2001,***81*, 2378-2388.

(9) Kubitscheck, U.; Kückmann, O.; Kues, T.; Peters, R., Imaging and tracking of single GFP molecules in solution. *Biophys. J.* **2000,***78*, 2170-2179.

(10) Einstein, A., On the movement of small particles suspended in stationary liquids required by the molecular-kinetic theory of heat. *Annalen der Physik* **1905,***17*, 549-560.

(11) Saxton, M. J.; Jacobson, K., Single-particle tracking: applications to membrane dynamics. *Annu. Rev. Biophys. Biomol. Struct.* **1997,***26*, 373-99.

(12) Martin, D. S.; Forstner, M. B.; Kas, J. A., Apparent subdiffusion inherent to single particle tracking. *Biophys. J.* **2002,***83*, 2109-17.

(13) Saxton, M. J., A biological interpretation of transient anomalous subdiffusion. II. Reaction kinetics. *Biophys. J.* **2008,***94*, 760-71.

(14) Suzuki, K.; Ritchie, K.; Kajikawa, E.; Fujiwara, T.; Kusumi, A., Rapid hop diffusion of a G-protein-coupled receptor in the plasma membrane as revealed by single-molecule techniques. *Biophys. J.* **2005,***88*, 3659-3680.

(15) Destainville, N.; Salomé, L., Quantification and correction of systematic errors due to detector time-averaging in single-molecule tracking experiments. *Biophys. J.* **2006,***90*, L17-L19.

(16) Ehrensperger, M.-V.; Hanus, C.; Vannier, C.; Triller, A.; Dahan, M., Multiple association states between glycine receptors and gephyrin identified by SPT analysis. *Biophys. J.* **2007,***92*, 3706-3718.

(17) Crocker, J. C.; Grier, D. G., Methods of digital video microscopy for colloidal studies. *J. Colloid Interface Sci.* **1996,***179*, 298-310.

(18) Jaqaman, K.; Loerke, D.; Mettlen, M.; Kuwata, H.; Grinstein, S.; Schmid, S. L.; Danuser, G., Robust single-particle tracking in live-cell time-lapse sequences. *Nat. Methods* **2008,***5*, 695-702.

(19) Smith, C. S.; Joseph, N.; Rieger, B.; Lidke, K. A., Fast, single-molecule localization that achieves theoretically minimum uncertainty. *Nat. Methods* **2010,***7*, 373-375.
(20) Ram, S.; Prabhat, P.; Chao, J.; Sally Ward, E.; Ober, R. J., High accuracy 3D quantum dot tracking with multifocal plane microscopy for the study of fast intracellular dynamics in live cells. *Biophys. J.* **2008,***95*, 6025-6043.
(21) Sbalzarini, I. F.; Koumoutsakos, P., Feature point tracking and trajectory analysis for video imaging in cell biology. *J. Struct. Biol.* **2005,***151*, 182-95.

The chapter 3 was originally published by ACS (Chang, J.C.& Rosenthal, S.J. (2012) Visualization of lipid raft membrane compartmentalization in living RN46A neuronal cells using single quantum dot tracking. ACS Chemical Neuroscience, 3 (10), 737–743). Permission is granted for the author's request for the dissertation use and for the benefit of the author's institution.

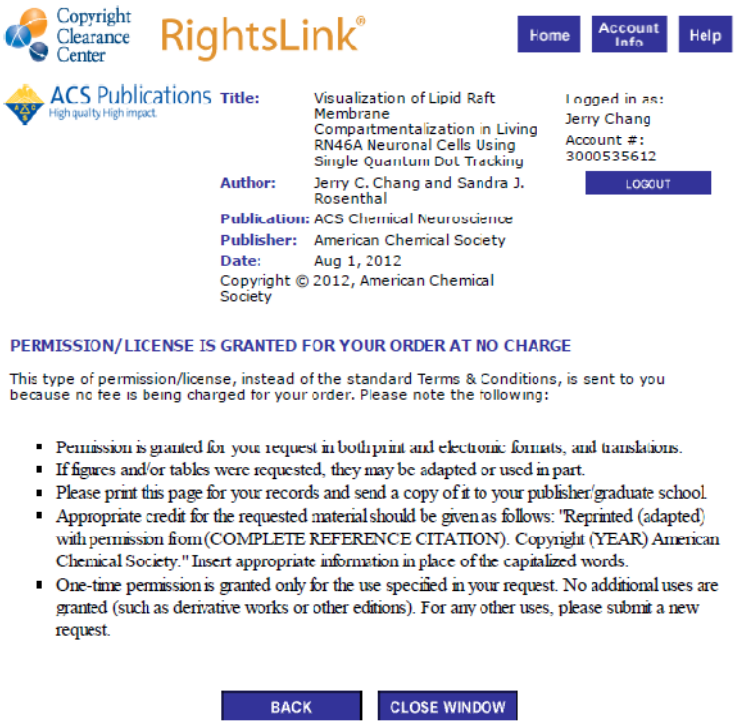

All other uses, reproduction and distribution, including without limitation commercial reprints, selling or licensing copies or access, or posting on open internet sites, your personal or institution's website or repository, without permission from the publisher are prohibited.

CHAPTER 3

PROBING MEMBRANE DYNAMICS OF LIPID RAFTS WITH SINGLE-QUANTUM DOT IMAGING

3.1 Introduction

Cholesterol-enriched membrane microdomains, known as lipid rafts, have been proposed to participate in cellular signal transduction by providing the microenvironment necessary for complex protein-protein interactions.[1] Early evidence based on the simplified membrane models showed that the presence of rigid cholesterol in the membrane essentially acts as glue, which packs the sphingolipids and unsaturated phospholipids closely together to form a highly directional, organized, and detergent-resistant state.[1] These specialized membrane domains were found abundantly and contained sets of associated proteins, especially the glycosyl-phosphatidylinositol (GPI)-anchored proteins, and were hypothesized to facilitate the regulation of membrane proteins through establishing boundaries between the raft and fluid compartments in the plasma membrane.[1, 2] The roles of lipid rafts in neuronal signaling have received increased attention in recent years.[3] However, studies on how lipid rafts participate in neuronal signaling still mostly rely on biochemical methods, such as using detergents to isolate the insoluble membrane fraction,[4] which lack dynamic information to help decipher the roles of lipid rafts in membrane compartmentalization.

In this chapter, single QDot tracking was adapted to investigate the membrane dynamics of lipid raft constituent ganglioside GM1 in the living RN46A neuronal cells. Importantly, our data point to a long-term stability of lipid rafts, as single QDot-labeled GM1 complexes show lateral confinement persisting on the order of tens of seconds.

3.2 Material and Methods

3.2.1 Single QDot Labeling of Ganglioside GM1 in RN46A cells

The immortalized serotonergic neural cell line, RN46A, was provided by Dr. Whittemore (University of Miami School of Medicine).[5] RN46A cells were cultured in DMEM/F12 (1:1; Life Technologies, Grand Island, NY) supplemented with 10% FBS and incubated in a humidified atmosphere with 5% CO_2 at 37°C. For experiments involving the labeling of ganglioside GM1 in the plasma membrane, RN46A cells were first incubated with 200 nM biotinylated CTxB (CTxB:biotin molar ratio ≈ 1:1 to avoid cross-linking, Sigma, St. Louis, MO) for 30 min prior to a 5 min 0.5 nM SAv-QDot (Life Technologies, Grand Island, NY) incubation. Importantly, ganglioside GM1-CTxB association has been shown to elicit endocytosis.[6] To avoid endocytosis and to achieve successful assessments in membrane dynamics, all optical live-cell time-lapse image series were taken immediately after QDot labeling.

3.2.2 Microscopy

Confocal images were obtained on a Zeiss LSM 5 Live confocal system (Carl Zeiss Jena GmbH, Jena, Germany) and viewed with a Zeiss 63×/1.4 NA oil immersion objective lens. Excitation was provided by a 488 nm 100-milliwatt diode laser. Single QDot emission was collected using a bandpass 610/20 mm filter (for QDot 605) or a long pass 650 mm filter (for QDot 655). Each sequence of time-lapse images was acquired at 10 frames per second for 30 -60 seconds with scan format of 512×128 pixels. All live-cell imaging were performed at 37 °C. Analysis of raw data images were processed using Zeiss LSM Image Examiner.

3.2.3 Subpixel Localization and Trajectory Generation

To calculate a subpixel estimate of single QDot position, the single QDot intensity distribution (Fig. 1C) was fitted with a 2D Gaussian function:[7]

$$I_{xy} = A_0 + A \cdot e^{-\frac{(x-x_0)^2+(y-y_0)^2}{w^2}} \quad [1]$$

, where I_{xy} is the intensity of the pixel, x_0 and y_0 is the designated local maximum coordinates of the Gaussian, A is the amplitude of the signal with local background A_0, and w is the width of the Gaussian curve. Note that the coordinate (x_0, y_0) acquired by 2D Gaussian fit is not a true position but only an estimate. The accuracy is dependent upon the respective signal-to-noise ratio (*SNR*), which is defined as:

$$SNR = \frac{I_0}{\sqrt{\sigma_{bg}^2 + \sigma_{I_0}^2}} \quad [2]$$

, where I_0 is the maximum signal intensity above background, σ_{bg}^2 is the variance of the background intensity values, and $\sigma_{I_0}^2$ is the true variance of the maximum signal intensity above the background. Since w width is approximately equal to the wide-field diffraction limit (for visible light is about 250 nm), the uncertainty of the fitted coordinate ($\Delta\sigma$) is approximately given by:

$$\Delta\sigma \approx \frac{250}{SNR} \text{ (nm)} \quad [3]$$

which is ±10-15 nm in our case (3 independent experiments, n = 873). In addition, QDot blinking was used to assure single-molecule events. For trajectory generation, raw data files were extracted to generate stacks of individual 16-bit TIF images and then processed with Matlab (the MathWorks, Inc., Natick, MA) routines originally developed by Jaqaman K. and colleagues.[8]

3.2.4 Instantaneous Velocity

The distribution of single step displacement over a time increment (100 ms in our case) was carried out to calculate the instantaneous velocity. For temporary lateral confinement of a diffusing protein due to local environmental constraints such as interaction with lipid rafts or cytoskeletal corrals, the motion pattern can be best described as anomalous subdiffusion.[9] The statistical distribution of instantaneous velocities is thus close to a Lévy function instead of a Gaussian function, which is given by:

$$f(x) = \left[\pi \cdot r \cdot \left(1 + \frac{x - x_0}{r} \right)^2 \right]^{-1} \quad [4]$$

, where x_0 is the location parameter (the best fit instantaneous movement) and *r* represents the interquartile range (the half-width at half-maximum) of the fitted step distance, meaning the statistical dispersion of the probability distribution. For practical applications, the Lévy probability distribution function can be simplified as a truncated Cauchy distribution:

$$f(x) = \left[b \cdot \left(1 + \frac{x - x_0}{a} \right)^2 \right]^{-1} \quad [5]$$

, where *a* and*b* are only treated as fit coefficients in the defined function, and the goodness of the fit is judged by the R^2 value. In all of our analyses, the R^2 values of the fit of instantaneous velocity are higher than 95 %, indicating high reliability of our fits.

3.2.5 Diffusion Coefficients and Membrane Confinement

After exporting trajectory coordinates, mean-square displacement (MSD) values for individual trajectories were calculated according to the formula listed below:[10]

$$MSD(n\Delta t) = (N - 1 - n)^{-1} \sum_{j=1}^{N-1-n} \left\{ [(x(j\Delta t + n\Delta t) - x(j\Delta t)]^2 + [(y(j\Delta t + n\Delta t) - y(j\Delta t)]^2 \right\} \quad [6]$$

, where $[x(j\Delta t+ n\Delta t)$, $y(j\Delta t+ n\Delta t)]$ are the position of the QDot starting at position $[x(j\Delta t)$, $y(j\Delta t)]$, Δt is the time resolution, N is total number of frames, $n\Delta t$ is the time interval over which the MSD is calculated. To achieve statistical significance, single QDot trajectories without a minimum of 100 time steps were discarded.

In a two-dimensional Brownian motion, also known asrandom walk, the MSD over time is linear. The standard method to calculate the diffusion coefficient D is to perform a linear fit of MSD over time since the MSD is given by:

$$\mathrm{MSD}(t) = 4D\Delta t \qquad [7]$$

, where $\Delta t$is the time-resolution.

For the case of confined diffusion, which is evident by a negative curvature on the MSD over time plot, we followed the method described by Daumas et al.[10] The MSD is given by

$$MSD(t) = 2L^2(1 - \mathrm{e}^{-t/\tau}) + 4D_M\tau \text{ , and } \tau = \frac{L^2}{2D_\mu} \qquad [8]$$

, where a short-term diffusion coefficient,D_μ, isused to describe a rapid, “microscopic” diffusion behavior, and a long-term diffusion coefficient,D_M, indicatesaslower, “macroscopic” movement. L is the characteristic size of the short-termconfiningdomain and $\tau$is the so-called “equilibration” or “relaxation” time on the short time-scales.

3.3 Results

3.3.1 Instrument response and single-molecule sensitivity inspection

To ensure spatial and temporal resolution of our imaging approach, carboxyl functionalized, amphiphilic poly(acrylic acid) polymer-coated QDots (AMP QDots) were first spin-casted onto a cover glass and then observed on a Zeiss line-scanning confocal microscope system (Fig. 3.1).[11] Time-lapse fluorescence imaging of QDots was used to assess temporal and spatial characteristics of single QDot fluorescence (Fig. 3.2 upper panel). In addition, Qdot blinkingwas demonstratedas a single-molecule criterion (Fig. 3.2 lower left panel).[12, 13] Furthermore, the intensity distribution coming from a single QDot shows a diffraction-limited pattern (Fig. 3.2 ROI 3, lower right panel), representing another signature of single-molecule.[14] Further analysis using 2D Gaussian fit of the intensity distribution provides an estimate of the localization of a single QDot with accuracy measured at ±10~15 nm (see section 2.2).[7]

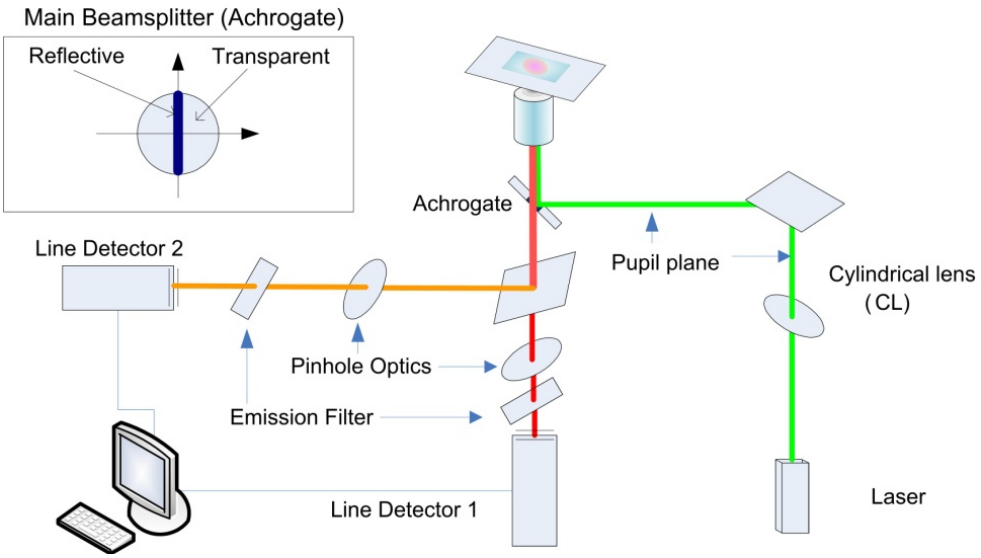

Figure 3.1 Schematic of the optical setup of the line-scanning confocal microscope. Through the use of the cylindrical lens (CL), single point laser light is recreated to form a pupil plane. This line excitation is then directed to Achrogate (left inset) for sample excitation. Fluorescent signal which passes the Achrogate and pinhole optics is collected onto the line detectors.

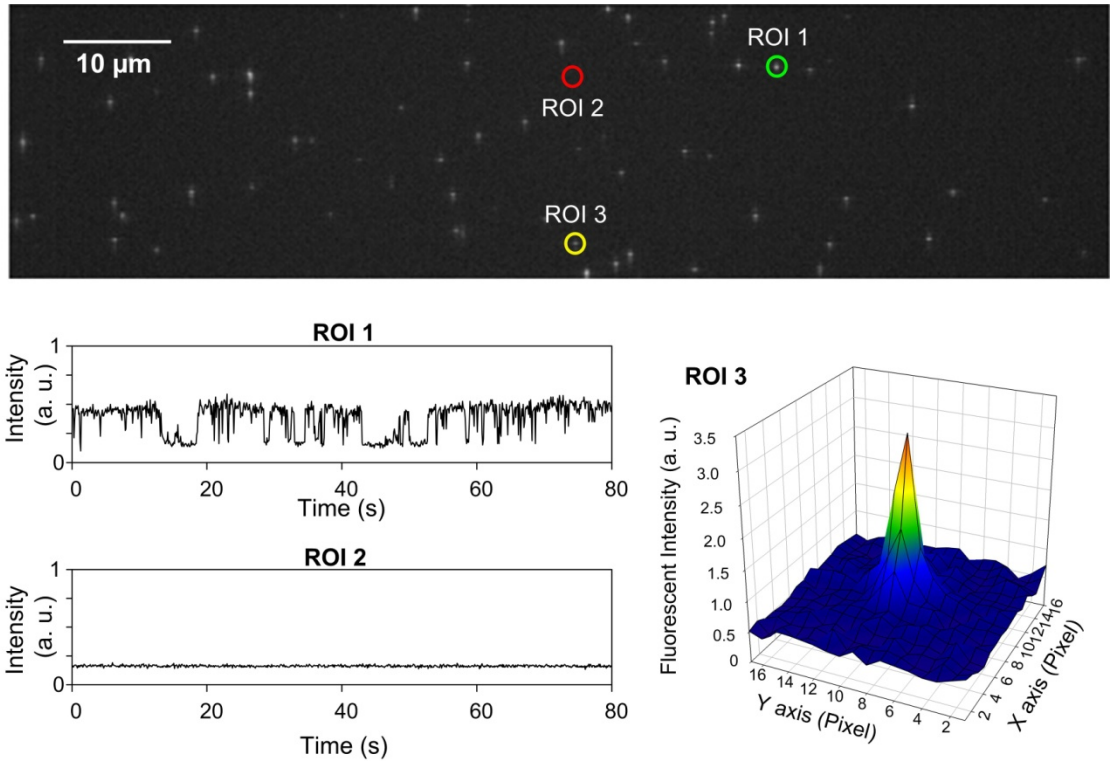

Figure 3.2 Visualization of single QDots on a glass support. Upper panel provides a single frame from time lapse imaging of QDots taken with the high-speed line scanning confocal microscope at 10 Hz scan rate. Spin-casting ITK carboxyl-modified 605 nm QDots were immobilized on the glass coverslip bottomed MetTek dish for imaging. Two randomly selected blinking QDots (ROI 1, ROI 3) and a randomly selected background region (ROI 2) are indicated by circles. Scale bar = 10 µm. Lower left panels provide time-dependent intensity traces of the selected ROIs. Fluorescence intensity of ROI 1 QDot is constant during the "on" state and shifts to a similar intensity level as background indicated by the intensity time trace of ROI 2. A 3D intensity plot of QDot (ROI 3) was used to provide an estimate of the spatial resolution achieved with our imaging paradigm (central position uncertainty = ±10~15 nm, one pixel = 200 nm).

3.3.2 Basal membrane diffusion in living RN46A Cells

Several previous studies have indicated that water-soluble AMP QDots, which were generated from passivating the hydrophobic QDots with amphiphilic polymers, nonspecifically interact with the cellular membrane via hydrophobic interaction.[15, 16] This artifact of QDot biological staining turns out to be a successful molecular probe for studying the lateral mobility of the neuronal membrane. To ensure the spatial separation of single QDots in regions greater than the diffraction-limited distance for single molecule tracking, AMP QDots are used at an extremely low concentration (< 10 picomoles) in RN46A cells. Fig. 3.3 shows typical trajectories of AMP QDots attached on the surface of a living RN46A cells via hydrophobic interaction. Although various moving patterns can be observed, the majority of trajectories exhibit a distinct, Brownian-type motion mode. We must also note that neither distinct orientation nor clear membrane compartmentalization is predominantly displayed (Fig. 3.4), suggesting that no particular force governs the motion of AMP QDots in the plasma membrane (i.e. active movements). To gain a quantitative assessment of the velocity of the diffused QDots, we analyzed the distribution of instantaneous velocity (single step displacement over a time increment τ = 100 ms, see methods). As shown in Fig.3.3B, single AMP QDots display a bimodal distribution of instantaneous velocity with a majority falling in the fast population (ν_{slow} = 0.51 ± 0.03 μm/s, 11.6%; ν_{fast} =1.46 ± 0.04 μm/s, 88.4%).

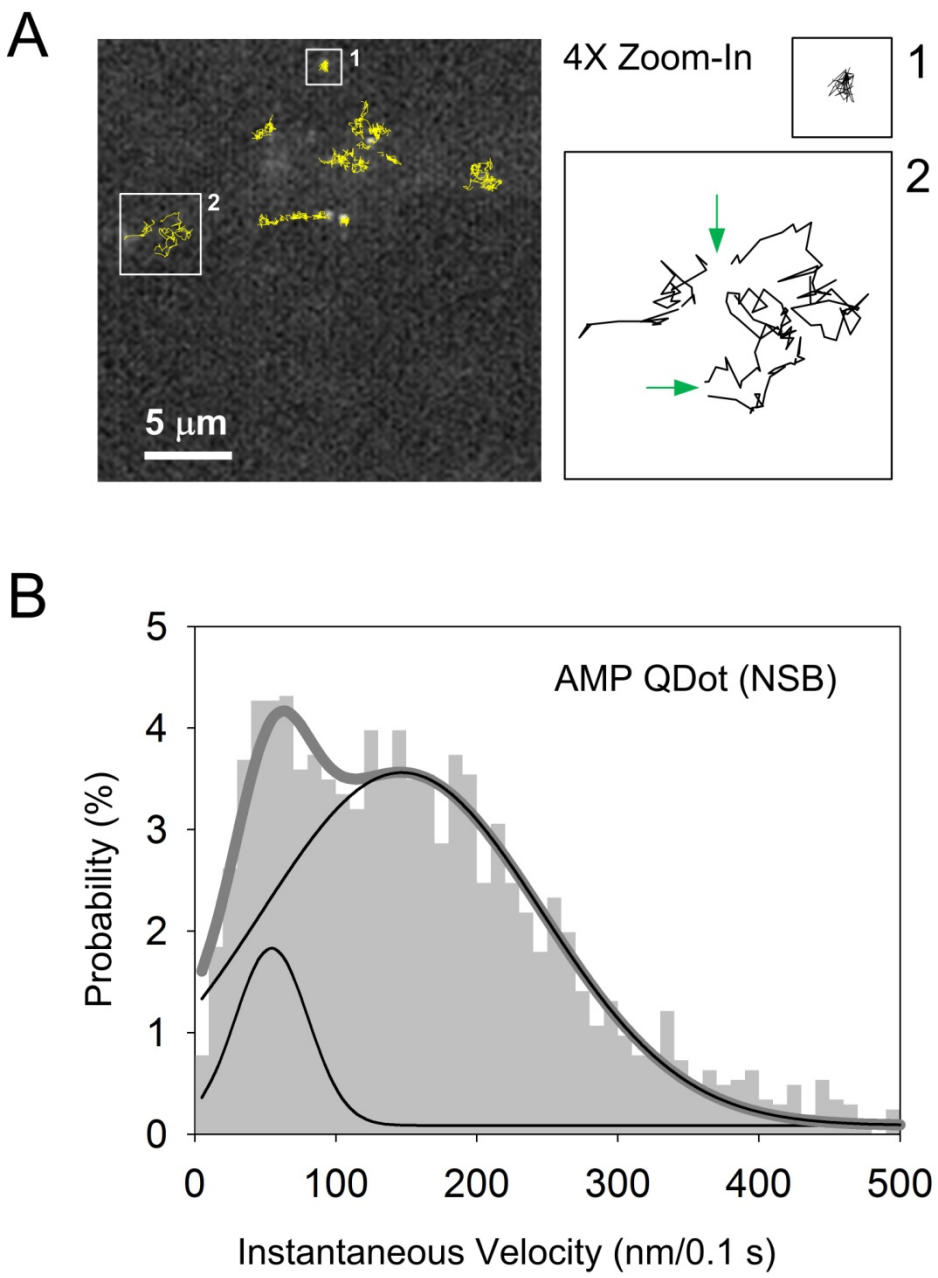

Figure 3.3 Trajectories and instantaneous velocity of AMP QDots non-specifically bound to the plasma membrane of living RN46A cells. (A) A single frame from a time-lapse recording of single AMP QDots diffuse in the native membrane of a RN46A cell that was superimposed upon the trajectories throughout the recording. Trajectories on the right are 4X zoom-in of the selected ones on the left, and green arrows note the blinking events. Although the motion of AMP QDots can be generally categorized as being one of two types — confined (as indicated in box 1) or non-confined (as indicated in box 2), trajectories shown a non-confined pattern are dominantly displayed. (B) The instantaneous velocity plot of AMP QDots is shown for the data from 4122 steps. The data points are well-fitted to a bimodal distribution where a majority falling in the fast population (ν_{slow} = 0.51 ± 0.03 μm/s, 11.6%; ν_{fast} =1.46 ± 0.04 μm/s, 88.4%).

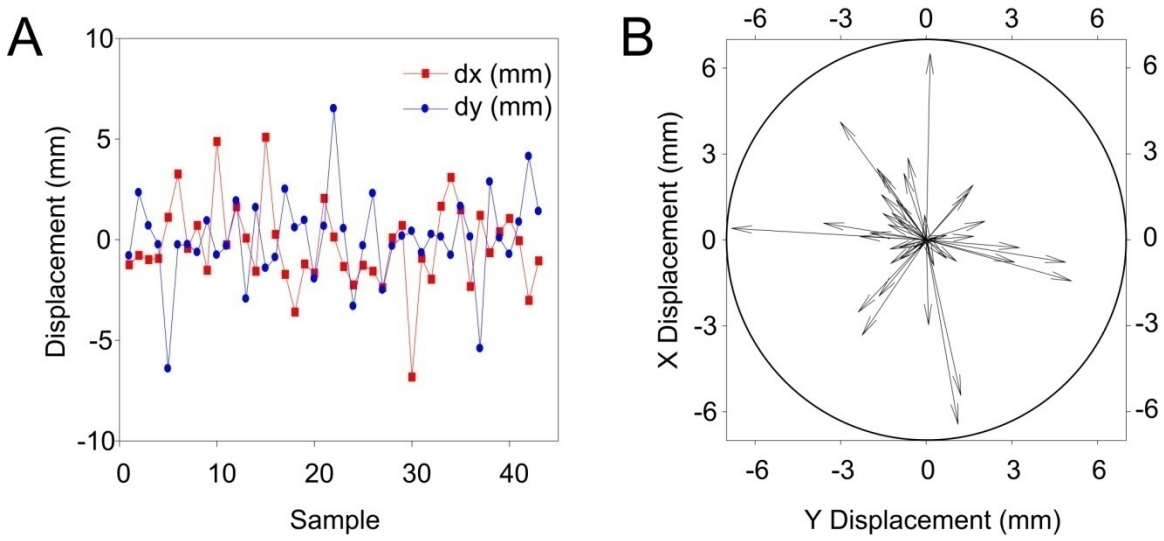

Figure 3.4 Membrane diffusion of AMP QDots shows a non-directional random walk. (A) Magnitude of x- and y- directional displacements of all collected trajectories over the same time-period recording (30 sec, n=43). (B) Vector representation of all collected trajectories over the same time-period recordings. All starting coordinates are normalized to the central position.

3.3.3 Single quantum dot tracking of lipid raft constituent ganglioside GM1

To perform single QDot tracking of lipid raft constituent ganglioside GM1, a two-step labeling approach was implemented in which RN46A cells were initially incubated with biotinylated cholera toxin B subunit (CTxB),[6, 17] a protein that binds specifically to ganglioside GM1, followed by the incubation with streptavidin-conjugated QDots (SA-QDots). The single molecule property of the QDot conjugates was further evaluated via blinking behavior inspection (Fig. 3.5A). Shown in Figure 3.5B are typical trajectories of single QDot-GM1 complexes in the membrane of RN46A cells, where apparently only the confined motion pattern can be found. The analysis of the distribution of instantaneous velocity was then carried out to correlate the confined movements (Fig. 3.5C). As expected, the distribution is well-fitted with a single population and the fitted instantaneous velocity was estimated as $\nu = 0.88 \pm 0.03$ μm/s.

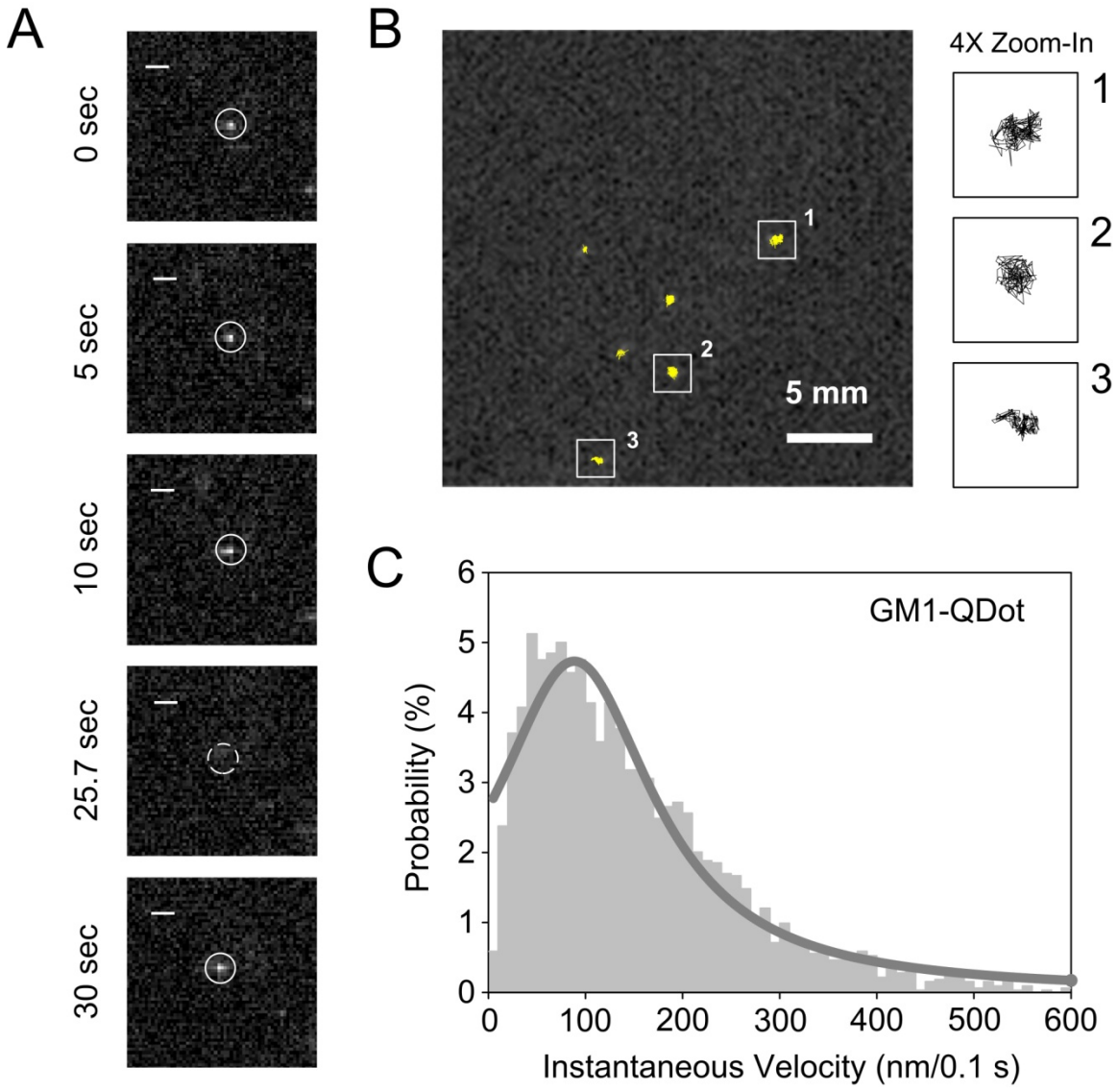

Figure 3.5 Trajectories and instantaneous velocity of single QDot-conjugated GM1 complexes in the plasma membrane of living RN46A cells. (A) Representative snapshots from a time-lapse series of single QDot-GM1 complexes via the bridge of CTxB. The white circles indicate the QDot being followed and the dash circle (t = 25.7 sec) notes a blinking event (scalebar = 1.5 μm). (B) A single frame from a time-lapse recording of single QDots bound to GM1 in the native membrane of a RN46A cell that was superimposed upon the trajectories throughout the recording. Three representative trajectories (right boxes) show a confined motion pattern and their 4X zoom-in (left boxes) are displayed. (B) The instantaneous velocity plot of AMP QDots is shown for the data from 3240 steps. The data points are well-fitted to a single distribution (ν = 0.88 ± 0.03 μm/s).

The dependence of the mean square displacement (MSD) on the time interval was then used to dissect the lateral diffusion and membrane confinements (Fig. 3.6). As seen in Fig. 4A, the diffusion of AMP QDots in the membrane appears to be Brownian since a linear correlation of MSD with time can be observed. From the linear fit, we obtained a diffusion coefficient D = 0.393 ± 0.002 $\mu m^2/s$ (mean ± SEM), similar to the reported diffusion coefficients of lipid probes in the native membrane on the order of 0.1~1 $\mu m^2/s$.[18] In comparison, the MSD versus time plot of single QDot-labeled ganglioside GM1 shows a curvature, indicating restricted diffusion. Consequently, a confined diffusion mode was used to calculate the diffusion coefficient and the characteristic size of the short-termconfiningdomain$L$(seesection 2.3), yielding the values of D = (7.87 ± 0.04)×$10^{-2}\mu m^2/s$ and L= 198 ± 33 nm. The diffusion distributions of AMP QDots and QDot-labeled GM1 were further evaluated using a cumulative probability plot (Fig. 3.6). Although visual inspection only shows minimal overlap between the two cases, the diffusion coefficients of QDot-labeled GM1 are mostly restricted to the slow timescales (10^{-2}~$10^{-3}\mu m^2/s$), whereas AMP QDots in the membrane diffuse significantly faster (*p* value <0.05, Shapiro–Wilk test) and exhibit a large range of diffusion rates.

The diffusion dynamics of QDot-labeled GM1 molecules in comparison to AMP Qdots suggests that lipid rafts in cell membrane produce a strong stabilization effect. We therefore sought to take advantage of the inherent photostability of QDots to follow GM1 movements over longer time-scales (30-60 seconds). Shown in Figure3.7 is a spatiotemporal 3D graph of QDot-labeled GM1 complexes in the native membrane of RN46A cells, where the majority of individual QDot-GM1 complexes exhibit movements less than 1 μm in distance throughout the entire recording. In comparison, ~80% of the AMP QDots display overall movement larger than 1 μm (Fig. 3.4B, *n* = 43).

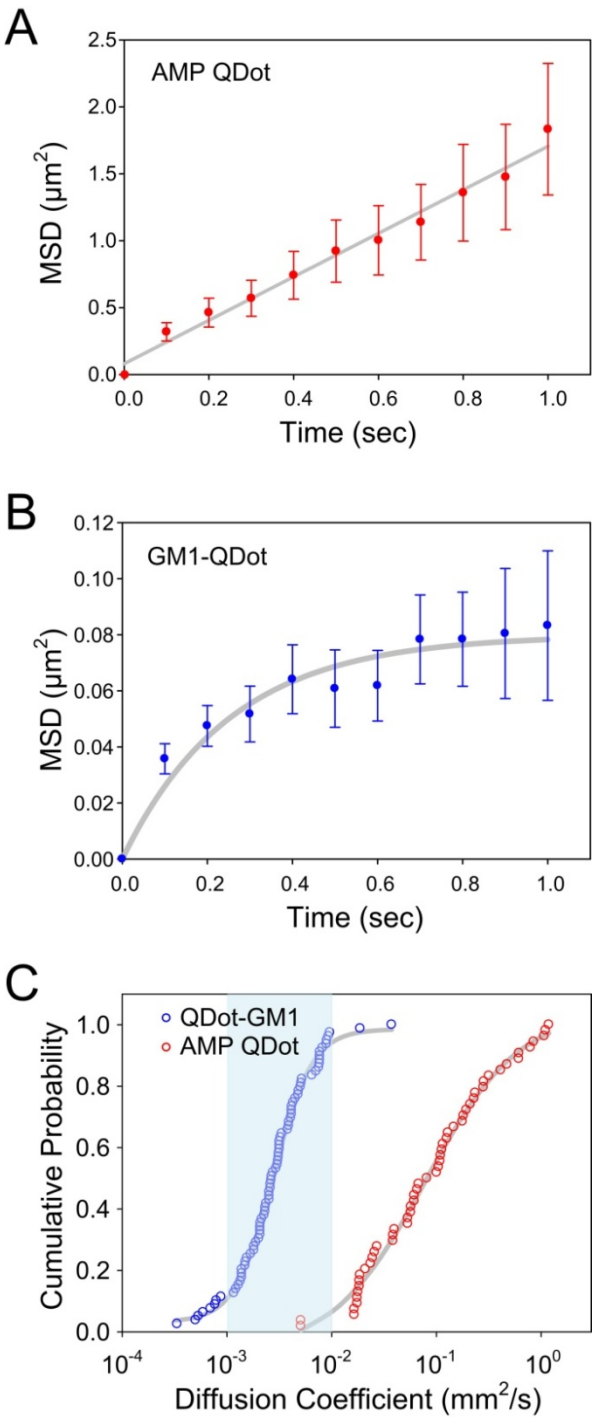

Figure 3.6 Comparison of diffusion behavior of single AMP QDots and QDot-labeled GM1 complexes in the RN46A cells. (A) Averaged MSD as a function of time for single AMP QDots. Solid gray line is computed based on linear regression, indicating a simple diffusion. (B) Averaged MSD as a function of time for single AMP QDot-GM1 complexes. Solid gray curve is the best fit based on an exponential function (see methods), indicating a confined diffusion. (C) Cumulative distribution of the diffusion coefficients. Blue shadow which indicates $10^{-3}<D<10^{-2}$ is used for visual comparison.

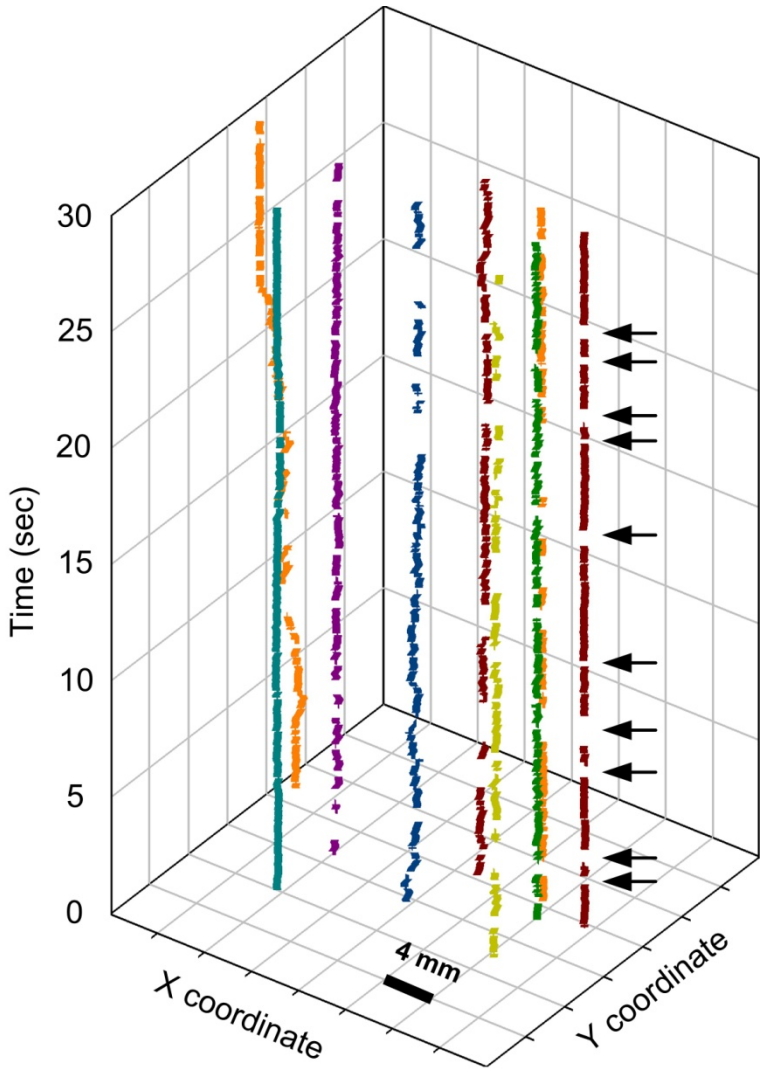

Figure 3.7 Spatiotemporal 3D representation of movement of the single QDot-GM1 complexes in living RN46A cells. Fluorescent intermittency ("blinking") of a single QDot on an example trajectory is noted by a black arrow.

3.4 Summary

The diffusion coefficient,D, dwelling time,τ, and the putative confinement domain,L, of lipid rafts have been previously estimated by various approaches. The study presented herein was designed to directly follow the motion of a lipid raft constituent GM1, while the native membrane integrity was preserved. Using a single QDot labeling approach, we reveal GM1 comprised lipid rafts slowly diffuse within a confinement zone, which has a diameter of ~200 nm. Further inspection of the long-term time-dependent trajectories (Fig. 5) features the persistent confinement of lipid rafts in RN46A cells (L = 200 nm, D = 7.8 × 10^{-2}μm^2/s, τ> 10 s). In comparison, Schütz et al. adopted liposome-facilitated delivery of a saturated acyl-chain fluorescent lipid probe (1,2-dimyristoyl-*sn*-glycero-3-phosphoethanolamine, DMPE-Cy5) for single-molecule tracking. In their analyses, lipid rafts were found to be localized in relatively larger partitioning domains along with faster diffusion rates and a long dwelling time in HSAM cells (L= 0.2 - 2 μm, D = 0.6-0.9 μm^2/s, τ~ 13 s).[19] Interestingly, a recent stimulated emission depletion (STED) microscopy study reported by Eggeling et al. showed that lipid raft-associated constituents, including the sphingolipids and GPI-anchored proteins, are transiently trapped in nanoscale domains for only tens of milliseconds with a relatively slower diffusion rate in the PtK2 cells (L< 20 nm,D = 2 ×10^{-2}μm^2/s, τ = 10 ~ 20 ms).[20] As lipid rafts are known to contain various components and participate in dynamic membrane trafficking and signaling, it is perhaps not surprising that differences in detecting approaches, experimental time-resolutions, targeted molecules, as well as cell models would have a substantial impact on the estimates of raft diffusion properties. Clearly, a systematic examination of various lipid raft constituents is required for a more general understanding of membrane dynamics of lipid rafts.

Presently how lipid rafts contribute to biological signaling is an open question. A closely related point of view is that, for a lipid raft to be able to act as a signaling platform, the lifetime of a lipid raft should be at least partially relevant to a biological signaling duration (i.e. the timescales over which biological signaling persists). Since protein signaling networks typically operate on timescales of seconds to minutes, the lifetime of lipid rafts are likely to exist on similar timescales, which is consistent with the findings reported in this study. In addition, if lipid rafts are membrane subdomains that facilitate the signaling of raft-associated proteins, proteins residing in the lipid rafts should share a similar confined diffusion mode as we observed in this research. In a recent study, Andrews *et al.* followed the motion of individual high affinity IgE receptors (FcεRI), a class of raft-dependent receptors, with monovalent antibody-conjugated QDots in living cells and identified confined diffusion with seconds of cross-linking in FcεRI signaling.[21] A similar confined diffusion mode was observed with single QDot labeled GPI anchored proteins,[22] α7 neuronal nicotinic acetylcholine receptors,[23] and serotonin transporters.[24] However, the question of whether lipid rafts dynamically govern protein signaling remains unanswered. Consequently, a multichannel single QDot tracking protocol for simultaneous multi-target analysis (i.e. one color of QDot labeling for raft constituent and another color of QDot labeling for the raft-associated protein) may hold high potential in the acquisition of information to address the above question.

As mentioned in the introduction, common attempts to perform real-time tracking of membrane constituents mostly rely on the use of organic fluorophores or micron to submicron-sized polymeric particles. The main advantage of organic fluorophores in real-time tracking is their small size ($\leq$ 1 nm). This property makes them particularly useful for tracking movements of individual receptors in distinct subcellular structures such as synapse or caveolae.[25] Up until now, the real bottleneck of dye-based single-

molecule microscopy is still the photostability of the organic fluorophores, which limits the tracking time to only a few seconds.[25, 26] In contrast, polymeric particles, owing to their superior strength in photostability, have been popularly used for following membrane dynamics since the 1990's.[27] However, the large size of the particles (> 100 nm), which inevitably leads to cross-linking of the labeling targets, call into question the diffusion characteristics measured.[28] So how can we address these shortcomings from both sides? The current best compromise is perhaps the use of photostableQDots for real-time tracking. Although the diameter of QDots compared to the organic fluorophores is still relatively large (10-20 nm) and the monovalent QDots are not commercially accessible, with appropriate adjustment in conjugation protocol (i. e. fine-tune the QDot/ligand molar ratio in conjugation conditions)[18, 29] single QDot tracking can be regarded as a single-molecule technique. Importantly, differences of QDot-conjugated and dye-conjugated approaches in measured diffusion coefficients are minimal,[18, 25, 30] indicating the applicability of QDots to substitute organic fluorophores for single-molecule tracking.

In conclusion, our single-QDot tracking study documents the diffusion properties of ganglioside GM1 in the plasma membrane of RN46A cells. The valuable information on membrane dynamics of lipid rafts as well as our straightforward, readily transferrable single QDot experimental protocol presented herein may form a basis for not just raft studies but also membrane protein research in living cells. It will be interesting to dissect the functional implications of the lateral confinement of lipid rafts in the neuronal membrane. In a preliminary treatment study, we observed a non-Brownian, actin cytoskeleton-dependent membrane dynamic in GM1 movements.[24] Further analysis of the connection between lipid rafts and cytoskeleton may yield useful insights into the compositional heterogeneity of lipid raft-associated signaling.[2]

3.5 References

(1) Munro, S., Lipid rafts: Elusive or illusive? *Cell* **2003,***115*, 377-388.

(2) Allen, J. A.; Halverson-Tamboli, R. A.; Rasenick, M. M., Lipid raft microdomains and neurotransmitter signalling. *Nat. Rev. Neurosci.* **2007,***8*, 128-40.

(3) Korade, Z.; Kenworthy, A. K., Lipid rafts, cholesterol, and the brain. *Neuropharmacology* **2008,***55*, 1265-73.

(4) Eckert, G. P., Manipulation of lipid rafts in neuronal cells. *Open Biol. J.* **2010,***3*, 32-38.

(5) White, L. A.; Eaton, M. J.; Castro, M. C.; Klose, K. J.; Globus, M. Y.; Shaw, G.; Whittemore, S. R., Distinct regulatory pathways control neurofilament expression and neurotransmitter synthesis in immortalized serotonergic neurons. *J. Neurosci.* **1994,***14*, 6744-6753.

(6) Orlandi, P. A.; Fishman, P. H., Filipin-dependent inhibition of cholera toxin: evidence for toxin internalization and activation through caveolae-like domains. *J Cell Biol* **1998,***141*, 905-15.

(7) Cheezum, M. K.; Walker, W. F.; Guilford, W. H., Quantitative comparison of algorithms for tracking single fluorescent particles. *Biophys. J.* **2001,***81*, 2378-2388.

(8) Jaqaman, K.; Loerke, D.; Mettlen, M.; Kuwata, H.; Grinstein, S.; Schmid, S. L.; Danuser, G., Robust single-particle tracking in live-cell time-lapse sequences. *Nat. Methods* **2008,***5*, 695-702.

(9) Martin, D. S.; Forstner, M. B.; Kas, J. A., Apparent subdiffusion inherent to single particle tracking. *Biophys. J.* **2002,***83*, 2109-17.

(10) Daumas, F.; Destainville, N.; Millot, C.; Lopez, A.; Dean, D.; Salome, L., Confined diffusion without fences of a g-protein-coupled receptor as revealed by single particle tracking. *Biophys. J.* **2003,***84*, 356-66.

(11) Ralf, W.; Bernhard, Z.; Michael, K., High-speed confocal fluorescence imaging with a novel line scanning microscope. *J. Biomed. Opt.* **2006,***11*, 064011.

(12) Nirmal, M.; Dabbousi, B. O.; Bawendi, M. G.; Macklin, J. J.; Trautman, J. K.; Harris, T. D.; Brus, L. E., Fluorescence intermittency in single cadmium selenide nanocrystals. *Nature* **1996,***383*, 802-804.

(13) Yao, J.; Larson, D. R.; Vishwasrao, H. D.; Zipfel, W. R.; Webb, W. W., Blinking and nonradiant dark fraction of water-soluble quantum dots in aqueous solution. *Proc. Natl. Acad. Sci. U.S.A.* **2005,***102*, 14284-14289.

(14) Schmidt, T.; Schutz, G. J.; Baumgartner, W.; Gruber, H. J.; Schindler, H., Imaging of single molecule diffusion. *Proc. Natl. Acad. Sci. U.S.A.* **1996,***93*, 2926-9.

(15) Bentzen, E. L.; Tomlinson, I. D.; Mason, J.; Gresch, P.; Warnement, M. R.; Wright, D.; Sanders-Bush, E.; Blakely, R.; Rosenthal, S. J., Surface modification to reduce nonspecific binding of quantum dots in live cell assays. *Bioconjug. Chem.* **2005,***16*, 1488-94.

(16) Warnement, M. R.; Tomlinson, I. D.; Chang, J. C.; Schreuder, M. A.; Luckabaugh, C. M.; Rosenthal, S. J., Controlling the Reactivity of Ampiphilic Quantum Dots in Biological Assays through Hydrophobic Assembly of Custom PEG Derivatives. *Bioconjug. Chem.* **2008,***19*, 1404-1413.

(17) Kenworthy, A. K.; Petranova, N.; Edidin, M., High-resolution FRET microscopy of cholera toxin B-subunit and GPI-anchored proteins in cell plasma membranes. *Mol. Biol. Cell* **2000,***11*, 1645-1655.

(18) Murcia, M. J.; Minner, D. E.; Mustata, G.-M.; Ritchie, K.; Naumann, C. A., Design of quantum dot-conjugated lipids for long-term, high-speed tracking experiments on cell surfaces. *J. Am. Chem. Soc.* **2008,***130*, 15054-15062.
(19) Schutz, G. J.; Kada, G.; Pastushenko, V. P.; Schindler, H., Properties of lipid microdomains in a muscle cell membrane visualized by single molecule microscopy. *EMBO J.* **2000,***19*, 892-901.
(20) Eggeling, C.; Ringemann, C.; Medda, R.; Schwarzmann, G.; Sandhoff, K.; Polyakova, S.; Belov, V. N.; Hein, B.; von Middendorff, C.; Schonle, A.; Hell, S. W., Direct observation of the nanoscale dynamics of membrane lipids in a living cell. *Nature* **2009,***457*, 1159-U121.
(21) Andrews, N. L.; Lidke, K. A.; Pfeiffer, J. R.; Burns, A. R.; Wilson, B. S.; Oliver, J. M.; Lidke, D. S., Actin restricts FcepsilonRI diffusion and facilitates antigen-induced receptor immobilization. *Nat. Cell Biol.* **2008,***10*, 955-63.
(22) Pinaud, F.; Michalet, X.; Iyer, G.; Margeat, E.; Moore, H.-P.; Weiss, S., Dynamic partitioning of a glycosyl-phosphatidylinositol-anchored protein in glycosphingolipid-rich microdomains imaged by single-quantum dot tracking. *Traffic* **2009,***10*, 691-712.
(23) Burli, T.; Baer, K.; Ewers, H.; Sidler, C.; Fuhrer, C.; Fritschy, J. M., Single particle tracking of alpha7 nicotinic AChR in hippocampal neurons reveals regulated confinement at glutamatergic and GABAergic perisynaptic sites. *PLoS One* **2010,***5*, e11507.
(24) Chang, J. C.; Tomlinson, I. D.; Warnement, M. R.; Ustione, A.; Carneiro, A. M. D.; Piston, D. W.; Blakely, R. D.; Rosenthal, S. J., Single molecule analysis of serotonin transporter regulation using antagonist-conjugated quantum dots reveals restricted, p38 MAPK-dependent mobilization underlying uptake activation. *J. Neurosci.* **2012,***32*, 8919-8929.
(25) Groc, L.; Lafourcade, M.; Heine, M.; Renner, M.; Racine, V.; Sibarita, J. B.; Lounis, B.; Choquet, D.; Cognet, L., Surface trafficking of neurotransmitter receptor: comparison between single-molecule/quantum dot strategies. *J. Neurosci.* **2007,***27*, 12433-7.
(26) Vrljic, M.; Nishimura, S. Y.; Moerner, W. E., Strengths and weaknesses of single-molecule tracking. *Biophysical society discussions speaker paper* **2004,***13*, SP13 A-J.
(27) Saxton, M. J.; Jacobson, K., Single-particle tracking: applications to membrane dynamics. *Annu. Rev. Biophys. Biomol. Struct.* **1997,***26*, 373-99.
(28) Wieser, S.; Schutz, G. J., Tracking single molecules in the live cell plasma membrane-Do's and Don't's. *Methods* **2008,***46*, 131-40.
(29) Lidke, D. S.; Nagy, P.; Heintzmann, R.; Arndt-Jovin, D. J.; Post, J. N.; Grecco, H. E.; Jares-Erijman, E. A.; Jovin, T. M., Quantum dot ligands provide new insights into erbB/HER receptor-mediated signal transduction. *Nat. Biotechnol.* **2004,***22*, 198-203.
(30) Dahan, M.; Levi, S.; Luccardini, C.; Rostaing, P.; Riveau, B.; Triller, A., Diffusion dynamics of glycine receptors revealed by single-quantum dot tracking. *Science* **2003,***302*, 442-445.

The chapter 4 was originally published in *the Journal of Neuroscience* (Chang, J.C., Tomlinson, I.D., Warnement, M.R., Ustione, A., Carneiro, A.M.D., Piston, D.W., Blakely, R.D. & Rosenthal, S.J. (2012) Single molecule analysis of serotonin transporter regulation using antagonist-conjugated quantum dots reveals restricted, p38 MAPK-dependent mobilization underlying uptake activation. *Journal of Neuroscience*, 32, 8919-8929). Permission is granted for the author's request for the dissertation use and for the benefit of the author's institution.

From: jn permissions <jnpermissions@sfn.org>
To: 'Jerry Chang' <jerry@femto.cas.vanderbilt.edu>
Date: 06/13/12 1:27 PM
Subject: RE: Permission Request (manuscript # 2087)

Dear Jerry Chang,
Permission is granted to reproduce the requested material listed below with NO fee in print and electronic format for use in your doctoral thesis/dissertation.

Please contact me if you have any questions or if you need another form of permission.
Respectfully,

SfN Central Office

Title: Single Molecule Analysis of Serotonin Transporter Regulation Using Antagonist-Conjugated Quantum Dots Reveals Restricted, p38 MAPK-Dependent Mobilization Underlying Uptake Activation
Author: Jerry C. Chang et al.
Publication: The Journal of Neuroscience
Date: June 27, 2012
Copyright © 2012 by the Society for Neuroscience
DOI: 10.1523/JNEUROSCI.0048-12.2012

All other uses, reproduction and distribution, including without limitation commercial reprints, selling or licensing copies or access, or posting on open internet sites, your personal or institution's website or repository, without permission from the publisher are prohibited.

CHAPTER 4

SINGLE MOLECULE ANALYSIS OF SEROTONIN TRANSPORTER REGULATION USING ANTAGONIST-CONJUGATED QUANTUM DOTS

4.1 Introduction

In the brain and periphery, signaling by the neurotransmitter serotonin (5-hydroxytryptamine, 5-HT) relies on efficient, transporter-mediated reuptake to terminate synaptic signals. The presynaptic, antidepressant-sensitive 5-HT transporter (SERT, 5HTT), encoded in humans by the *SLC6A4* gene, is primarily responsible for 5-HT clearance and has been the focus of much attention as a determinant of neuropsychiatric disease risk.[1] Both transcriptional and post-translational mechanisms exert powerful control over SERT-mediated 5-HT transport, though many aspects of SERT regulation are as yet ill-defined.[2] SERT is known to undergo both regulated membrane trafficking as well as transitions between low and high activity states, with multiple, intracellular signaling pathways involved, including pathways linked to the activation of PKC, PKG and p38 MAPK.[2, 3] These stimuli may act directly, for example via transporter phosphorylation.[3, 4] Additionally, biochemical studies indicate that SERT exhibits dynamic associations with cytoskeletal binding proteins.[2, 5] As altered posttranslational regulation of SERT by these mechanisms is a feature of coding variants identified in subjects with obsessive-compulsive disorder (OCD) and autism,[6-9] a more detailed mechanism that supports regulation of the wildtype transporter is needed.

Biochemical studies that assess the distribution of large populations of molecules indicate that SERT proteins and related transporters localize to cytoskeleton-associated, cholesterol-rich membrane microdomains, compartments that may also dictate aspects of transporter regulation.[5, 10, 11] Such studies, however, do not provide sufficient

resolution to monitor the behavior of individual molecules that, collectively, contribute to the macroscopic features of transporter behavior. Ion channels can be monitored at the single molecule level by patch clamp recording techniques. Generally, cell surface transporters and receptors cannot be studied with this approach due to low or absent electrogenicity needed for patch-clamp recordings. Antibody-based optical methods have been utilized to identify a few single membrane proteins,[12, 13] however, many proteins lack suitable extracellular domains that can be targeted by antibodies without functional disruption. Taking advantage of their remarkable brightness and extraordinary photostability properties, quantum dots (QDots) are increasingly being used for the detection of biomolecules in living cells.[14-16] Compared to conventional ensemble biochemical methods, single-QDot tracking allows for a detailed biophysical characterization of protein movements that can provide a real-time report of the unitary events associated with regulation.[13] In this report, we implement a ligand-conjugated QDot approach[17] to monitor single QDot-labeled SERT proteins in living, neuronal cells, providing evidence that actin-based mechanisms dictate p38 MAPK-dependent transporter activation. More generally, our successful use of QDots targeted to cell surface proteins by high-affinity ligands establishes a paradigm that should be of broad utility in defining the single molecule behavior of drug targets.

4.2 Materials and Methods

4.2.1 Cell Culture, Treatments, and SERT Activity Assay

The immortalized serotonergic neural cell line, RN46A,[18] was provided by Dr. Whittemore (University of Miami School of Medicine). Cells were cultured in DMEM/F12 (1:1; Gibco) supplemented with 10% FBS and incubated in a humidified atmosphere with 5% CO_2 at 37°C. Although RN46A cells endogenously express functional SERT proteins, an increase in SERT expression can be obtained by incubating cells in DMEM/F12 (1:1) containing a 1% B27 supplement (Invitrogen) plus 1 μM 5-HT for 24 hours prior to single molecule labeling experiments.

For experiments involving peptide treatments, RN46A cells were preincubated with a synthetic peptide at 10 μM for 30 min (37 °C; 5% CO_2) prior to the assay. Synthetic peptides (>95% purity) used in the study were purchased from Thermo Scientific, and carried the sequences as followed:

C-SERT: YGRKKRRQRRR(TAT)-ETPTEIPCGDIRMNAV

U-SERT: YGRKKRRQRRR(TAT)-PGTFKERIIKSITPETPREI

SERT activity in living RN46A cells was examined by using IDT307, a fluorescent neurotransmitter substrate.[19] IDT307 is nonfluorescent in solution but fluoresces as the substrate is accumulated, affording real time kinetic evaluation of SERT activity. A straightforward assay to verify successful SERT expression in RN46A cells simply involved the addition of IDT307 directly to the culture media at a final concentration of 5 μM and incubating at 37 °C for 30 minutes. Time-lapse fluorescent images were then acquired immediately after IDT307 addition, and successful transporter expression was evident by an observable increase in intracellular fluorescence. No additional rinsing was required since IDT307 is only fluorescent in intracellular environments, and any excess of IDT307 in solution did not result in any observable fluorescent background.

4.2.2 Labeling RN46A Cells with Ligand-Conjugated Quantum Dots

For single QDot labeling of SERT proteins, biotinylated IDT318 ligand was first incubated with RN46A cells followed by three washes to remove unbound ligand. Streptavidin-conjugated Quantum Dots (SA-QDots) (Invitrogen) were then added to detect the biotinylated moiety of antagonist-associated linker. To minimize the possibility of cross-linking of ligands and the overlap of QDot trajectories, we adapted the QDot-based, single molecule labeling protocol of Triller and colleagues [20], where the ligand concentration (0.5 μM) is set well below saturation (saturation concentration: ≥ 10 μM). In addition, low concentrations (0.5 nM) of SA-QDots were used to detect ligand binding at the lowest recommended concentration as studied by Triller and colleagues [20].

For experiments involving cholesterol depletion, cells were incubated with 5 μM methyl-β-cyclodextrin (MβCD) (Sigma) at 37°C for 30 min prior to two-step QDot-SERT labeling. The MβCD cholesterol depletion protocol we utilized does not result in overt changes in RN46A cell morphology, though more prolonged incubations (90 min) of RN46A cells with 10 m MβCD at 37 °C produce cell rounding paralleled by a decrease in SERT mobility.

For experiments involving the labeling of plasma membrane GM1 ganglioside, RN46A cells were first incubated with 0.2 μM biotinylated cholera toxin subunit B (CTxB) (CTxB:biotin molar ratio ≈ 1:1 to avoid cross-linking, Sigma) for 30 min prior to a 5 min 0.5 nM SAv-QDot incubation. Importantly, GM1 ganglioside-CTxB association has been shown elicit endocytosis.[21, 22] To avoid endocytosis and to achieve successful quantification in dual-channel imaging, all optical live-cell images were taken immediately after QDot labeling. Endocytosis from longer labeling experiments could be readily detected by an accumulation of larger clusters of QDots within the endosomes.

4.2.3 Microscopy

Confocal images were obtained on a Zeiss LSM 510META confocal imaging system. A dual fluorescent, Differential Interference Contrast (DIC) imaging setup was used for conventional point scanning confocal microscopy. Images were collected using a Zeiss Plan-Apochromat 63×/1.4 numerical aperture (NA) oil immersion objective lens and excited by an Argon laser at 488 nm. All images were 512×512 pixels in size and had an 8-bit pixel depth. IDT307 or Alexa 488-labeled CTxB signals were collected through a 520/20 bandpass filter. QDot655 labeling was collected through a 650 nm long bandpass filter. Dual channel fluorescent signals were collected individually to ensure that fluorescent signals could be selected without emission wavelength overlap. Images were processed using Zeiss Image LSM Examiner or Matlab routines originally designed by Esposito A. and colleagues.[23] All images acquired for comparison were thresholded equivalently.

For high speed line-scanning confocal microscopy, images were obtained on a Zeiss LSM 5 Live confocal system and viewed with a Zeiss 63×/1.4 NA oil immersion objective lens. Excitation was provided by a 488 nm 100-milliwatt diode laser. Imaging was performed at 37 °C. Single QDot emission was collected using a long pass 650 filter. Line scan images with scan format of 512x128 pixels were processed using Zeiss LSM Image Examiner.

4.2.4 Data Analysis of Single Quantum Dot Imaging

Raw data files were extracted to generate stacks of individual 16 bit TIF images for single molecule analyses of velocity and trajectory, performed using MATLAB routines. For details, see section 3.23- 3.2.5

4.3 Results

4.3.1 Single Molecule Analysis of QDot-labeled SERT Reveals a Membrane Microdomain-Associated Subpopulation of Transporters With Confined Diffusion

The schematic in Figure 4.1A illustrates our QDot-SERT labeling strategy and depicts the chemical structure of our custom-synthesized SERT ligand, IDT318, which consists of the indoleamine derivative 5-Methoxy-3-(1,2,5,6-tetrahydro-4-pyridinyl)-1H-indole,[24] attached to a biotinylated polyethylene glycol (PEG 5000) linker via an alkyl spacer. The ligand has been previously shown to act as a competitor for SERT-dependent, 5-HT uptake and antagonist binding,[24, 25] and the ligand specificity and affinity were previously described in detail.[25] A two-step labeling of SERT by SA-QDots was designed to permit fluorescence-based detection of surface SERT proteins. We labeled single SERT proteins in differentiated, RN46A cells that are derived from rat embryonic raphe neurons.[18] These cells express low levels of SERT, facilitating the tracking of single SERT molecules.[26] We monitored single SERT proteins in living RN46A cells across 10 sec time-lapse sequences at 10 Hz (Fig.4.1B), where individual QDots show a pattern of fluorescence intermittency ("blinking"), a hallmark of single QDot detection.[27]

Adkins and co-workers,[28] utilizing transfected cells and conventional fluorescence methods to study transporter populations, visualized dopamine transporters in cholesterol-rich membrane microdomains (often referred to as "lipid rafts or "membrane rafts").[29, 30] Magnani and co-workers,[10] using classical biochemical approaches, provided evidence that extraction of membrane cholesterol from brain preparations reduce SERT activity. To determine whether native SERT associates with these microdomains in living, neuronal cells and whether these domains represent membrane rafts, we performed dual-color, live-cell confocal imaging of RN46A cells[18] with the two-step labeling methods as described above. Cholesterol-rich microdomains were identified using Alexa

Fluor 488-conjugated CTxB, a protein that binds specifically to ganglioside GM1, a molecule that has previously been shown to localize to membrane rafts.[31] As shown in Figure 4.1C, images of RN46A cells revealed extensive CTxB/SERT co-labeling, including the presence of single particles as defined above. To verify that the pattern of the clustered SERT/GM1 co-labeling indeed derives from cholesterol-rich membrane microdomains; we extracted cholesterol with methyl-β-cyclodextrin (MβCD), followed by subsequent dual marker labeling.[11] As predicted, this manipulation dispersed the punctate labeling of both CTxB and QDot-SERT labeling of RN46A cells (Fig. 4.1C, Right).

Next, we obtained real-time trajectory data for single QDot-SERT complexes under control and MβCD-treatedconditions (Fig. 4.2A-B). Inspecting these trajectories reveals that lateral movement of single SERT molecules are nonuniform in both cases, with a mixture of movements distinguished by distinct rates but with a relative continuity of motion. Notably, single QDot complexes predominantly display limited movement under control conditions (Fig. 4.2A), whereas single SERT proteins in cholesterol-depleted cells displayed noticeably accelerated, lateral movements (Fig. 4.2B).

For the demonstration of standard protocols for diffusion analyses prior to an introduction of analyses for larger ensembles, a representative time-lapse example from each group is given (Fig. 4.2C). In Figure 2D, we quantified the impact of MβCD on time-dependent displacements (step movements) of single QDot-SERT complexes. As revealed in the greater slope of particle displacement, plotted as a function to time, cholesterol-depleted conditions resulted in significantly faster QDot-SERT movements (red trace) ($P<0.0001$ from averaged traces, Student's t-test), consistent with a mobilization of transporters following disruption of membrane microdomains. These elevated step velocities can be derived from confined diffusion, Brownian movement, or

directed movement, and thus do not describe how a target protein interacts with the surrounding membrane microenvironment. Since single QDot-labeled SERT proteins predominantly displaied limited movement (Fig. 4.2A), we assumed that single SERT proteins are restricted to membrane microdomains. In that case, the diffusion property of single SERT proteins can be appropriately characterized as anomalous subdiffusion,[32] a time-dependent decrease of the diffusion coefficient as a result of temporary confinement (i.e. interaction with lipid rafts or cytoskeletal corrals) of a diffusing protein.[33] Following the relation between transient diffusion coefficient $D(t)$ and tracking time lags(t), free diffusion versus anomalous subdiffusion can be readily distinguished by a plot of log $D(t)$ versus log t (log-log plot), in which a line of negative slopereflects subdiffusion whereas a horizontal line indicates free diffusion. The transient anomalous diffusion coefficient $D(t)$ can be calculated as the mean squared displacement (MSD or $\langle r^2 \rangle$), $D(t)=\langle r^2 \rangle \propto t^{\alpha}$, where α is the anomalous exponent.[32] Shown in Figure 4.2E is the log-log plot of single SERT proteins using the same position data as shown in Figure 4.2D. As expected, the single QDot-SERT complex under control condition exhibited restricted, anomalous subdiffusion. In contrast, and consistent with macroscopic assessments, the diffusion property of single SERT protein is best fit to a model dominated by free diffusion after MβCD treatment.

To further distinguish transporter movements from control and cholesterol-depleted cells, we inspected the trajectories of a larger number of single SERT molecules. Consistent with the findings from the representative experiments indicated in Figure 4.2C, examination of total displacement of single SERT molecules as a function of time (n>50, from 3 independent experiments) demonstrates an approximately two times faster average rate of movement for MβCD treated cells versus control cells (Fig. 4.3A). Since the single SERT trajectories collected in our experiments varied from 5 to 30 sec in duration, using the mean slope from the total displacement over time to calculate

single SERT velocity could have impacted our results. A better assessment of single SERT mobility can be achieved by the calculation of an instantaneous velocity where the distribution of a single step displacement (x) can be fitted into a Lévy probability distribution function (see Materials and Methods). Note that the dynamic behavior of nanoscale assemblies in the plasma membrane of live cells must be observed on the subsecond timescale or below,[34] hence our use of an instantaneous velocity approach. Although the PEG linker we utilized to tether the SERT ligand appears to reduce the steric interference of QDots with SERT, this linker may also increase the uncertainty of SERT velocity assessments. We minimized this uncertainty by calculating instantaneous velocity from a large ensemble of instantaneous displacements (>3000). From these fits, we determined a mean, instantaneous velocity of QDot-SERT molecules of 0.75 ± 0.06 μm/s (mean ± 95% confidence limits) in untreated cells (Fig. 4.3B). Consistent with our mean slope-based estimates, fits from MβCD-treated cells yielded a significant increase in instantaneous velocity (1.74 ± 0.08 μm/s, P<0.0001, Student's t-test). The log-log plot of MβCD-treated cells also clearly show an increase in slope, indicative of reduced constraints on lateral mobility (compare Fig. 4.4A and Fig. 4.4C). The population distribution of single particle diffusion coefficients from untreated cells reveals two components (Fig. 4.4B) with a majority of the SERT proteins residing in the component with lower diffusion coefficients (10^{-3}~10^{-2} μm^2/s). In contrast, only a single distribution of diffusion coefficients could be detected for SERT proteins in MβCD-treated cells (Fig. 4.4D), matching the minority population detected in untreated cells (10^{-2}~10^{-1} μm^2/s).

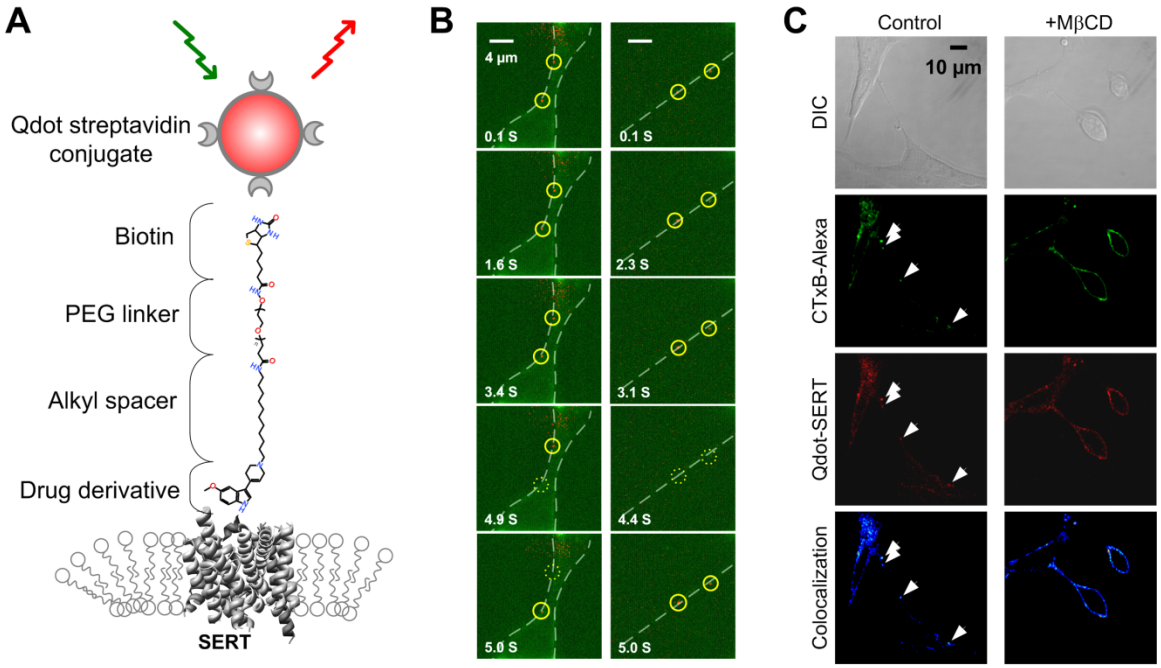

Figure 4.1 Tracking of QDot-labeled single SERT proteins. ***A***, Schematic of QDot nanoconjugates for SERT labelling. The SERT ligand (IDT318) incorporates a biotin moiety to permit conjugation by SAv-QDot, a PEG chain to reduce steric interference and non-specific binding, an alkyl spacer to provide accessibility to the binding site, and a SERT-selective drug derivative to facilitate specific recognition of SERT. ***B***, Time series images of single QDot-SERT proteins on the surface close to the cell body (left column) or neuritic process (right column) of living RN46A cells. Time points where QDot-labeled SERT proteins exhibit “blinking” are indicated by the dashed circles. ***C***, Presence of SERT proteins within GM1 enriched membrane microdomains and their mobility in control and cholesterol depleted cells. 1st column: DIC images. 2nd column: staining of membrane rafts using Alexa 488-conjugated CTxB. 3rd column: QDot-SERT proteins. 4th column: colocalization of CTxB and QDot labeling. Arrowheads note the presence of puncta labeled for both markers.

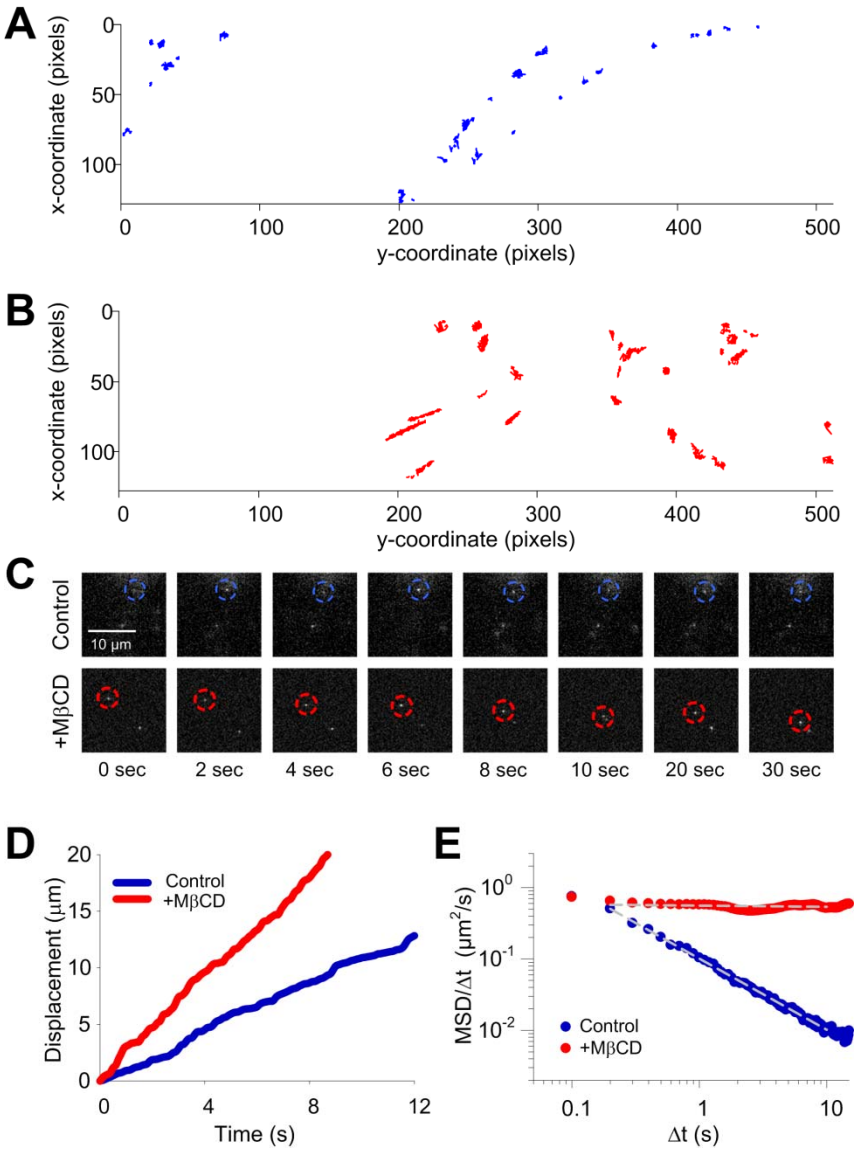

Figure 4.2 Single QDot-SERT tracking in living serotonergic RN46A cells under control and MβCD-treated conditions. ***A***, Full trajectory reconstruction from 30 sec time-lapse videos of single QDot-labeled SERT proteins in control ***A*** and cholesterol depleted ***B*** RN46A cells. Video frame size: 512X128 pixels, pixel size: 0.2 µm. Note the more mobile behavior of single SERT trajectories after MβCD treatment. ***C***, Temporal profile of representative QDot-labeled, single SERT proteins with and without MβCD treatment. ***D***, Comparison of displacement over time of the representative single QDot-SERT complexes in ***C***. ***E***, Plot of MSD/Δt as a function of Δt of the representative single SERT proteins in C on a log-log scale. Single SERT under MβCD treated condition shows the pattern expected of free diffusion whereas SERT from untreated cells demonstrates a pattern consistent with motion restriction, or anomalous subdiffusion. White, dashed lines in E represent a least squares best-fit of the data.

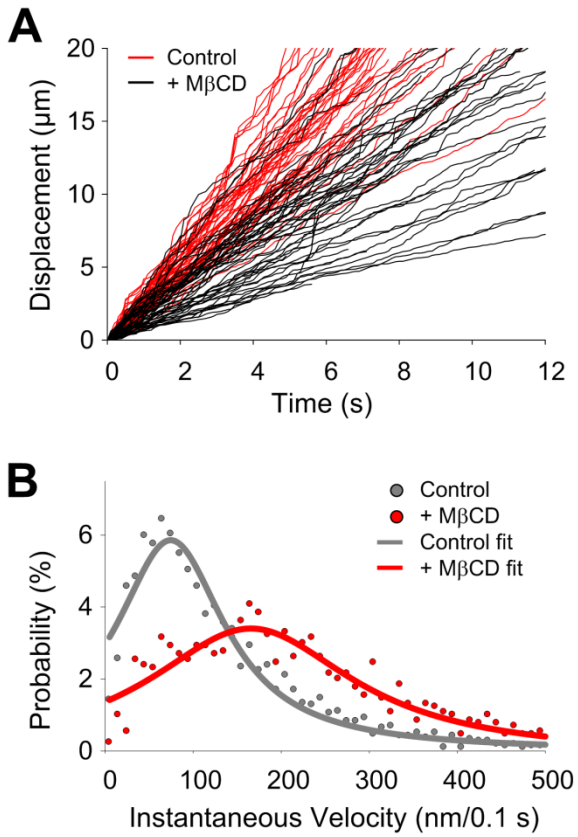

Figure 4.3 Single QDot-labeled SERT proteins demonstrate elevated SERT lateral mobility after membrane raft disruption.***A***, Distributions of the instantaneous displacement of single SERT proteins in control (black, n=52) and MβCD treated (red, n=51) conditions. ***B***, Comparison of instantaneous velocities of single SERT proteins in untreated and MβCD treated RN46A cells. Each set of data was collected from 3 independent experiments.

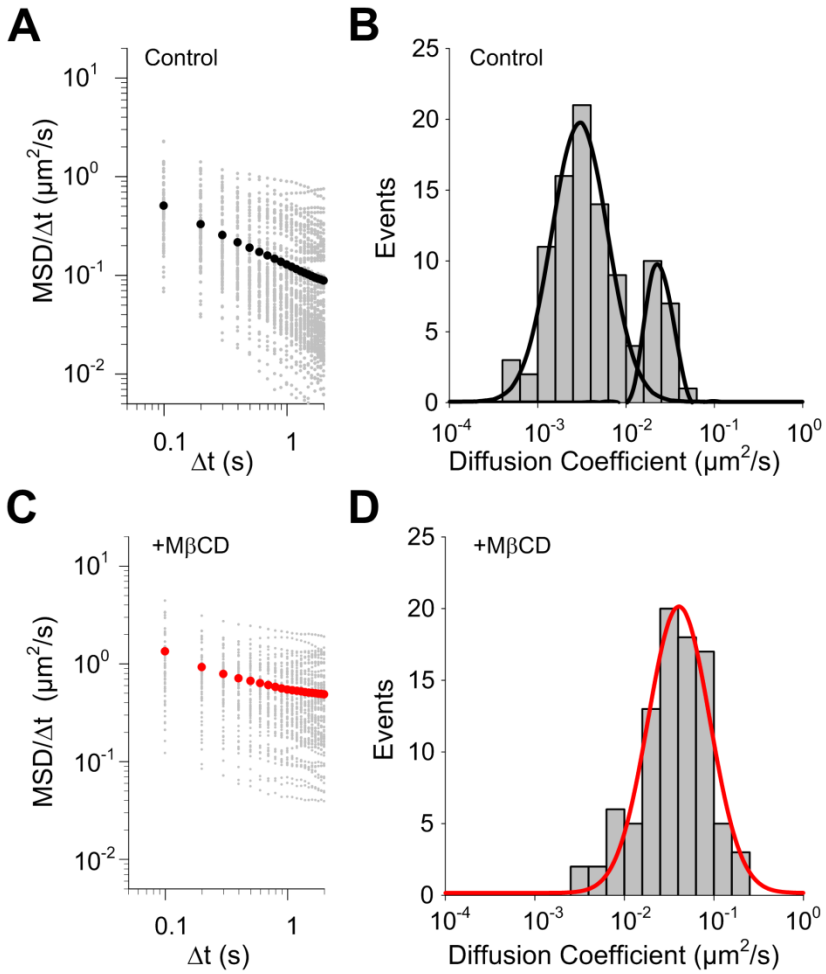

Figure 4.4 Characterization of the dynamic behavior of single SERT proteins. Plots of MSD/Δt as a function of Δt and distribution of diffusion coefficient of single SERT proteins in control cells (***A-B***;*n*=98) and in MβCD treated cells (***C-D***,*n*=91). ***A***, ***B***, Although the variability exists in both cases, the majority of SERT proteins in untreated cells display confined diffusion pattern with lower diffusion coefficient values. ***C***, ***D***,In contrast, single SERT proteins after MβCD treatmentfollow free diffusion with higher diffusion coefficients. Black circles in ***A*** and red circles in ***C*** present the average MSD/Δt. Panels ***B*** and ***D*** were fit to double and single Gaussian distributions, respectively.

4.3.2 Single Qdot-Labeled SERT Proteins Demonstrate Increased SERT Lateral Mobility, Despite a Confined Distribution, after 8-Br-cGMP Treatment

Although our direct observations, along with the chemical manipulation of RN46A cells, revealed inherent restrictions in the mobility of single, plasma membrane SERT proteins, such treatments do not address the degree to which mobility restrictions contribute to physiologically relevant features of transporter regulation. As noted above, SERT membrane trafficking and catalytic activity are under tight regulation by multiple signaling pathways[2] that are affected by OCD and autism SERT mutations.[6-9] Activation of PKG by cGMP analogs in both SERT-transfected and native SERT expressing, RN46A cells triggers SERT phosphorylation, enhanced SERT surface trafficking, and an increase in 5-HT uptake rates.[2] Moreover, OCD- and autism-associated SERT coding variants display altered PKG-dependent SERT phosphorylation, trafficking and/or catalytic activation *in vitro* and *in vivo*.[6-8, 35] We thus sought to determine whether PKG activation produces an altered motion behavior of SERT proteins localized to membrane subdomains. To investigate the above hypothesis, we compared the instantaneous velocity of single SERT proteins in control and 8-bromo cGMP (8-Br-cGMP) (a membrane-permeable cGMP analog that activates PKG) treated RN46A cells. Interestingly, we detected a significant, ~2 fold, increase in the mean instantaneous velocity after 8-Br-cGMP treatment (Fig. 4.5A) (1.60 ± 0.03 μm/s versus 0.75 ± 0.06 μm/s, $P<0.0001$, Student's t-test.). Additionally, when we performed diffusion coefficient analysis on 8-Br-cGMP treated cells, the distribution of SERT diffusion rates after 8-Br-cGMP treatment still resulted in bimodal behavior (Fig. 4.5B), although a significant increase in higher diffusion rates was observed compared to the untreated cells (Fig. 4.4B).

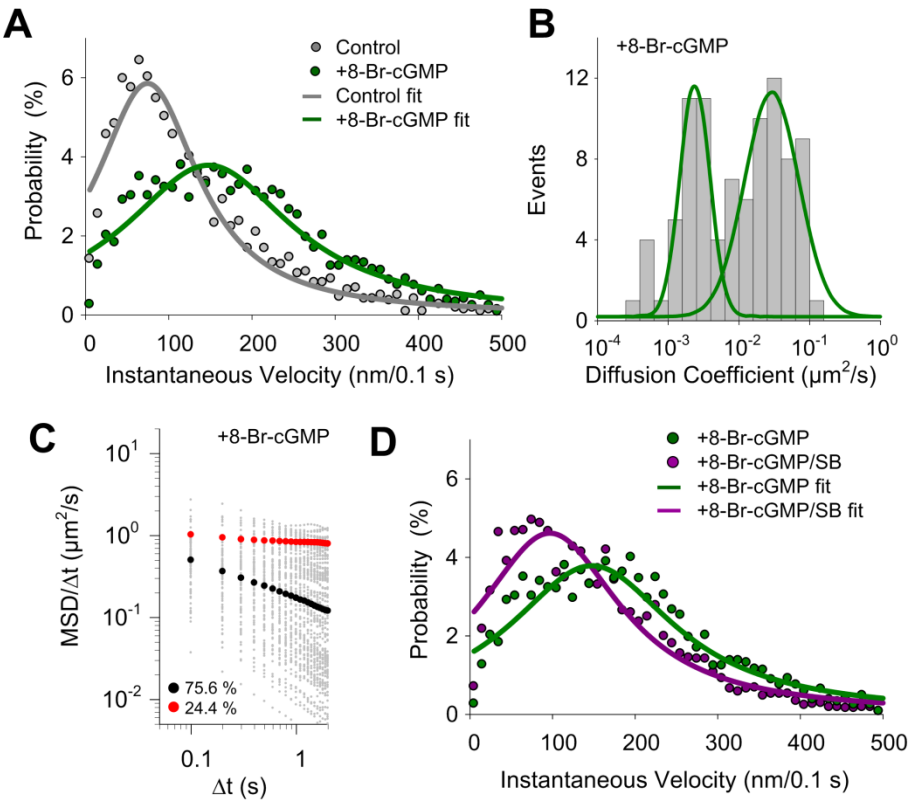

Figure 4.5 Effect of 8-Br-cGMP on SERT lateral mobility. ***A***, Comparison of instantaneous velocities of single SERT proteins in untreated and 8-Br-cGMP stimulated cells. ***B***, Distribution of diffusion coefficient of single SERT proteins (*n*=90) after 8-Br-cGMP treatment and fit with double Gaussian distributions. ***C***, Plots of MSD/Δt as a function of Δt of single SERT proteins (*n*=90) in MβCD treated cells are shown. Black circles and red circles show the average MSD/Δt of constrained (75.6%) and mobile (24.5%) population of single SERT trajectories. ***D***, Comparison of instantaneous velocities of single SERT proteins in 8-Br-cGMP stimulated or 8-Br-cGMP plus SB203580 (SB) co-treated cells. Data derived from 3-6 independent experiments.

The increase in SERT instantaneous velocity, accompanied by elevated diffusion rates, following 8-Br-cGMP treatment that are known to elevate SERT activity were surprising. As above, we noted that we increased SERT mobility accompanies MβCD treatment that produce a reduction in SERT activity.[10, 11] Furthermore, the anomalous exponent α derived from log-log plots (Fig. 4.5C) indicates that 75.6 % of SERT proteins in 8-Br-cGMP treated cells exhibit confined lateral diffusion, similar to the fraction (89.8 %) observed with untreated cells. Thus, despite the observation that accelerated SERT movements are evident for a large fraction of SERT molecules following 8-Br-cGMP treatment, the majority of SERT proteins appear to remain highly constrained in membrane microdomains.

4.3.3 The p38 MAPK Inhibitor SB203580 Attenuates 8-Br-cGMP Induced Enhancements in SERT Lateral Mobility

Treatment of RN46A cells with 8-Br-cGMP induces a PKG-dependent mobilization of intracellular SERT loaded vesicles, leading to an increase of SERT cell surface density.[2] Since our QDot-SERT surface labeling paradigm should be insensitive to the trafficking of unlabeled intracellular SERT proteins to the cell surface, we suspect that the altered mobility of SERT proteins after 8-Br-cGMP treatment might relate to the transport rate enhancement (catalytic activation) of surface transporters that arises subsequent to PKG-stimulated membrane trafficking.[2, 6] Previously, we showed that SERT catalytic activation arises as a result of PKG-triggered p38 MAPK activation that in turn stabilizes SERT in a conformation recognizing serotonin with higher-affinity.[36, 37] Therefore, we asked whether p38 MAPK activation is essential for the observed changes in SERT movements following 8-Br-cGMP treatment by co-incubating cells treated with 8-Br-cGMP with the specific p38 MAPK inhibitor SB203580. As shown in

Figure 5D, co-incubation of 8-Br-cGMP treated RN46A cells with SB203580 significantly attenuated the increase in SERT instantaneous velocity observed with 8-Br-cGMP alone.

To visualize better the displacements of single SERT movements following different treatments, we plotted lateral trajectories of single transporter movements over a 5 sec recording interval (d_{5S}), comparing control, MβCD, and 8-Br-cGMP treatments (Fig. 4.6A-C). Whereas instantaneous velocity is used to monitor the dynamic behavior at a relatively short timescale, 5 sec displacement measures provide an estimation of the extent of lateral movement, thereby estimating the borders of the membrane compartment occupied by single SERT proteins. As can be seen in Figure 4.5A-B, single SERT proteins in untreated cells displayed limited displacement, whereas the movements in MβCD-treated cells exhibit significantly greater dispersal. Our results demonstrate that 8-Br-cGMP treatment (or 8-Br-cGMP/SB203580 co-treatment) generates SERT displacements that are indistinguishable from untreated cells when monitored at a longer timescale (Fig. 4.6C-D). Thus, cGMP-linked signaling pathways appear to enhance SERT activity without a dissociation of transporters from the membrane microdomains in which they were initially labeled.

4.3.4 IL-1β Activated Single SERT Proteins Reveal p38 MAPK-Dependent Subpopulation

Having linked increased mobility of SERT proteins within the membrane rafts to p38 MAPK-dependent pathways, we asked whether a natural stimulus that produces p38 MAPK-dependent SERT activation, independent of PKG, would reproduce the mobility changes induced by 8-Br-cGMP. We have shown that the inflammatory cytokine IL-1β acts through plasma membrane IL-1 receptors[38] to produce a p38 MAPK-dependent catalytic activation of SERT proteins in RN46A cells, as well as in brain

synaptosomes. As shown in Figure 4.6F, IL-1β treatment (100 ng/mL; 30 min; 37°C) of RN46A cells produces a rightward shift in the instantaneous velocities of single SERT molecules, in comparison to untreated cells, documenting enhanced transporter velocity. The distribution of velocities is well-fit to a model comprised of two populations: one aligned with the low mobility distribution that was observed under untreated conditions and a second aligned with the distribution previously described following 8-Br-cGMP stimulation. We also found that treatment with IL-1β, like 8-Br-cGMP, caused an increase in the fraction of SERT molecules exhibiting accelerated velocity (Fig. 4.6F) with high diffusion coefficients (Fig.4.6G). As with 8-Br-cGMP treatment, the 2D displacements of single SERT molecules did not differ from that observed in untreated cells (Fig. 4.6E), and SERT remained localized to CTxB-labeled membrane microdomains. These results provide strong support that both 8-Br-cGMP and IL-1β-induced stimulation of SERT activity arises via a p38 MAPK-dependent mobilization of transporter proteins that remain confined to membrane microdomains.

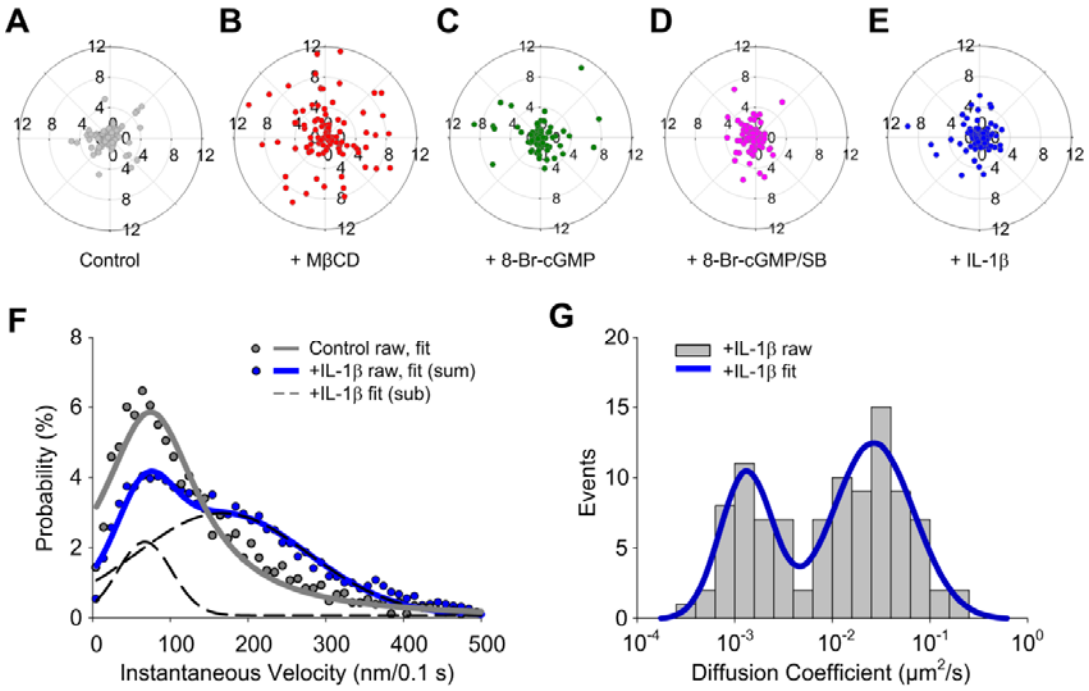

Figure 4.6 p38 MAPK-dependent increase in SERT mobility in the absence of lateral dispersion. ***A-E***, 2D Polar plots of 5 sec displacements (d_{5s}) of single SERT movements, normalized to their starting coordinates under control, MβCD, 8-Br-cGMP, 8-Br-cGMP plus SB203580, and IL-1β treated conditions, respectively. Plots provide data in pixel units (200 nm/pixel). Data were collected from 3-6 independent experiments with 90-100 trajectories for each condition. ***F***, Comparison of instantaneous velocities of single SERT proteins in untreated and IL-1β stimulated cells. The best-fit velocity distribution of IL-1β treated SERT proteins reveals a dominant population (76.9 %) with higher velocities and a minor population (23.1%) with lower velocities. ***G***, Distribution of diffusion coefficient of single SERT proteins (*n*=99) after IL-1β treatment (double Gaussian fit).

4.3.5 Cytoskeletal Disruption Mobilizes SERT Molecules That Remain Confined to Membrane Microdomains

A possible mechanism responsible for confined diffusion of SERT proteins in membrane microdomains, and one that could be a target for p38 MAPK regulation associated with transporter activation, is the liberation of transporters from juxtamembrane cytoskeletal networks that could confine movements of raft-localized transporters.[2] To determine whether SERT lateral mobility within these domains is restricted by cytoskeletal interactions, we treated cells with the actin filament disrupter cytochalasin D (CytoD) (0.5 μg/ mL; 30min; 37°C) a dose that does not produce gross changes in cell morphology. Like 8-Br-cGMP and IL-1β treatments, this treatment produced a bimodal distribution of diffusion rates for single QDot-labeled SERT molecules (Fig.4.7), with an increased representation of the more mobile population. CytoD treatment produces an increase in diffusion rates for both subpopulations, as compared to 8-Br-cGMP and IL-1β treatments (fitted Gaussian center D value: relative immobile population increases from $(1.32 \pm 0.04)\times10^{-3}$ to $(1.05 \pm 0.03)\times10^{-2}\mu m^2/s$; relative mobile population increases from $(2.63 \pm 0.04)\times10^{-2}$ to $(6.92 \pm 0.01)\times10^{-2}\mu m^2/s$), consistent with a contribution of cytoskeletal interactions also constraining SERT lateral mobility to some degree outside of lipid rafts. Compared to untreated cells, the instantaneous velocity of single QDot-labeled SERT proteins from CytoD treated cells was significantly elevated (Fig. 4.8A), with 93% of the transporters fit to a higher velocity component (1.51 ± 0.06 μm/s vs 0.75 ± 0.06 μm/s for untreated cells). We found very similar results in monitoring the instantaneous movements of membrane rafts using single QDot-labeled GM1/CTxB complexes following the same CytoD treatment (Fig. 4.8B). However, CytoD treatment did not disperse CTxB labeling as seen with MβCD treatment, consistent with an actin-independent contribution to microdomain integrity.

Importantly, SERT proteins remained colocalized with CTxB/GM1 (Fig. 4.7B). When IL-1β (100 ng/mL; 30 min; 37°C) was added to cells pretreated with CytoD, no further increase in SERT velocity was achieved (Fig. 4.8C). We do not believe that this is a ceiling effect on velocity as MβCD treatment increase rates beyond this level (higher velocity component: 1.82 ± 0.06 μm/s, Fig. 5A +8-Br-cGMP data fit with double Gaussian). Together, these data support the hypothesis that IL-1β activation of SERT arises as a result of the release of transporters from cytoskeleton-associated anchors, though the transporters remained trapped within membrane microdomains.

SERT is known to associate through N and C-terminal cytoplasmic domains with multiple integral membrane and cytosolic proteins, several of which have been suggested to coordinate SERT regulation via cytoskeletal interactions.[2, 39] In this regard, the SERT C-terminus has been shown not only to complex with integrins and integrin-associated proteins that interact dynamically with the cytoskeleton[5, 40] but also to interact with the PKG-linked signaling molecule nitric oxide synthetase (NOS).[39] To determine whether SERT C-terminal protein interactions could account for microdomain-restricted mobility of transporters, we incubated RN46A cells with membrane permeate TAT-C-terminal SERT peptides (C-SERT peptide) prior to single QDot-SERT tracking. As seen with IL-1β treatment, C-SERT peptide treatment generated a shift of the distribution to more rapid transporter diffusion rates (Fig.4.9A). In contrast to the untreated RN46A cells (Fig. 4.4B), TAT-conjugated SERT peptide derived from sequences upstream of those of the C-terminal SERT peptide (interior or U-SERT peptide) produced a similar SERT diffusion rate distribution (Fig. 4.9B) to that of untreated cells (Fig. 4.4B). Importantly, and as with IL-1β treatment, the C-SERT peptide produced an increase in SERT transport activity (Fig.4.9C).

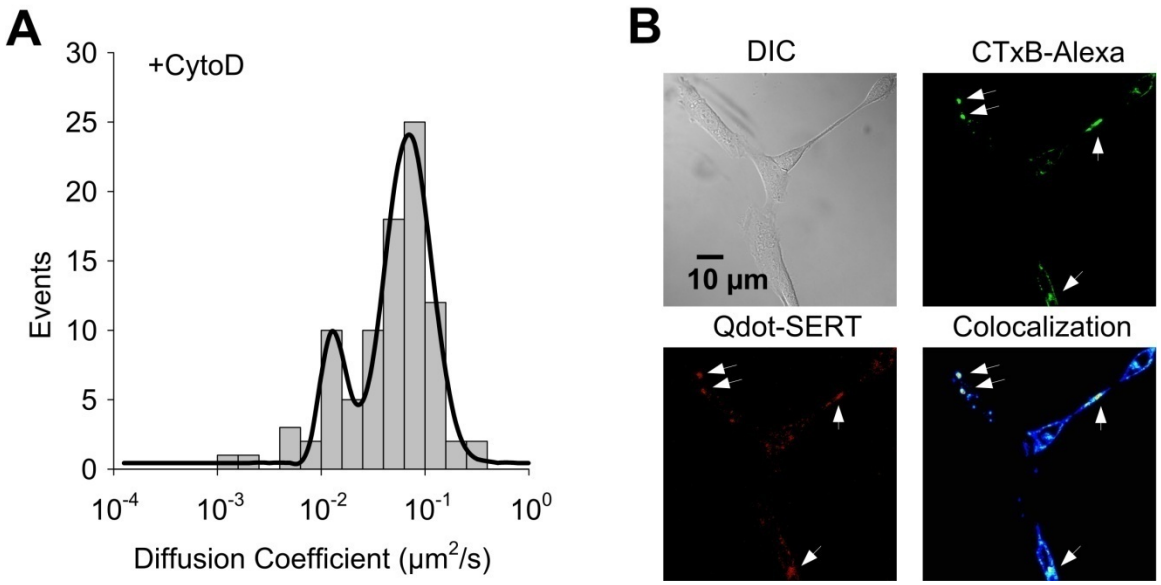

Figure 4.7 Cytoskeletal disruption mobilizes SERT molecules that remain confined to membrane microdomains. ***A***, Increased lateral diffusion of QDot labeled SERT proteins after CytoD treatment. Data fit with double Gaussian distributions. ***B***, Retention of SERT proteins within membrane rafts in CytoD-pretreated RN46A cells. Upper left: DIC image; Upper right: staining of membrane rafts using Alexa 488-conjugated CTxB; Lower left: QDot-SERT proteins; Lower right: colocalization of CTxB and QDot labeling. Arrowheads denote the presence of multiple puncta labeled for both markers.

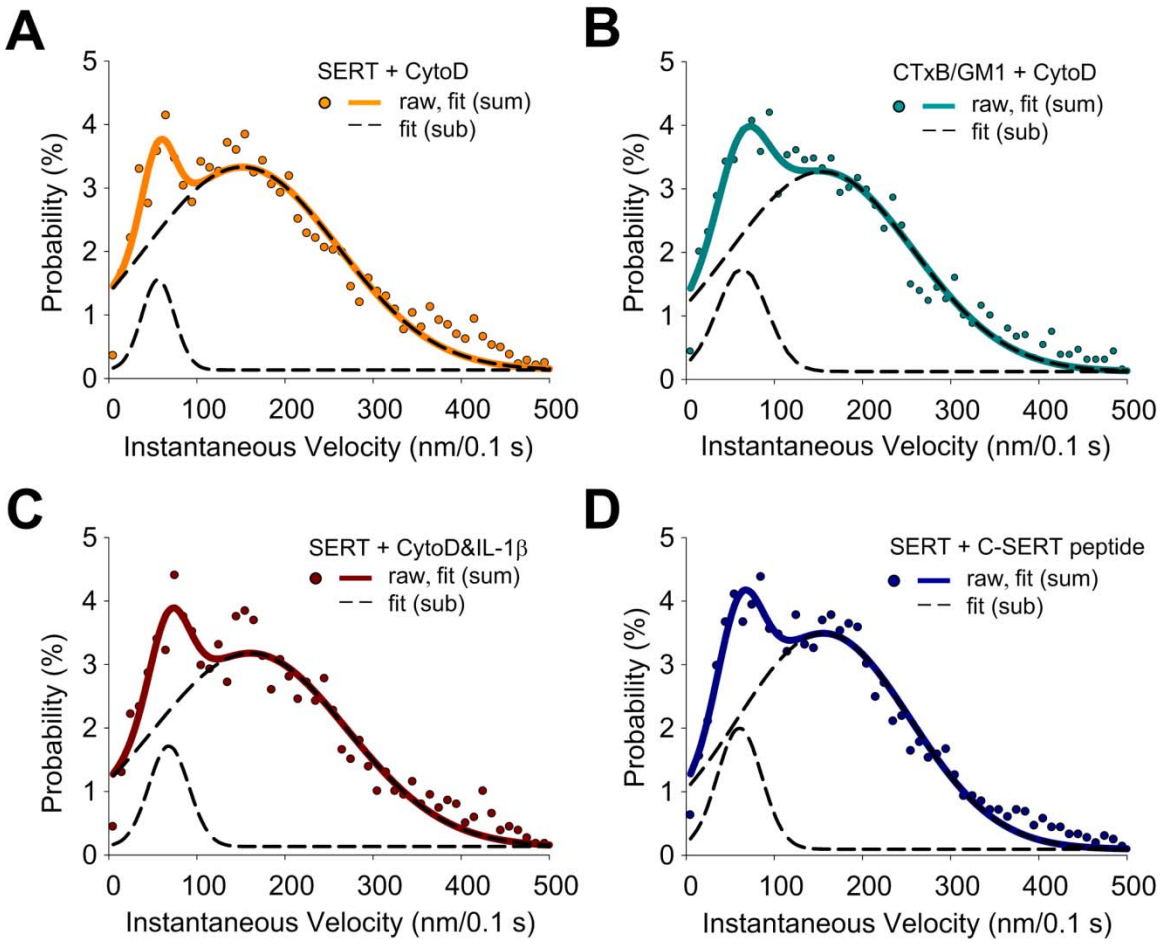

Figure 4.8 Actin cytoskeleton restricts SERT mobility within membrane microdomains in a p38 MAPK and SERT C-terminus dependent manner. Plots of instantaneous velocity of ***A***, single QDot-labeled SERT proteins in RN46A cells treated with CytoD, ***B***, single QDot-labeled GM1/CTxB complexes in RN46A cells treated with CytoD, ***C***, single QDot-labeled SERT proteins in RN46A cells treated with CytoD after IL-1β stimulation, and ***D***, single QDot-labeled SERT proteins in RN46A cells treated with C-SERT peptide. Each condition represents results of three independent experiments.

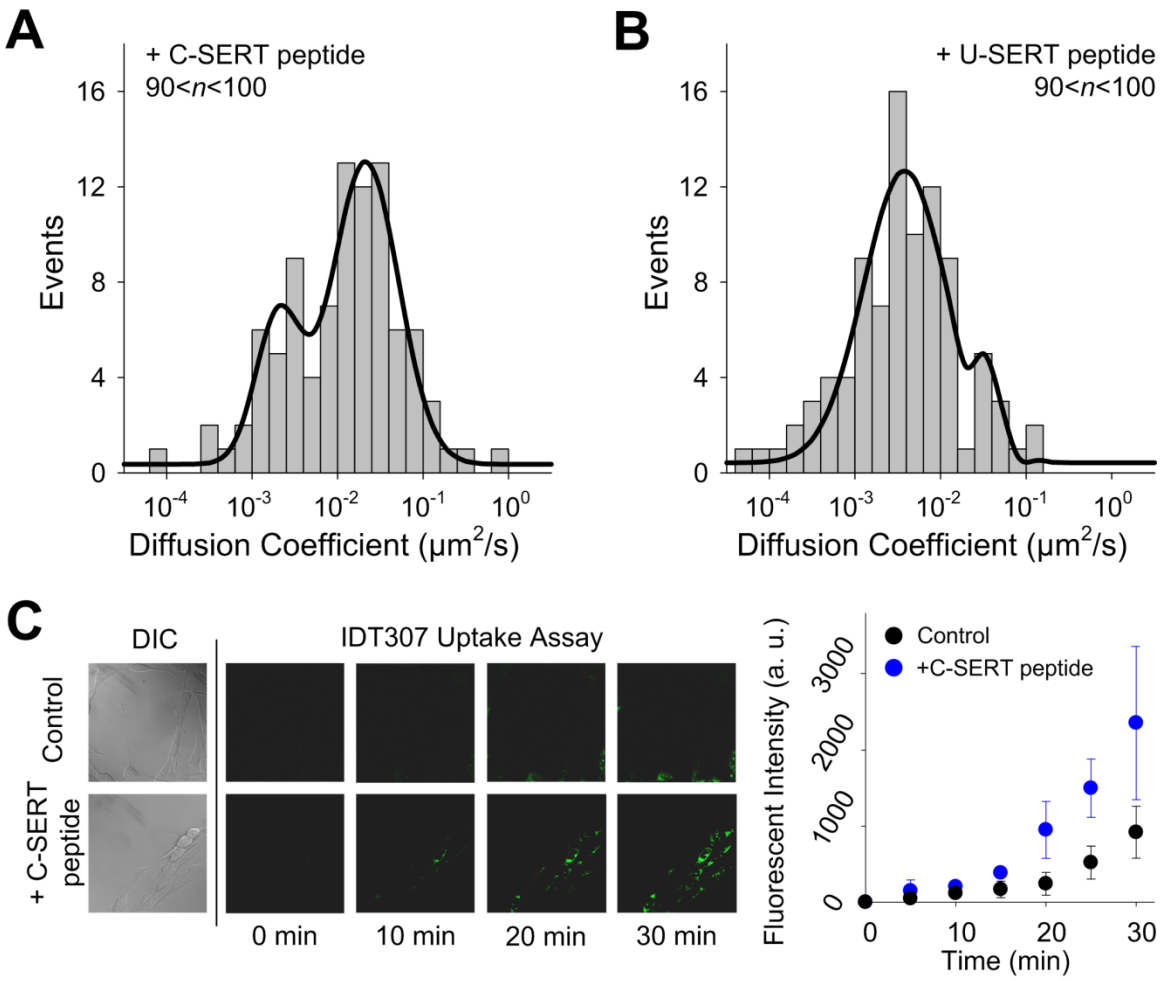

Figure 4.9 Dissociation of SERT C-terminus from cytoskeletal-associated proteins creates increases in single SERT diffusion and SERT transport activity.***A-B***, Distribution of diffusion coefficient of single SERT proteins after C-SERT ***A*** and U-SERT ***B*** peptide treatments and fit with double Gaussian distributions. Data collected from five independent experiments. ***C***, SERT activity in RN46A cells after U-SERT peptide treatment. SERT activity was monitored using the fluorescent monoamine transporter substrate IDT307 (see Materials and Methods). Data shown are representative of time-lapse microphotographs (right) and fluorescent quantification ($P < 0.01$, Student's t-test) (left) obtained in three independent experiments.

4.4 Discussion

Here we provide evidence that single QDot-labeled, plasma membrane-embedded SERT proteins distribute between freely mobile pools and relatively immobile, cholesterol-rich microdomains where restricted mobility is derived from C-terminal interactions with the actin cytoskeleton. Our findings, which to our knowledge are the first to describe the mobility of single transporter proteins, were achieved by fusing the single molecule detection capacity of QDots to the specificity and high affinity of a pharmacological probe. The linker between the SERT antagonist and the SA-QDots was developed to provide both access of the ligand to its high-affinity binding site that lies midway through the plasma membrane[41] and to enhance linker solubility. Although multiple biotin binding sites are theoretically available on the SA-QDots, the surface density of SERT proteins is very low on RN46A cells,[38] and we used subsaturating concentrations of ligand as well as low concentrations of QDots to minimize multivalent labeling.[20] Importantly, our antagonist-conjugated SA-QDots do not limit our ability to detect free diffusion kinetics of a subpopulation of SERT molecules nor to detect regulation of SERT through cGMP and p38 MAPK-linked pathways. Previously, we achieved population detection of SERT,[17, 25] GABA receptor,[42] and dopamine transporter (DAT)[43] proteins using ligand-conjugated QDots. With respect to the prior SERT study, these efforts involved direct conjugation of 5-HT to QDots, prior to the application of this complex to cells. In subsequent studies, we found this approach to be of insufficient sensitivity and reliability for the detection of transporters on natively-expressing cells, due to the lower affinity of 5-HT, the higher nonspecific binding of the QDot conjugate, and the stability of the QDot complexes after binding. Nonetheless, our success in these efforts provided critical evidence that a modification of this approach could be generalized and enhanced to achieve detection of SERT diffusion dynamics. Many more small molecule ligands, including therapeutic compounds, are available that target

membrane proteins rather than surface-epitope antibodies, and thus the methods presented here appear well-suited to the detection of other receptors, ion channels and transporters targeted by widely available pharmacological tools and medications.

In our report, we establish that SERT instantaneous velocity is significantly enhanced by both chemical depletion of membrane cholesterol and activation of p38 MAPK-dependent signaling pathways, two manipulations that exert opposite influences on SERT activity. In resolving this puzzle, we discovered a previously unsuspected correlation of SERT activation involving the mobilization of transporters from juxtamembrane tethers within cholesterol-rich microdomains. Importantly, mobilized transporters do not leave these membrane microdomains, providing a mechanism for reversibility of associations that can both increase and decrease surface-resident SERT proteins.Membrane cholesterol has been reported to have a varied effect on the diffusion of surface proteins.[11, 44] Cholesterol extraction using MβCD increases the diffusion coefficient of dopamine transporter populations assessed by fluorescence recovery after photobleaching (FRAP).[28] In contrast, extraction of membrane cholesterol results in plasma membrane changes that reduce diffusion of MHC II proteins.[45] The degree to which SERT protein function *in vivo* depends on membrane cholesterol is unknown, though one advantage to our *in vitro* studies is the use of a serotonergic neuronal model that expressed endogenous SERT proteins, limiting potential artifacts due to heterologous expression. Human clinical studies report inconsistent findings on the impact of reduced cholesterol and/or cholesterol-lowering therapy risk for mood disorders or their treatments.[46, 47] Interestingly, a recent study in rats demonstrated that lovastatin treatment enhances the ability of the SERT-directed antidepressant fluoxetine to reverse despair behavior,[48] findings that should be investigated to determine whether they reflect, at least in part, alterations in SERT membrane dynamics. Additionally, antidepressant drugs have been reported to concentrate in membrane microdomains[49]

and whether this partitioning might influence SERT membrane dynamics as well as block re-uptake should be explored. Finally, we have shown recently that A3 adenosine receptors physically associate with SERT and regulate SERT catalytic function in RN46A cells via p38 MAPK.[50] Our results are most consistent with this regulation being highly localized and provide an explanation for how signaling pathways that act on many other targets within the cell can be limited to specific targets, in this case toward SERT.

What molecular mechanisms support the single molecule findings associated with p38 MAPK-dependent SERT regulation? SERT is known to reside in macromolecular complexes whose composition changes as a function of regulatory stimuli.[2, 50] The association of several proteins with SERT can be altered by stimuli that influence SERT activity, including syntaxin 1A and the focal adhesion interactor Hic-5.[5, 51] Hic-5 is a focal adhesion-associated protein known to associate with both the SERT C-terminus and the actin-rich, membrane cytoskeleton. We have shown that Hic-5 addition to resealed membrane vesicles *in vitro* reduces SERT activity.[5] Furthermore, SERT/Hic-5 associations are enhanced by stimuli, such as PKC activation, that lead to initial SERT catalytic inactivation and subsequent internalization. Therefore, we hypothesize that the orchestrated dissociation from the SERT C-terminus of cytoskeletal-associated proteins, such as Hic-5, places the transporter in a more active conformation, and that such dissociation accounts for both the increase in SERT mobility we observed and the increase in SERT activity found upon manipulation of SERT cytoskeletal interactions (Fig. 4.10). In support of this idea, Hong and Amara have recently provided evidence that cholesterol-rich microdomains favor an outward facing conformation of DAT[52] and we have previously shown that activation of p38 MAPK enhances the affinity of the transporter for 5-HT.[37]

To conclude, we show here that the diffusion rate distribution of single QDot labeled SERT proteins under control, 8-Br-cGMP, and IL-1β treated conditions exhibit a

bimodal distribution, with populations exhibiting higher rates of mobility increased after 8-Br-cGMP (Fig. 4.5B) and IL-1β (Fig. 4.6G) treatments. These changes in mobility are not the same as those generated through cholesterol depletion and elimination of membrane rafts, which also reduce SERT activity. Importantly, the actin cytoskeleton and the SERT C-terminus appear to play critical roles in the mobilization of SERT within these membrane microdomains. Thus, we believe that a major aspect of SERT regulation relies on a tightly controlled, and dynamic, cytoskeletal interaction (Fig. 4.10). The ability of Il-1β to stimulate SERT mobility places our findings in a physiological context, given that our findings that this receptor regulates SERT activity *in vitro* and *in vivo*,[38, 53] and is consistent with prior findings that Il-1 signaling arises from raft-like membrane microdomains.[54] Finally, we hypothesize that OCD and autism-associated SERT mutations that are known to constitutively enhance SERT activity and to disrupt PKG and p38 MAPK-dependent regulation[6, 9] derive their pathophysiological impact from perturbed SERT cytoskeletal associations in membrane microdomains.

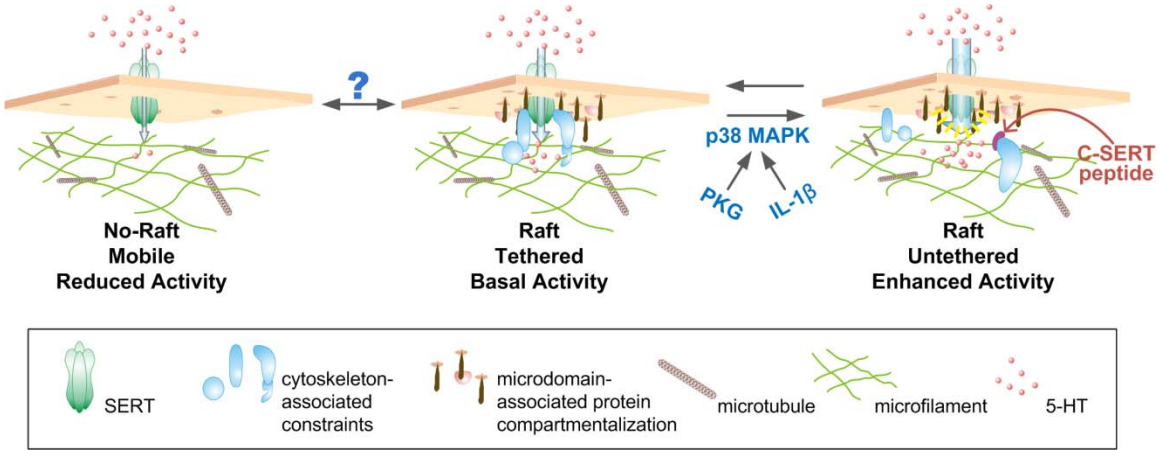

Figure 4.10 Model for SERT-cytoskeletal interactions dictating cell surface transporter regulation. In the resting state, SERT is present in two compartments, one that permits free diffusion in the membrane (left), and a second compartment that represents confinement to membrane microdomains (center) where transporters are immobilized by cytoskeleton-associated proteins (middle). When cytoskeleton-associated constraints are relaxed in response to PKG/IL-1β/p38 MAPK activation (or through actin destabilizers or C-SERT peptide treatments), SERT remains confined to membrane microdomains (right), though now transporters can adopt conformations that favor increased transport activity. Question mark overlying transitions into and out of membrane microdomains denotes the possibility that such movements could also play a role in SERT regulation, though they are not features of the PKG and p38 MAPK-dependent SERT regulation detected in the current study.

4.5 References

(1) Murphy, D. L., Fox, M. A., Timpano, K. R., Moya, P. R., Ren-Patterson, R., Andrews, A. M., Holmes, A., Lesch, K. P., and Wendland, J. R. (2008) How the serotonin story is being rewritten by new gene-based discoveries principally related to SLC6A4, the serotonin transporter gene, which functions to influence all cellular serotonin systems. *Neuropharmacology55*, 932-960.

(2) Steiner, J. A., Carneiro, A. M., and Blakely, R. D. (2008) Going with the flow: trafficking-dependent and -independent regulation of serotonin transport. *Traffic9*, 1393-1402.

(3) Ramamoorthy, S., Shippenberg, T. S., and Jayanthi, L. D. (2011) Regulation of monoamine transporters: Role of transporter phosphorylation. *Pharmacol. Ther.129*, 220-238.

(4) Ramamoorthy, S., and Blakely, R. D. (1999) Phosphorylation and sequestration of serotonin transporters differentially modulated by psychostimulants. *Science285*, 763-766.

(5) Carneiro, A. M. D., and Blakely, R. D. (2006) Serotonin-, protein kinase C-, and Hic-5-associated redistribution of the platelet serotonin transporter. *J. Biol. Chem.281*, 24769-24780.

(6) Prasad, H. C., Zhu, C.-B., McCauley, J. L., Samuvel, D. J., Ramamoorthy, S., Shelton, R. C., Hewlett, W. A., Sutcliffe, J. S., and Blakely, R. D. (2005) Human serotonin transporter variants display altered sensitivity to protein kinase G and p38 mitogen-activated protein kinase. *Proc. Natl. Acad. Sci. U.S.A.102*, 11545-11550.

(7) Prasad, H. C., Steiner, J. A., Sutcliffe, J. S., and Blakely, R. D. (2009) Enhanced activity of human serotonin transporter variants associated with autism. *Philos. Trans. R. Soc. Lond. B364*, 163-173.

(8) Ozaki, N., Goldman, D., Kaye, W. H., Plotnicov, K., Greenberg, B. D., Lappalainen, J., Rudnick, G., and Murphy, D. L. (2003) Serotonin transporter missense mutation associated with a complex neuropsychiatric phenotype. *Mol. Psychiatry8*, 933-936.

(9) Sutcliffe, J. S., Delahanty, R. J., Prasad, H. C., McCauley, J. L., Han, Q., Jiang, L., Li, C., Folstein, S. E., and Blakely, R. D. (2005) Allelic heterogeneity at the serotonin transporter locus (SLC6A4) confers susceptibility to autism and rigid-compulsive behaviors. *Am. J. Hum. Genet.77*, 265-279.

(10) Magnani, F., Tate, C. G., Wynne, S., Williams, C., and Haase, J. (2004) Partitioning of the serotonin transporter into lipid microdomains modulates transport of serotonin. *J. Biol. Chem.279*, 38770-38778.

(11) Scanlon, S. M., Williams, D. C., and Schloss, P. (2001) Membrane cholesterol modulates serotonin transporter activity. *Biochemistry40*, 10507-10513.

(12) Fichter, K. M., Flajolet, M., Greengard, P., and Vu, T. Q. (2010) Kinetics of G-protein-coupled receptor endosomal trafficking pathways revealed by single quantum dots. *Proc. Natl. Acad. Sci. U.S.A.107*, 18658-18663.

(13) Dahan, M., Levi, S., Luccardini, C., Rostaing, P., Riveau, B., and Triller, A. (2003) Diffusion dynamics of glycine receptors revealed by single-quantum dot tracking. *Science302*, 442-445.

(14) Alivisatos, P. (2004) The use of nanocrystals in biological detection. *Nat. Biotechnol.22*, 47-52.

(15) Howarth, M., Liu, W., Puthenveetil, S., Zheng, Y., Marshall, L. F., Schmidt, M. M., Wittrup, K. D., Bawendi, M. G., and Ting, A. Y. (2008) Monovalent, reduced-size quantum dots for imaging receptors on living cells. *Nat. Methods5*, 397-399.

(16) Michalet, X., Pinaud, F. F., Bentolila, L. A., Tsay, J. M., Doose, S., Li, J. J., Sundaresan, G., Wu, A. M., Gambhir, S. S., and Weiss, S. (2005) Quantum dots for live cells, in vivo imaging, and diagnostics. *Science307*, 538-544.
(17) Rosenthal, S. J., Tomlinson, I., Adkins, E. M., Schroeter, S., Adams, S., Swafford, L., McBride, J., Wang, Y., DeFelice, L. J., and Blakely, R. D. (2002) Targeting cell surface receptors with ligand-conjugated nanocrystals. *J. Am. Chem. Soc.124*, 4586-4594.
(18) White, L. A., Eaton, M. J., Castro, M. C., Klose, K. J., Globus, M. Y., Shaw, G., and Whittemore, S. R. (1994) Distinct regulatory pathways control neurofilament expression and neurotransmitter synthesis in immortalized serotonergic neurons. *J. Neurosci.14*, 6744-6753.
(19) Blakely, R. D., Mason, J. N., Tomlinson, I. D., and Rosenthal, S. J. (2011) Fluorescent substrates for neurotransmitter transporters, In *United States Patent No. US 7,947,255 B2*.
(20) Bannai, H., Levi, S., Schweizer, C., Dahan, M., and Triller, A. (2006) Imaging the lateral diffusion of membrane molecules with quantum dots. *Nat. Protoc.1*, 2628-2634.
(21) Orlandi, P. A., and Fishman, P. H. (1998) Filipin-dependent inhibition of cholera toxin: evidence for toxin internalization and activation through caveolae-like domains. *J. Cell Biol.141*, 905-915.
(22) Balasubramanian, N., Scott, D. W., Castle, J. D., Casanova, J. E., and Schwartz, M. A. (2007) Arf6 and microtubules in adhesion-dependent trafficking of lipid rafts. *Nat. Cell Biol.9*, 1381-1391.
(23) Esposito, A., Dohm, C. P., Kermer, P., Bahr, M., and Wouters, F. S. (2007) alpha-Synuclein and its disease-related mutants interact differentially with the microtubule protein tau and associate with the actin cytoskeleton. *Neurobiol. Dis.26*, 521-531.
(24) Adkins, E. M., Barker, E. L., and Blakely, R. D. (2001) Interactions of tryptamine derivatives with serotonin transporter species variants implicate transmembrane domain I in substrate recognition. *Mol. Pharmacol.59*, 514-523.
(25) Chang, J. C., Tomlinson, I. D., Warnement, M. R., Iwamoto, H., DeFelice, L. J., Blakely, R. D., and Rosenthal, S. J. (2011) A fluorescence displacement assay for antidepressant drug discovery based on ligand-conjugated quantum dots. *J. Am. Chem. Soc.133*, 17528-17531.
(26) Steiner, J., Carneiro, A., Wright, J., Matthies, H., Prasad, H., Nicki, C., Dostmann, W., Buchanan, C., Corbin, J., Francis, S., and Blakely, R. (2009) cGMP-dependent protein kinase Ia associates with the antidepressant-sensitive serotonin transporter and dictates rapid modulation of serotonin uptake. *Mol. Brain2*, 26.
(27) Nirmal, M., Dabbousi, B. O., Bawendi, M. G., Macklin, J. J., Trautman, J. K., Harris, T. D., and Brus, L. E. (1996) Fluorescence intermittency in single cadmium selenide nanocrystals. *Nature383*, 802-804.
(28) Adkins, E. M., Samuvel, D. J., Fog, J. U., Eriksen, J., Jayanthi, L. D., Vaegter, C. B., Ramamoorthy, S., and Gether, U. (2007) Membrane mobility and microdomain association of the dopamine transporter studied with fluorescence correlation spectroscopy and fluorescence recovery after photobleaching. *Biochemistry46*, 10484-10497.
(29) Schutz, G. J., Kada, G., Pastushenko, V. P., and Schindler, H. (2000) Properties of lipid microdomains in a muscle cell membrane visualized by single molecule microscopy. *EMBO J.19*, 892-901.

(30) Allen, J. A., Halverson-Tamboli, R. A., and Rasenick, M. M. (2007) Lipid raft microdomains and neurotransmitter signalling. *Nat. Rev. Neurosci.8*, 128-140.
(31) Kenworthy, A. K., Petranova, N., and Edidin, M. (2000) High-resolution FRET microscopy of cholera toxin B-subunit and GPI-anchored proteins in cell plasma membranes. *Mol. Biol. Cell11*, 1645-1655.
(32) Saxton, M. J. (2007) A biological interpretation of transient anomalous subdiffusion. I. Qualitative model. *Biophys. J.92*, 1178-1191.
(33) Martin, D. S., Forstner, M. B., and Kas, J. A. (2002) Apparent subdiffusion inherent to single particle tracking. *Biophys. J.83*, 2109-2117.
(34) Simons, K., and Gerl, M. J. (2010) Revitalizing membrane rafts: new tools and insights. *Nat. Rev. Mol. Cell Biol.11*, 688-699.
(35) Veenstra-VanderWeele, J., Muller, C. L., Iwamoto, H., Sauer, J. E., Owens, W. A., Shah, C. R., Cohen, J., Mannangatti, P., Jessen, T., Thompson, B. J., Ye, R., Kerr, T. M., Carneiro, A. M., Crawley, J. N., Sanders-Bush, E., McMahon, D. G., Ramamoorthy, S., Daws, L. C., Sutcliffe, J. S., and Blakely, R. D. (2012) Autism gene variant causes hyperserotonemia, serotonin receptor hypersensitivity, social impairment and repetitive behavior. *Proc. Natl. Acad. Sci. U.S.A.109*, 5469-5474.
(36) Zhu, C. B., Hewlett, W. A., Feoktistov, I., Biaggioni, I., and Blakely, R. D. (2004) Adenosine receptor, protein kinase G, and p38 mitogen-activated protein kinase-dependent up-regulation of serotonin transporters involves both transporter trafficking and activation. *Mol. Pharmacol.65*, 1462-1474.
(37) Zhu, C. B., Carneiro, A. M., Dostmann, W. R., Hewlett, W. A., and Blakely, R. D. (2005) p38 MAPK activation elevates serotonin transport activity via a trafficking-independent, protein phosphatase 2A-dependent process. *J. Biol. Chem.280*, 15649-15658.
(38) Zhu, C. B., Blakely, R. D., and Hewlett, W. A. (2006) The proinflammatory cytokines interleukin-1beta and tumor necrosis factor-alpha activate serotonin transporters. *Neuropsychopharmacology31*, 2121-2131.
(39) Chanrion, B., Mannoury la Cour, C., Bertaso, F., Lerner-Natoli, M., Freissmuth, M., Millan, M. J., Bockaert, J., and Marin, P. (2007) Physical interaction between the serotonin transporter and neuronal nitric oxide synthase underlies reciprocal modulation of their activity. *Proc. Natl. Acad. Sci. U.S.A.104*, 8119-8124.
(40) Carneiro, A. M. D., Cook, E. H., Murphy, D. L., and Blakely, R. D. (2008) Interactions between integrin aIIbb3 and the serotonin transporter regulate serotonin transport and platelet aggregation in mice and humans. *J. Clin. Invest.118*, 1544-1552.
(41) Kaufmann, K. W., Dawson, E. S., Henry, L. K., Field, J. R., Blakely, R. D., and Meiler, J. (2009) Structural determinants of species-selective substrate recognition in human and Drosaphila serotonin transporters revealed through computational docking studies. *Proteins74*, 630-642.
(42) Gussin, H. A., Tomlinson, I. D., Little, D. M., Warnement, M. R., Qian, H. H., Rosenthal, S. J., and Pepperberg, D. R. (2006) Binding of muscimol-conjugated quantum dots to GABA(c) receptors. *J. Am. Chem. Soc.128*, 15701-15713.
(43) Kovtun, O., Tomlinson, I. D., Sakrikar, D. S., Chang, J. C., Blakely, R. D., and Rosenthal, S. J. (2011) Visualization of the cocaine-sensitive dopamine transporter with ligand-conjugated quantum dots. *ACS Chem. Neurosci.2*, 370-378.
(44) Wang, Q., Zhang, X., Zhang, L., He, F., Zhang, G., Jamrich, M., and Wensel, T. G. (2008) Activation-dependent hindrance of photoreceptor G protein diffusion by lipid microdomains. *J Biol Chem283*, 30015-30024.

(45) Nishimura, S. Y., Vrljic, M., Klein, L. O., McConnell, H. M., and Moerner, W. E. (2006) Cholesterol depletion induces solid-like regions in the plasma membrane. *Biophys. J.90*, 927-938.
(46) Lalovic, A., Levy, E., Luheshi, G., Canetti, L., Grenier, E., Sequeira, A., and Turecki, G. (2007) Cholesterol content in brains of suicide completers. *Int. J. Neuropsychopharmacol.10*, 159-166.
(47) Vevera, J., Fisar, Z., Kvasnicka, T., Zdenek, H., Starkova, L., Ceska, R., and Papezova, H. (2005) Cholesterol-lowering therapy evokes time-limited changes in serotonergic transmission. *Psychiatry Res.133*, 197-203.
(48) Renshaw, P. F., Parsegian, A., Yang, C. K., Novero, A., Yoon, S. J., Lyoo, I. K., Cohen, B. M., and Carlezon, W. A., Jr. (2009) Lovastatin potentiates the antidepressant efficacy of fluoxetine in rats. *Pharmacol. Biochem. Behav.92*, 88-92.
(49) Eisensamer, B., Uhr, M., Meyr, S., Gimpl, G., Deiml, T., Rammes, G., Lambert, J. J., Zieglgansberger, W., Holsboer, F., and Rupprecht, R. (2005) Antidepressants and antipsychotic drugs colocalize with 5-HT3 receptors in raft-like domains. *J. Neurosci.25*, 10198-10206.
(50) Zhu, C. B., Lindler, K. M., Campbell, N. G., Sutcliffe, J. S., Hewlett, W. A., and Blakely, R. D. (2011) Colocalization and regulated physical association of presynaptic serotonin transporters with a3 adenosine receptors. *Mol. Pharmacol.80*, 458-465.
(51) Quick, M. W. (2003) Regulating the conducting states of a mammalian serotonin transporter. *Neuron40*, 537-549.
(52) Hong, W. C., and Amara, S. G. (2010) Membrane cholesterol modulates the outward-facing conformation of the dopamine transporter and alters cocaine binding. *J. Biol. Chem.285*, 32616-32626.
(53) Zhu, C. B., Lindler, K. M., Owens, A. W., Daws, L. C., Blakely, R. D., and Hewlett, W. A. (2010) Interleukin-1 receptor activation by systemic lipopolysaccharide induces behavioral despair linked to MAPK regulation of CNS serotonin transporters. *Neuropsychopharmacology35*, 2510-2520.
(54) Veluthakal, R., Chvyrkova, I., Tannous, M., McDonald, P., Amin, R., Hadden, T., Thurmond, D. C., Quon, M. J., and Kowluru, A. (2005) Essential role for membrane lipid rafts in interleukin-1beta-induced nitric oxide release from insulin-secreting cells: potential regulation by caveolin-1^{+}. *Diabetes54*, 2576-2585.

CHAPTER 5

Summary and Future Perspective

5.1 Introduction

Plasma membrane, the physical barrier of the smallest living unit, a single cell, consists mainly of bilayer phospholipids with embedded proteins. It not only allows for accomplishing vital biological functions but also governs the movement of materials and signals in and out of the cell. For the past four decades, the most well-known model of plasma membrane is the fluid mosaic model,[1] in which the membrane proteins are viewed as freely floating boats in the phospholipid "sea." However, recent investigations have found that the diffusivity of cellular membranes in eukaryotes has fewer degrees of freedom as was predicted in the fluid mosaic model, suggesting the regulatory role of the surrounding lipid environment in membrane signaling/interaction.[2] It has become increasingly clear that the cell membrane is far from homogeneous but contains various small microdomains for specialized functions.[2-4] In many cases, the cholesterol-enriched membrane microdomains, also known as lipid rafts, were indicated to participate in cellular signaling by providing the microenvironment necessary for complex protein-protein interactions.[4, 5] In addition, recent biochemical studies demonstrated a connection between membrane microdomains and the cytoskeleton. This connection found to influence membrane compartmentalization,[2, 5] further suggests the role of membrane microdomains in the secretary and endo-exocytotic pathways. Together, these largely underdeveloped properties explain the recent emergence of the studies in membrane dynamics and vesicle trafficking.

To date, various techniques based on optical microscopy have been created to allow observation and quantification of membrane dynamics. These approaches can be

generally categorized into two groups based on the collected data types: the first group, such as fluorescence recovery after photobleaching (FRAP) and conventional immunofluorescence microscopy, is developed to depict the ensemble average response of the movement of fluorescently labeled molecules; while the second, known as single molecule microscopy, is designed to extract diffusion parameters from probing multiple single events.[6] The ensemble-averaging approach, although convenient and widely used, presents an obvious disadvantage regarding the representativeness of the experimental data: the lost of sub-population distribution in the ensemble average.[6] To characterize the diffusion rates in different domains of the plasma membrane, the single-molecule tracking (SMT) approach is clearly a better choice.[2] The basis of SMT is to follow the real-time movement of individual biological targets using high-speed fluorescent microscopy (typical time resolution: 10-100 milliseconds) with high spatial resolution (at the nanometer scale), resulting in a map of the real-time dynamics upon observing many individual events. Based on the above definition, an ultimate sensitivity is required, which allows individual single molecules to be monitored in a picoliter- to femtoliter-sized microscope sampling volume. A fundamental limit is, however, subject to Abbe's optical diffraction limit, which is ~ 250 nm in the visible spectrum. To achieve a sub-pixel localization in SMT, the FIONA (*F*luorescence *I*maging with *O*ne-*N*anometer *A*ccuracy) approach is typically performed (Figure 5.1).[7] Single emitters viewed through a microscope produce an Airy disc diffraction pattern in the image plane. In the FIONA approach, this pattern is analyzed in terms of the point spread function (PSF) where the localized centroid is determined by fitting the PSF to a 2-D Gaussian profile with a least-squares estimator:

$$I_{xy} = A_0 + A \cdot e^{-\frac{(x-x_0)^2+(y-y_0)^2}{w^2}} \qquad [1]$$

, where I_{xy} is the intensity of the pixel, x_0 and y_0 is the designated local maximum coordinates of the Gaussian, A is the amplitude of the signal with local background A_0, and w is the width of the Gaussian curve. It is important to note that the coordinate (x_0, y_0) acquired by fitting function [1] is not a true position but only an estimate; the accuracy is strongly dependent upon the respective signal-to-noise ratio (SNR), which is defined as:

$$SNR = \frac{I_0}{\sqrt{\sigma_{bg}^2 + \sigma_{I_0}^2}} \quad [2]$$

, where I_0 is the maximum signal intensity above background, σ_{bg}^2 is the variance of the background intensity values, and $\sigma_{I_o}^2$ is the true variance of the maximum signal intensity above the background. However, common organic fluorophores used in single-molecule imaging have a very limited photon yield and a narrow Stokes shift(the difference between excitation and emission wavelengths), which makes them difficult to produce a sufficient SNR for single molecule imaging. In addition, photobleaching associated with organic fluorophores prevents their usefulness in long-term monitoring. Hence, these shortcomings associated with organic fluorophores places a high demand for new fluorescent materials for single-molecule tracking.

Fluorescent quantum dots (QDots) are semiconductor nanomaterials with a size in the range of 2-10 nanometer, smaller than their Bohr exciton radius, which makes QDots display discrete, quantized energy levels. Extraordinary optical properties in QDots include high quantum yield, broad adsorption with monochromatic narrow emission, high molar extinction coefficients, and a large Stokes shift (for review, see Rosenthal *et al.*[8]).Over the past decade, QDots have been popularly used in biological labeling applications (for review, see Chang *et al.*[9]). As mentioned, the sub-pixel

localization in single molecule imaging is dependent upon the SNR, which is highly correlated to the total photons emitted and the Stokes shift of a single emitter. Unlike conventional fluorescent dyes, these two properties make QDots much more advantageous. Additionally the superior photostability makes QDots particularly useful for long-term tracking studies (minutes to hours). Since its emergence in the biological imaging field, single QDot imaging approach has played an essential role in investigating cellular signaling and regulation. In the following sections, we highlight recent biological applications using single QDot techniques, in particular the applications in exploring membrane dynamics and intracellular trafficking.

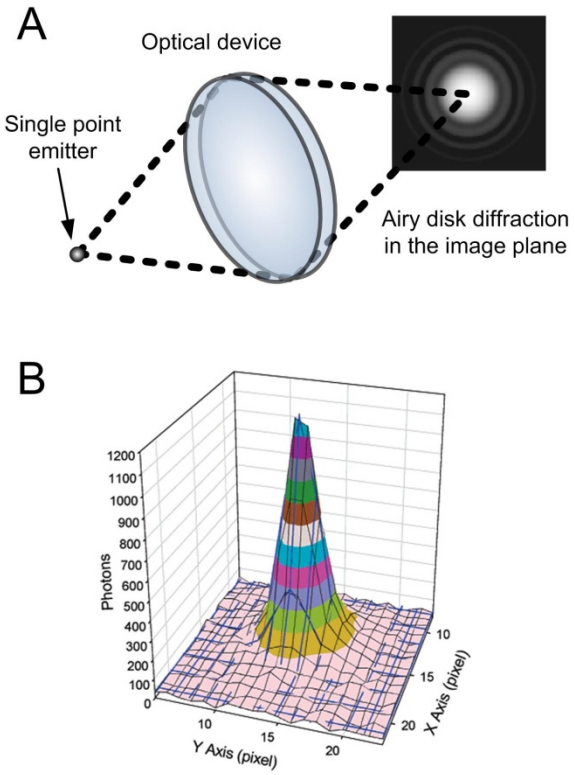

Figure 5.1 Schematic representation of the diffraction pattern from a point emitter passed through an optical device.(A) Owing to diffraction, the smallest distance to which an imaging system can optically resolve separate light sources is limited by the size of the Airy disk. (B) Fitting a 2D Gaussian function to the PSF of a single emitter yields nanometer precision, termed Fluorescence Imaging with One Nanometer Accuracy (FIONA). Adapted from reference (7).

5.2 Mapping Receptor Membrane Diffusion

By utilizing the superior fluorescent properties of QDots and a highquantum-efficiency back-illuminated electron multiplying charge-coupled device (EMCCD) camera, Dahan *et al.* first reported the use of single QDot imaging approach to investigating endogenous glycine receptors (GlyR) at the surface of cultured rat spinal cord neurons.[10] Importantly, the authors were able to characterize multipleGlyR diffusion domains in relation to the synaptic, perisynaptic, and extrasynaptic GlyR localization, which was unable to be determined by conventional ensemble methods. Since then, several studies inspired by this work are directed toward addressing the specific biological functions of membrane protein sub-populations.

In line with the above study, noticeable efforts in single QDot approach were made in recent years on the studies of the cholesterol and ganglioside GM1-enriched membrane microdomains.[4] Pinaid *et al.* developed a raft-associated glycosyl-phosphatidyl-inositolanchored avidin test probe (Av-GPI) to study the correlation between the diffusion of individual Av-GPI and the location of GM1-rich microdomains and caveolae in the transfected HeLa cells.[11] Single QDot-labeled Av-GPI complexes were found to exhibit dynamical partition in and out of GM1-rich microdomains in a cholesterol-dependent manner. In a native, non-transfected neuronal cell line, we used single QDot-labeled cholera toxin B subunit (CTxB) to investigate the diffusion dynamics and membrane compartmentalization of the GM1-rich microdomains.[12] Diffusion measurements revealed that single QDot-labeled CTxB-GM1 complexes undergo slow, confined lateral diffusion with a diffusion coefficient of $\sim 7.87 \times 10^{-2}$ μm^2/sec and a confinement domain about 200 nm in size. Further analysis of the trajectories showed lateral confinement persisting on the order of tens of seconds, comparable to the time scales of the majority of cellular signaling and biological reactions.

The importance of lipid rafts in membrane protein signaling and regulation was also tested with the single QDot approach. In a recent publication, we reported the first use of ligand-conjugated single QDots for the investigation of membrane dynamics of serotonin transporter, a primary target for antidepressant medications.[13] Two types of subpopulations of SERT were found in living neuronal cells: one exhibits relatively free diffusion and the other localize to cholesterol and GM1 ganglioside-enriched microdomains, which displays restricted mobility. Disruption of membrane rafts by gentle cholesterol depletion results in an increase of single SERT mobility and a loss of SERT confined diffusion (Figure 5.2). In addition, mobilization of transporters arises from a p38 MAPK-dependent untethering of the SERT C-terminus from the juxtamembrane actin cytoskeleton. This study demonstrates the potential of ligand-conjugated QDots for analysis of the behavior of single membrane proteins in relation to critical cellular signaling and regulation.

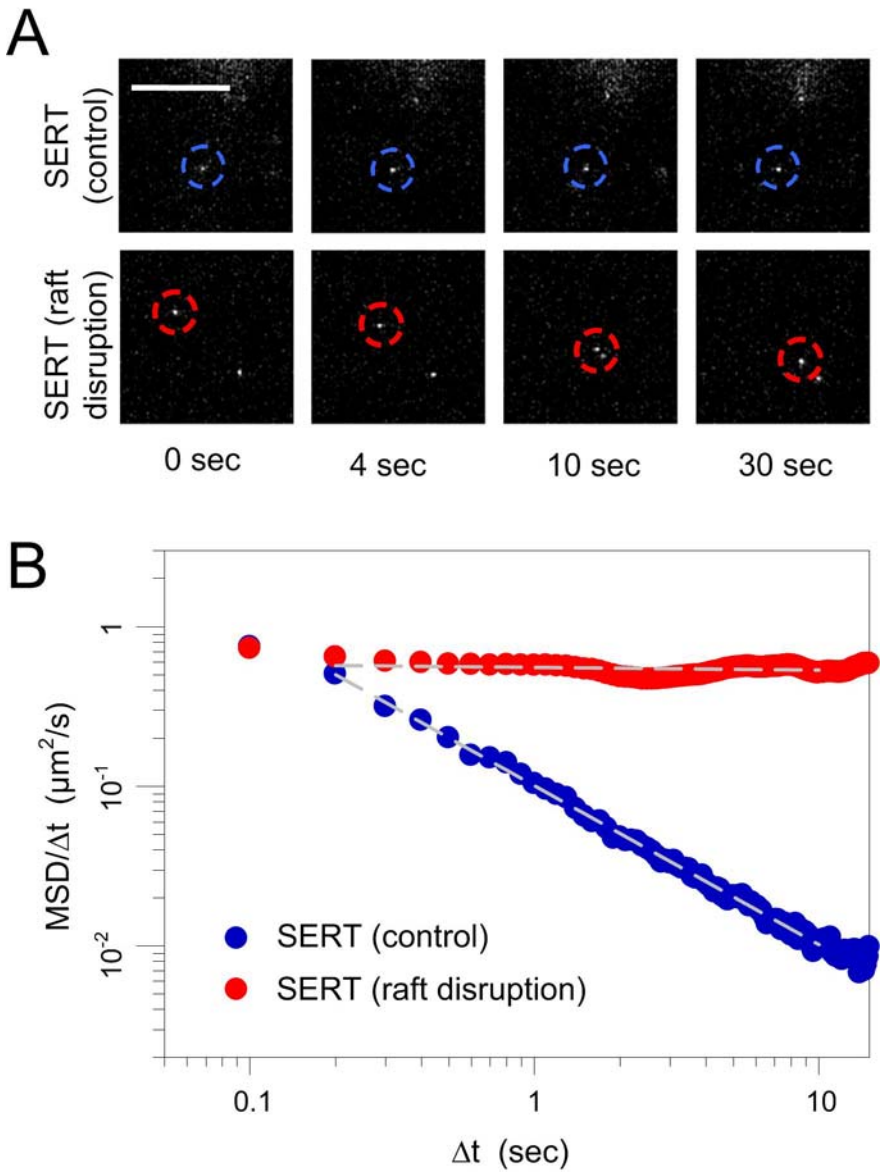

Figure 5.2 Single QDot-SERT tracking in living serotonergic RN46A cells under control and lipid raft-disrupted conditions. (A) Temporal profile of representative QDot-labeled, single SERTs with and without lipid raft disruption. Note the more mobile behavior of the single QDot after lipid raft disruption. (B) Comparison of the mean squared displacement over time of the representative single QDots in (A). Single SERT under a lipid raft-disrupted condition shows the pattern expected of free diffusion whereas single SERT from untreated cells demonstrates a pattern consistent with confined lateral diffusion. Adapted from reference (13).

5.3 Endosomal Trafficking and Endocytosis

Endosomal trafficking and endocytosis are known to be highly heterogeneous in space and time. However, it is a challenging field of research due to technical difficulties of visualizing the processes in real-time. Cui *et al.* presented a milestone study in which the real-time movement of nerve growth factor (NGF) axonal transport was followed with single QDot imaging approach in live rat dorsal root ganglion (DRG) neurons.[14] To achieve a monovalent presentation of NGF dimer on the QDot surface, a stoichiometric ratio of NGF to QDot of 1:1.2 was adapted in their conjugation procedure. In a clever setup, NGF–QDot conjugates were first added to the microfluidic chamber containing distal axons of DRG neurons and allowed to bind and form complexes with NGF receptors and undergo subsequent internalization into early endosomes. Interestingly, endosomes containing NGF–QDots were found to exhibit 'stop-and-go' retrograde transport toward the neuronal cell body with an average speed of 1.31 ± 0.03 μm/sec (Figure 5.3A). The presented research also underscores the potential utility of single QDot nanoconjugates for intracellular applications as the real-time observation of intracellular endosome movement is achieved in this study.

The same technique, with emphasis on the internalization measurement, was successfully extended by Fichter *et al.* to quantify the endocytosis of G-protein–coupled receptors (GPCRs), the biggest protein superfamily and the major drug targets.[15] In this study, a small group of 5-HT_{1A} receptors, a type of metabotropic G protein-coupled receptors, were labeled with single QDots and, importantly, the authors found that single QDot probes do not interfere with the internalization kinetics of receptors in live cells. In their analysis, sustained 5-HT exposure elicited receptor internalization that increased from 20 to ~ 60 – 70 % within 60 min, indicating sustained receptor internalization in response to continuous 5-HT stimulation (Figure 5.3B). Further research may allow for elucidating the actions of GPCR-targeted therapeutics.

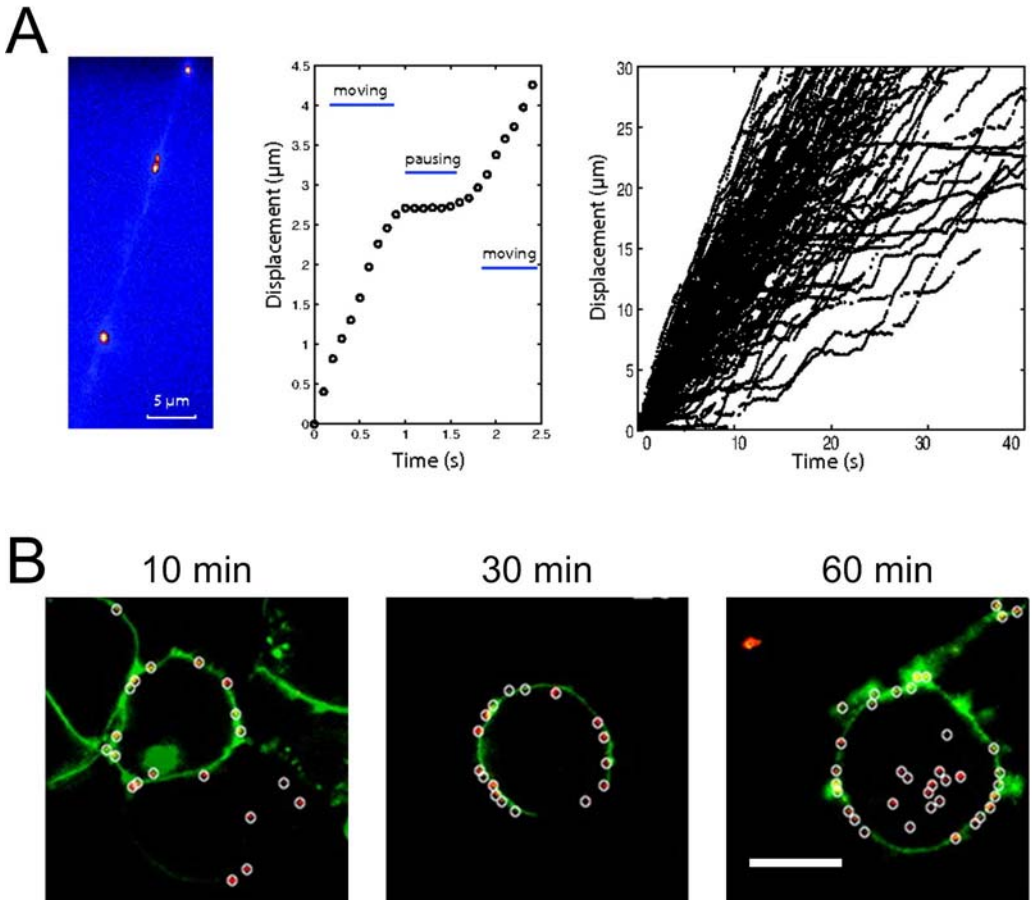

Figure 5.3 Single QDot imaging for endosomal trafficking and endocytosis(A) Live imaging reveals that single QD-NGF containing endosomes exhibit stop-and-go motion. Left: A typical axon showing four moving endosomes that contained QD-NGF in pseudocolor. Center: Trajectory of a typical endosome, showing a switch between moving and pausing. Right: Trajectories of 120 endosomes showing that the moving speed and the duration of pauses vary greatly from one endosome to another. Adapted from reference (14). (B) Cellular internalization of single QDot-labeled serotonin receptor complexes during continuous serotonin stimulation in transfected N2a cells. Red: QDot probe; green, plasma membrane, visualized with DiO. The scale bar is 10 μm. Adapted from reference (15).

5.4 Dynamic Processes of Intracellular Targets

Recently, several groups came up with brilliant ideas to take advantage of the nanoscale sized single QDots as a "molecular ruler" in measuring the dynamics of intracellular processes. In an exciting example, Zhang *et al.* used single QDot fluorescence to investigate the molecular mechanism of vesicular secretion of neurotransmitters in the living neurons.[16] Since a single synaptic vesicle is so small (lumen diameter ~ 24 nm) that it can only load one QDot (~ 15 nm) at a time, the authors used single QDot imaging to see if a full-collapse fusion (FCF) or a kiss-and-run fusion (K&R) is taking place during neuron firing; the former refers to a preloaded single QDot being released, while the latter depicts the single QDot being trapped in the vesicle. In addition to the size of the QDots, the authors also cleverly took advantage of another important character of single QDot, the pH-dependent fluorescence fluctuation, where the author found that the QDot fluorescence would increase by ~ 15% if the single QDots move from intravesicular space (pH ~ 5.48) to extracellular space (pH ~ 7.34). As such, in the K&R one could only capture the increase of QDot fluorescence but not the escape of QDot, while in the FCF similar Qdot brightening would appear followed by a complete loss of signal as the QDot escaped from the synaptic vesicle. Using this sophisticated yet elegant approach, a stochastic vesicle dynamic is established in which the authors successfully correlate the increased neurotransmitter release probability with a higher prevalence of K&R.

Another excellent example under this category is the use of peptide-conjugated QDots as a cargo to investigate the intracellular nuclear transport via nuclear pore complex (NPC).[17] It is known that NPC acts as the gatekeeper for traffic into and out of the nucleus. Unlike small molecules which can passively diffuse through NPC, the transportation of larger protein-based cargo into nucleus requires a dedicated transport mechanism. Generally the signal-dependent nuclear transport is facilitated by

nucleoplasmic shuttling receptors of the importins/karyopherins, which are associated with Ran GTPase. In the study reported by Lowe *et al.*, the authors conjugated the importin-β binding domain to QDots (IBB-QDot) and used single IBB-QDots as pseudo cargos to visualize the nuclear translocation process (Figure 5.4).[17] Additionally, the conjugated IBB-QDot complexes have a mean hydrodynamic diameter of 18 ± 4 nm, similar to the size of native cargos that translocate into nucleus via receptor-driven transport through NPC. Remarkably, with the precise single QDot imaging analysis the authors were, for the first time, able to calculate the multi-step processes of Ran GTPase-dependent importthrough NPC:cargo capture (25% success rate), filtering and translocation (80% success rate), and cargo release into the nucleus (50% success rate with Ran; > 99% abort without Ran).

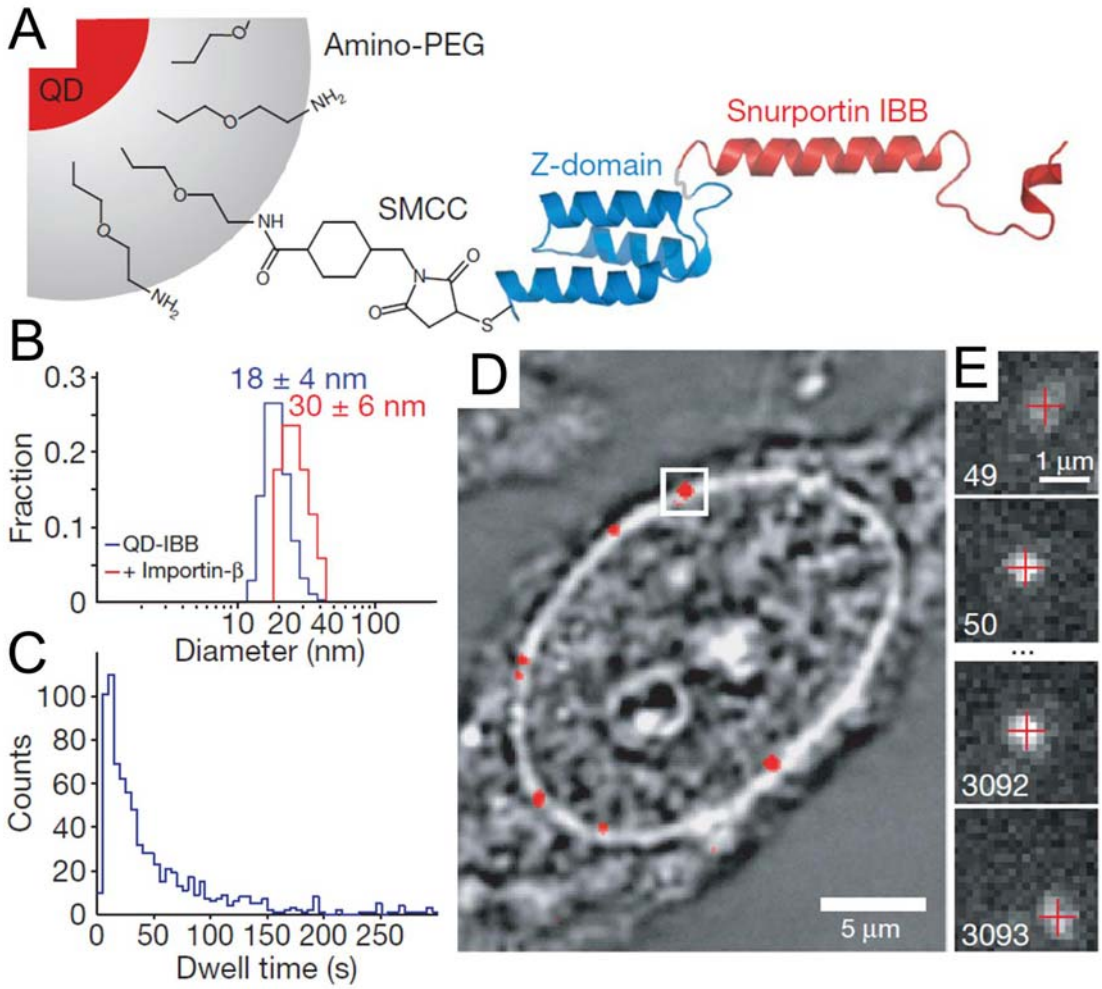

Figure 5.4 Characterization of nucleocytoplasmic transport with single QDot approach. (A) Diagram of QDot-based cargo. The snurportin-1 IBB/Z-domain fusion protein is coupled via a bifunctional SMCC crosslinker to the amino-PEG polymer coat of a fluorescent QDot. The three helix Z-domain acts as a spacer to correctly present the IBB for biological function. (B) Dynamic light scattering size distributions of QDot-IBB cargos in the presence and absence of importin-β. (C) Dwell time distribution of all QDot interactions with the NPC. The time axis is truncated at 300 sec. (D) Bright-field image of a nucleus with a QDot fluorescence image (with background subtraction applied) overlaid in red. A single QDot cargo at the nuclear envelope is boxed. (E) Individual consecutive frames from a single-molecule experiment showing the arrival (first frame) from the cytoplasm and departure (final frame) of the cargo into the nucleus. The centroids determined from the fitting of the PSF are overlaid as red crosses. Frame numbers are at the bottom left hand corner of each frame. Movies were captured at 40 Hz. Adapted from reference (17).

5.5 Single-Quantum Dot FRET

Fluorescence resonance energy transfer (FRET) is a photophysical process where the excited-state energy from a donor fluorophore can be non-radiatively transferred to a nearby acceptor fluorophore. The energy transfer is through a dipole-dipole coupling and the obtained distance has to be in the range of 1-10 nm (for a review of FRET principle, see Selvin[18]). Since the initial works of Willard *et al.*[19] and Medintz *et al.*[20] demonstrating the potential of QDot as a FRET donor for biosensing, similar concepts have been applied to various biological applications such as explosive 2,4,6-trinitrotoluene (TNT) detection,[21] proteolytic activity assay,[22-25] and molecular sensing of microenvironmental changes in pH,[26, 27] and calcium ions.[25]

The bottleneck in single molecule FRET studies is the low SNR. However, with the assistance of high SNR QDot probes Zhang *et al.* first developed a FRET-based single QDot nanosensor for specific nucleic acid detection (Figure 5.5).[28] A sandwich-type hybrid structure was designed to detect the target sequence by the presence of a biotin-labeled capture probe and a Cy5 labeled reporter probe. The hybridized sequence assembly then self-assembles on the streptavidin-conjugated QDot and thus forming a FRET donor–acceptor ensemble. Extremely high femtomole sensitivity was achieved in this study. This is about 100 times higher than the molecular beacon approach, the gold standard FRET method for nucleic acid detection. However, we wish to note that, despite various successes in molecular sensing, single QDot FRET probes are mostly limited in biochemical assays. To the best of our knowledge, studies have not yet been revealed to demonstrate live cell imaging applications.

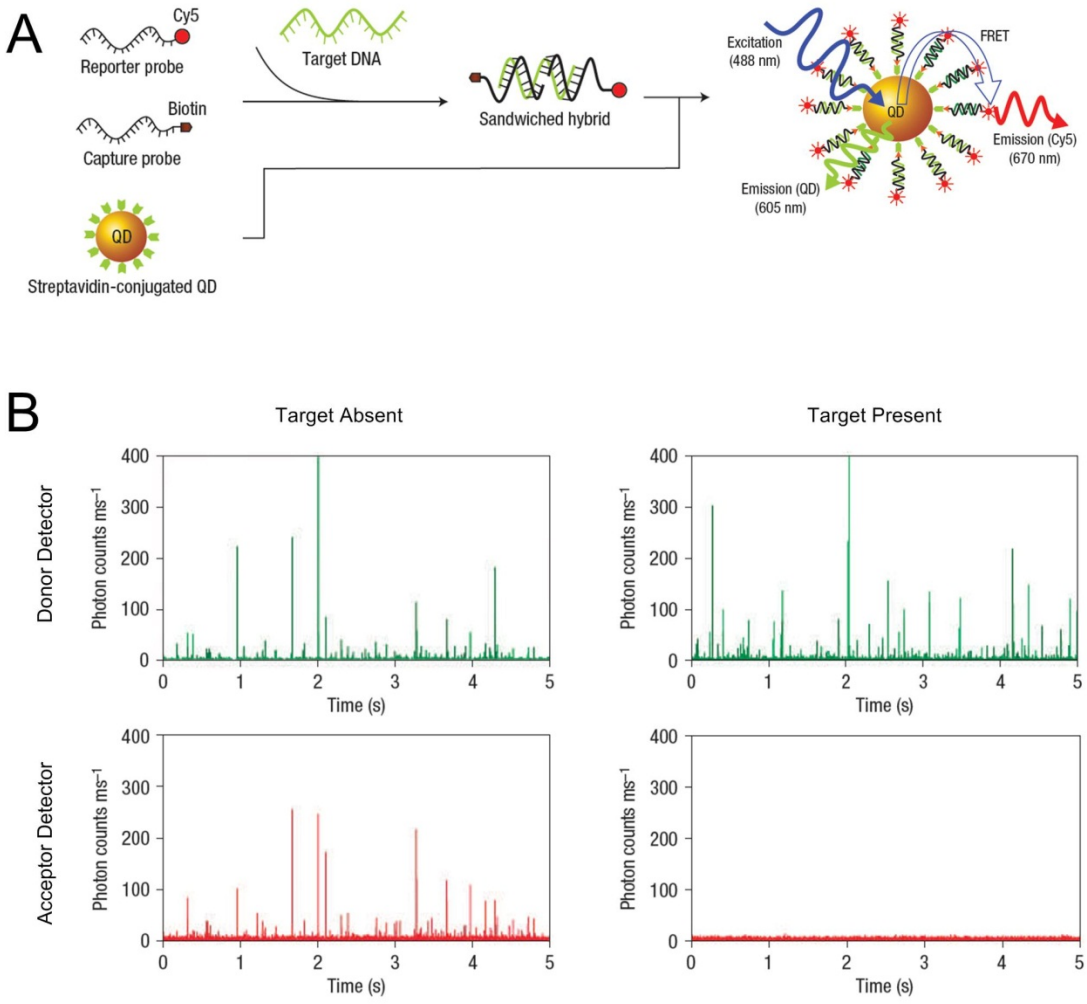

Figure 5.5 Single QDot-FRET for DNA detection (A) Conceptual scheme showing the formation of a single-QDdot based DNA nanosensor in the presence of targets. The resulting assembly brings the fluorophore acceptors and the QDot donor into close proximity, leading to energy transfer from QDot to acceptors. (B) Representative traces of fluorescent bursts detected with QDot nanosensors. Fluorescent signals are acquired by both the donor and the acceptor detectors. In the presence of targets, fluorescent bursts were detectable in both donor and acceptor detectors. When targets were absent, fluorescent bursts were only detected by the donor detector, not by the acceptor detector. Adapted from reference (28).

5.6 3-D Single Quantum Dot Tracking

While the application of live cell 3-D single QDot tracking is still in its infancy, recent advances in ultrasensitive detectors, in particular the high-speed ultrasensitive EMCCD cameras, offer great promise in this field. Two common approaches have been taken toward the construction of 3-D single QDot trajectories in real-time. Thefirst is to conduct multifocal plane imaging with a widefield fluorescent microscope. Photons generated from a targeted single QDot are split into multiple paths. In each light-path, the signal is turned at a specific calibrated distance that allows each detector to only reflect a specific focal plane (z) information.[29] An obvious advantage of this technique is to simultaneously track multiple focal planes over a large z-range, which enables the observation of whole cell events in real-time. By simultaneous projecting single QDot position into 4 EMCCD cameras, a recent report from Ram *et al.* demonstrated an amazing 10 micron z-range in 3-D single QDot tracking of the transferrin receptor in a live epithelial cell monolayer.[29] Although this approach is relatively straightforward and effective, it requires multiple high-end EMCCD cameras, which may not be a preferred method for general laboratory use from a cost-effectiveness point of view.

A different kind of 3-D tracking approach, which also uses a widefield fluorescent microscope, is aimed at 3-D localization from a single detector. An outstanding example established by the Moerner Lab is to engineer the PSF of a single emitter through a spatial light modulator.[30, 31] This enables the display of additional Z-directional information on a single detector, where the single emitter exhibits two lobes in the image plane that rotate continuously around the optical axis with propagation, terms “double-helix point spread function (DH-PSF)” (Figure 5.6A).In a recent study with the DH-PSF based 3-D fluorescent microscopy, Thompson *et al.* reported a nanometer localization accuracy along the x, y, and z directions, which allows following 3-D movement of a single QDot-labeled structure inside a living cell.[31] Interestingly, the 3-D single QDot

trajectory showed a variety of diffusive and linear transport characteristics in live cells (Figure 5.6B), which would be otherwise missing if processed with 2-D tracking.

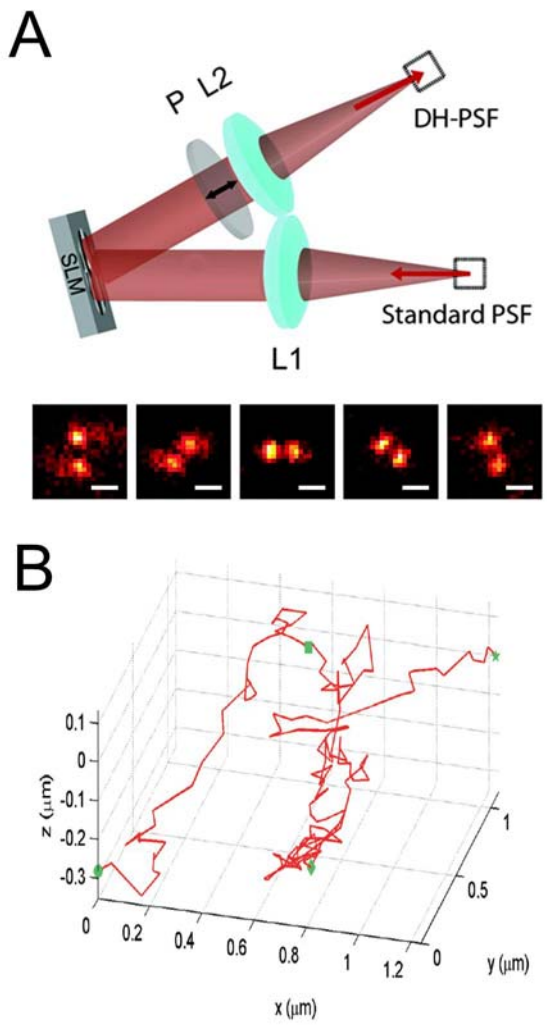

Figure 5.6 3-D single QDot tracking with DH-PSF imaging approach. (A) schematic of the DH-PSF imaging system. L1 and L2 are focal-length-matched achromatic lenses, and SLM is a liquid crystal spatial light modulator. Bottom images are a bead emitting on average 2000 photons/frame shown at five different axial positions (from left to right -960, -510, -20, 510, and 970 nm). Scale bar is 1 μm. (B) 3-D plot of a single QDot trajectory in live COLO205 cells, showing a variety of diffusive and linear transport characteristics. Adapted from reference (31).

5.7 Conclusion and Future Perspective

Since the first demonstrations in biological imaging, water-soluble QDots have become popular probes for various biological imaging and detection applications.[32, 33] Their unique photophysical properties render them particularly valuable for revealing dynamic biological processes. However, owing to the size and the surface chemistry, even single QDots can cause multivalent binding, which is a major drawback in regards to QDots for single molecule studies.[34] Recently, the preparation of monovalent QDots was demonstrated by Howarth et al., where each compact QDot was bound to only a single copy of monovalent streptavidin to enable the monovalent QDot-receptor labeling in living cells.[35] Without a doubt, if commercially available, this material will find many applications in the field of single QDot imaging.

Additionally, the pros and cons of QDot blinking in single QDot imaging have been previously discussed in great detail.[36] On one hand, this property is popularly used as a criterion for identifying single QDots in live cells.[10-17] On the other hand, it raises concern on the discontinuous trajectory of a single QDot tracking approach due to the temporary disappearance of the target position from the blinking events.[37] We would like to indicate that the synthesis of non-blinking QDots based on a multishell approach[38, 39] and gradient alloyed core/shell structure[37] were recently reported. Researchers are currently taking advantage of the non-blinking QDots in single QDot tracking experiments.[40] We can expect the biological applications of non-blinking QDots to increase.

In summary, the biological applications of QDots have moved from a simple alternative to fluorescent dyes to more specialized topics for advanced biological research. This is particularly obvious in the cases of the recent development in single QDot applications. Although there are some limitations due to the physical nature of the QDots, advances in QDot synthesis and surface chemistry show significant potential to

eliminate these pitfalls. Considering the applications of a single QDot approach in the past few years, we are optimistic that the use of single QDots will largely advance our understanding in the biological research field.

5.8 References

(1) Singer, S. J.; Nicolson, G. L., The fluid mosaic model of the structure of cell membranes. *Science* **1972,***175*, 720-731.

(2) Ritchie, K.; Shan, X. Y.; Kondo, J.; Iwasawa, K.; Fujiwara, T.; Kusumi, A., Detection of non-Brownian diffusion in the cell membrane in single molecule tracking. *Biophys J* **2005,***88*, 2266-77.

(3) Maxfield, F. R., Plasma membrane microdomains. *Curr Opin Cell Biol* **2002,***14*, 483-7.

(4) Allen, J. A.; Halverson-Tamboli, R. A.; Rasenick, M. M., Lipid raft microdomains and neurotransmitter signalling. *Nat. Rev. Neurosci.* **2007,***8*, 128-40.

(5) Simons, K.; Gerl, M. J., Revitalizing membrane rafts: new tools and insights. *Nat. Rev. Mol. Cell Biol.* **2010,***11*, 688-99.

(6) Moerner, W. E.; Fromm, D. P., Methods of single-molecule fluorescence spectroscopy and microscopy. *Rev. Sci. Instrum.* **2003,***74*, 3597-3619.

(7) Yildiz, A.; Selvin, P. R., Fluorescence imaging with one nanometer accuracy: application to molecular motors. *Acc. Chem. Res.* **2005,***38*, 574-82.

(8) Rosenthal, S. J.; McBride, J.; Pennycook, S. J.; Feldman, L. C., Synthesis, surface studies, composition and structural characterization of CdSe, core/shell and biologically active nanocrystals. *Surf. Sci. Rep.* **2007,***62*, 111-157.

(9) Chang, J. C.; Kovtun, O.; Blakely, R. D.; Rosenthal, S. J., Labeling of neuronal receptors and transporters with quantum dots. *WIREs Nanomed. Nanobiotechnol.* **2012,***4*, 605-619.

(10) Dahan, M.; Levi, S.; Luccardini, C.; Rostaing, P.; Riveau, B.; Triller, A., Diffusion dynamics of glycine receptors revealed by single-quantum dot tracking. *Science* **2003,***302*, 442-445.

(11) Pinaud, F.; Michalet, X.; Iyer, G.; Margeat, E.; Moore, H.-P.; Weiss, S., Dynamic partitioning of a glycosyl-phosphatidylinositol-anchored protein in glycosphingolipid-rich microdomains imaged by single-quantum dot tracking. *Traffic* **2009,***10*, 691-712.

(12) Chang, J. C.; Rosenthal, S. J., Visualization of lipid raft membrane compartmentalization in living RN46A neuronal cells using single quantum dot tracking. *ACS Chem. Neurosci.* **2012,***3*, 737-743.

(13) Chang, J. C.; Tomlinson, I. D.; Warnement, M. R.; Ustione, A.; Carneiro, A. M. D.; Piston, D. W.; Blakely, R. D.; Rosenthal, S. J., Single molecule analysis of serotonin transporter regulation using antagonist-conjugated quantum dots reveals restricted, p38 MAPK-dependent mobilization underlying uptake activation. *J. Neurosci.* **2012,***32*, 8919-8929.

(14) Cui, B.; Wu, C.; Chen, L.; Ramirez, A.; Bearer, E. L.; Li, W.-P.; Mobley, W. C.; Chu, S., One at a time, live tracking of NGF axonal transport using quantum dots. *Proc. Natl. Acad. Sci. U.S.A.* **2007,***104*, 13666-13671.

(15) Fichter, K. M.; Flajolet, M.; Greengard, P.; Vu, T. Q., Kinetics of G-protein-coupled receptor endosomal trafficking pathways revealed by single quantum dots. *Proc. Natl. Acad. Sci. U.S.A.* **2010,***107*, 18658-63.

(16) Zhang, Q.; Li, Y.; Tsien, R. W., The dynamic control of kiss-and-run and vesicular reuse probed with single nanoparticles. *Science* **2009,***323*, 1448-53.

(17) Lowe, A. R.; Siegel, J. J.; Kalab, P.; Siu, M.; Weis, K.; Liphardt, J. T., Selectivity mechanism of the nuclear pore complex characterized by single cargo tracking. *Nature* **2010,***467*, 600-3.

(18) Selvin, P. R., The renaissance of fluorescence resonance energy transfer. *Nat. Struct. Biol.* **2000,***7*, 730-734.

(19) Willard, D. M.; Carillo, L. L.; Jung, J.; Van Orden, A., CdSe-ZnS quantum dots as resonance energy transfer donors in a model protein-protein binding assay. *Nano Lett.* **2001,***1*, 469-474.
(20) Medintz, I. L.; Clapp, A. R.; Mattoussi, H.; Goldman, E. R.; Fisher, B.; Mauro, J. M., Self-assembled nanoscale biosensors based on quantum dot FRET donors. *Nat. Mater.* **2003,***2*, 630-8.
(21) Goldman, E. R.; Medintz, I. L.; Whitley, J. L.; Hayhurst, A.; Clapp, A. R.; Uyeda, H. T.; Deschamps, J. R.; Lassman, M. E.; Mattoussi, H., A hybrid quantum dot-antibody fragment fluorescence resonance energy transfer-based TNT sensor. *J. Am. Chem. Soc.* **2005,***127*, 6744-51.
(22) Medintz, I. L.; Clapp, A. R.; Brunel, F. M.; Tiefenbrunn, T.; Uyeda, H. T.; Chang, E. L.; Deschamps, J. R.; Dawson, P. E.; Mattoussi, H., Proteolytic activity monitored by fluorescence resonance energy transfer through quantum-dot-peptide conjugates. *Nat. Mater.* **2006,***5*, 581-9.
(23) Shi, L.; De Paoli, V.; Rosenzweig, N.; Rosenzweig, Z., Synthesis and application of quantum qots FRET-based protease sensors. *J. Am. Chem. Soc.* **2006,***128*, 10378-10379.
(24) Ghadiali, J. E.; Lowe, S. B.; Stevens, M. M., Quantum-dot-based FRET detection of histone acetyltransferase activity. *Angew. Chem., Int. Ed.* **2011,***50*, 3417-3420.
(25) Prasuhn, D. E.; Feltz, A.; Blanco-Canosa, J. B.; Susumu, K.; Stewart, M. H.; Mei, B. C.; Yakovlev, A. V.; Loukov, C.; Mallet, J. M.; Oheim, M.; Dawson, P. E.; Medintz, I. L., Quantum dot peptide biosensors for monitoring caspase 3 proteolysis and calcium ions. *ACS Nano* **2010,***4*, 5487-97.
(26) Snee, P. T.; Somers, R. C.; Nair, G.; Zimmer, J. P.; Bawendi, M. G.; Nocera, D. G., A ratiometric CdSe/ZnS nanocrystal pH sensor. *J. Am. Chem. Soc.* **2006,***128*, 13320-1.
(27) Dennis, A. M.; Rhee, W. J.; Sotto, D.; Dublin, S. N.; Bao, G., Quantum dot-fluorescent protein FRET probes for sensing intracellular pH. *ACS Nano* **2012,***6*, 2917-24.
(28) Zhang, C. Y.; Yeh, H. C.; Kuroki, M. T.; Wang, T. H., Single-quantum-dot-based DNA nanosensor. *Nat. Mater.* **2005,***4*, 826-31.
(29) Ram, S.; Kim, D.; Ober, R. J.; Ward, E. S., 3D single molecule tracking with multifocal plane microscopy reveals rapid intercellular transferrin transport at epithelial cell barriers. *Biophys. J.* **2012,***103*, 1594-603.
(30) Pavani, S. R. P.; Thompson, M. A.; Biteen, J. S.; Lord, S. J.; Liu, N.; Twieg, R. J.; Piestun, R.; Moerner, W. E., Three-dimensional, single-molecule fluorescence imaging beyond the diffraction limit by using a double-helix point spread function. *Proc. Natl. Acad. Sci. U.S.A.* **2009**.
(31) Thompson, M. A.; Lew, M. D.; Badieirostami, M.; Moerner, W. E., Localizing and tracking single nanoscale emitters in three dimensions with high spatiotemporal resolution using a double-helix point spread function. *Nano Lett.* **2010,***10*, 211-8.
(32) Bruchez, M.; Moronne, M.; Gin, P.; Weiss, S.; Alivisatos, A. P., Semiconductor nanocrystals as fluorescent biological labels. *Science* **1998,***281*, 2013-2016.
(33) Chan, W. C.; Nie, S., Quantum dot bioconjugates for ultrasensitive nonisotopic detection. *Science* **1998,***281*, 2016-8.
(34) Jaiswal, J. K.; Simon, S. M., Potentials and pitfalls of fluorescent quantum dots for biological imaging. *Trends Cell Biol.* **2004,***14*, 497-504.
(35) Howarth, M.; Liu, W.; Puthenveetil, S.; Zheng, Y.; Marshall, L. F.; Schmidt, M. M.; Wittrup, K. D.; Bawendi, M. G.; Ting, A. Y., Monovalent, reduced-size quantum dots for imaging receptors on living cells. *Nat. Methods* **2008,***5*, 397-399.
(36) Groc, L.; Lafourcade, M.; Heine, M.; Renner, M.; Racine, V.; Sibarita, J. B.; Lounis, B.; Choquet, D.; Cognet, L., Surface trafficking of neurotransmitter receptor: comparison between single-molecule/quantum dot strategies. *J. Neurosci.* **2007,***27*, 12433-7.

(37) Wang, X.; Ren, X.; Kahen, K.; Hahn, M. A.; Rajeswaran, M.; Maccagnano-Zacher, S.; Silcox, J.; Cragg, G. E.; Efros, A. L.; Krauss, T. D., Non-blinking semiconductor nanocrystals. *Nature* **2009,***459*, 686-9.
(38) Chen, Y.; Vela, J.; Htoon, H.; Casson, J. L.; Werder, D. J.; Bussian, D. A.; Klimov, V. I.; Hollingsworth, J. A., "Giant" multishell CdSe nanocrystal quantum dots with suppressed blinking. *J. Am. Chem. Soc.* **2008,***130*, 5026-5027.
(39) Mahler, B.; Spinicelli, P.; Buil, S.; Quelin, X.; Hermier, J. P.; Dubertret, B., Towards non-blinking colloidal quantum dots. *Nat. Mater.* **2008,***7*, 659-64.
(40) Marchuk, K.; Guo, Y.; Sun, W.; Vela, J.; Fang, N., High-precision tracking with non-blinking quantum dots resolves nanoscale vertical displacement. *J. Am. Chem. Soc.* **2012,***134*, 6108-11.

The Appendix A was originally published by ACS (Chang, J.C., Tomlinson, I.D., Warnement, M.R., Iwamoto, H., DeFelice, L.J., Blakely, R.D. & Rosenthal, S.J. (2011) A fluorescence displacement assay for antidepressant drug discovery based on ligand-conjugated quantum dots. *J Am Chem Soc*, 133, 17528–17531) as a rapid communication. Permission is granted for the author's request for the dissertation use and for the benefit of the author's institution.

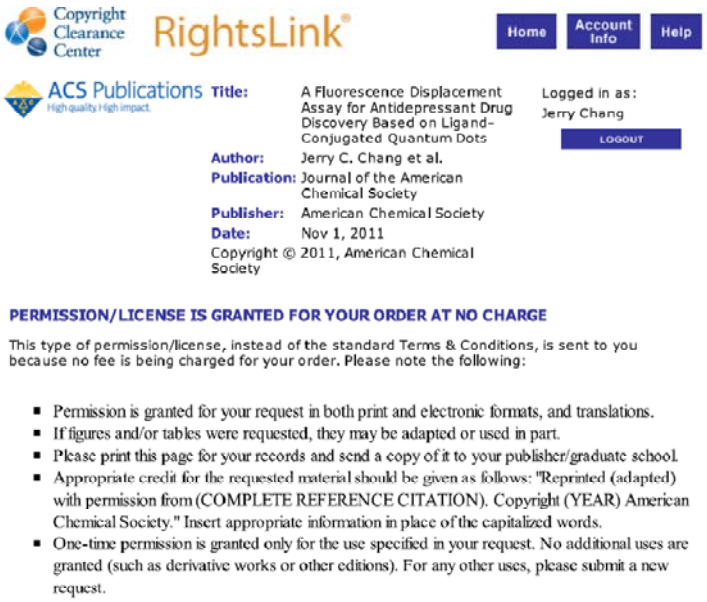

Copyright Clearance Center RightsLink®

Home | Account Info | Help

ACS Publications High quality. High impact.

Title: A Fluorescence Displacement Assay for Antidepressant Drug Discovery Based on Ligand-Conjugated Quantum Dots

Author: Jerry C. Chang et al.

Publication: Journal of the American Chemical Society

Publisher: American Chemical Society

Date: Nov 1, 2011

Copyright © 2011, American Chemical Society

Logged in as: Jerry Chang

LOGOUT

PERMISSION/LICENSE IS GRANTED FOR YOUR ORDER AT NO CHARGE

This type of permission/license, instead of the standard Terms & Conditions, is sent to you because no fee is being charged for your order. Please note the following:

- Permission is granted for your request in both print and electronic formats, and translations.
- If figures and/or tables were requested, they may be adapted or used in part.
- Please print this page for your records and send a copy of it to your publisher/graduate school.
- Appropriate credit for the requested material should be given as follows: "Reprinted (adapted) with permission from (COMPLETE REFERENCE CITATION). Copyright (YEAR) American Chemical Society." Insert appropriate information in place of the capitalized words.
- One-time permission is granted only for the use specified in your request. No additional uses are granted (such as derivative works or other editions). For any other uses, please submit a new request.

All other uses, reproduction and distribution, including without limitation commercial reprints, selling or licensing copies or access, or posting on open internet sites, your personal or institution's website or repository, without permission from the publisher are prohibited.

Appendix A

QUANTUM DOT DISPLACEMENT ASSAY FOR ANTIDEPRESSANT DRUG SCREENING

A.1 Abstract

The serotonin (5-hydroxytryptamine, 5-HT) transporter (SERT) protein plays a central role in terminating 5-HT neurotransmission and is the most important therapeutic target for the treatment of major depression and anxiety disorders. We report an innovative, versatile, and target-selective quantum dot (QDot) labeling approach for SERT in single Xenopus oocytes that can be adopted as a drug-screening platform. Our labeling approach employs a custom-made, QDot-tagged indoleamine derivative ligand, IDT318, that is structurally similar to 5-HT and that accesses the primary binding site with enhanced human SERT selectivity. Incubating QDot-labeled oocytes with paroxetine (Paxil), a high affinity SERT-specific inhibitor, showed a concentration- and time-dependent decrease in QDot fluorescence, demonstrating the utility of our approach for the identification of SERT modulators. Further, with the development of ligands aiming at other pharmacologically relevant targets, our approach may potentially form the basis for a multi-target drug discovery platform.

A.2 Introduction

Major depression occurs in 2 - 5% of the U. S. population and is the most common mental illness in modern society.[1, 2] Depression is not only devastating, but is a financial burden, costing the U.S. an estimated 100 billion dollars annually.[2] Selective serotonin reuptake inhibitors (SSRIs) that block the serotonin transporter (SERT) at brain synapses are, by far, the most frequently prescribed drugs for the management of depression.[1, 3-6] A well-known major drawback of current SSRIs is their slow onset of antidepressant activity, requiring 3-6 weeks of administration to produce a significant therapeutic benefit.[7]

To develop faster acting antidepressants, it was proposed that a multi-target strategy,[7] where antagonists are designed for several pharmacologically relevant targets. Several studies indicate that dual-acting antidepressants such as Desvenlafaxine,[8] a serotonin and norepinephrine reuptake inhibitor (SNRI), and SB-649915-B,[9] a 5-$HT_{1A/B}$ receptor antagonist and SSRI, may provide a faster onset of antidepressant action. Another emerging area in antidepressant drug discovery exploits allosteric antagonists.[10] In this approach, drug candidates can be engineered to act at a site of the transporter distinct from the high-affinity primary binding site, consequently mediating conformational changes of a substrate binding pocket and attenuating neurotransmitter uptake. No crystal structure of any neurotransmitter transporter is presently available, which makes it difficult to validate the allosteric antagonism. Several high-affinity SSRIs have been previously proposed as allosteric modulators for SERT, including paroxetine, (Paxil®), a high-affinity SERT-specific inhibitor and FDA-approved SSRI.[11]

Recently, several new multi-target antagonists and allosteric modulators have shown improved efficacy and success in clinical trials. However, progress in next-generation antidepressant drug discovery has been largely delayed by the lack of appropriate screening platforms.[7] At present, methods used to investigate transporter

binding/activity rely on conventional biochemical methods such as *in vitro* phosphorylation assay, electrophysiology,[12] or radio-labeled substrate uptake assay.[12] These methods are labor-intensive, time-consuming, and in the latter case, require isotope use.

Alternatively, fluorescent probes can be used for target-selective drug screening. However, when using common fluorophores, the two major limiting features are photostability and sensitivity. In recent years, QDot development has achieved promising results that overcome the disadvantages associated with conventional biolabelingfluorophores.[13-16] Previously, we have demonstrated the use of ligand-conjugated QDots for visualization of SERT, $GABA_C$ receptor, and most recently, the dopamine transporter.[17-19] In this report, we advance the ligand-conjugated QDot labeling approach as an antidepressant drug screening platform in single, living oocytes.

A.3 Experimental Section

A.3.1 IDT318 ligand synthesis

The synthesis details and spectroscopic characterization have been previously described in our recent publications.[20, 21] Brief scheme is shown in Figure 1. Initially, the parent drug 5-methoxy-3-(1,2,5,6-tetrahydro-4-pyridinyl)-1*H*-indole **(1)** was synthesized and coupled to 11-(1,3-Dioxo-1,3-dihydro-isoindol-2-yl)-undecyl bromide **(2)** to yield 2-(11-(4-(5-methoxy-1*H*-indol-3yl)-5,6-dihydropyridin-(2*H*)-yl)undecyl) isoindoline-1,3-dione **(3)** in the presence of triethylamine (Et_3N). The phthalimide protecting group was removed using hydrazine monohydrate to give 11-(4-(5-methoxy-1*H*-indol-3-yl)-5,6-dihydropyridin-1(2*H*)-yl)undecan-1- amine **(4).** This is then coupled to biotin-polyethylene glycol-*N*-hydroxysuccinimide ester to give the SERT ligand IDT318 **(5)** for the study.

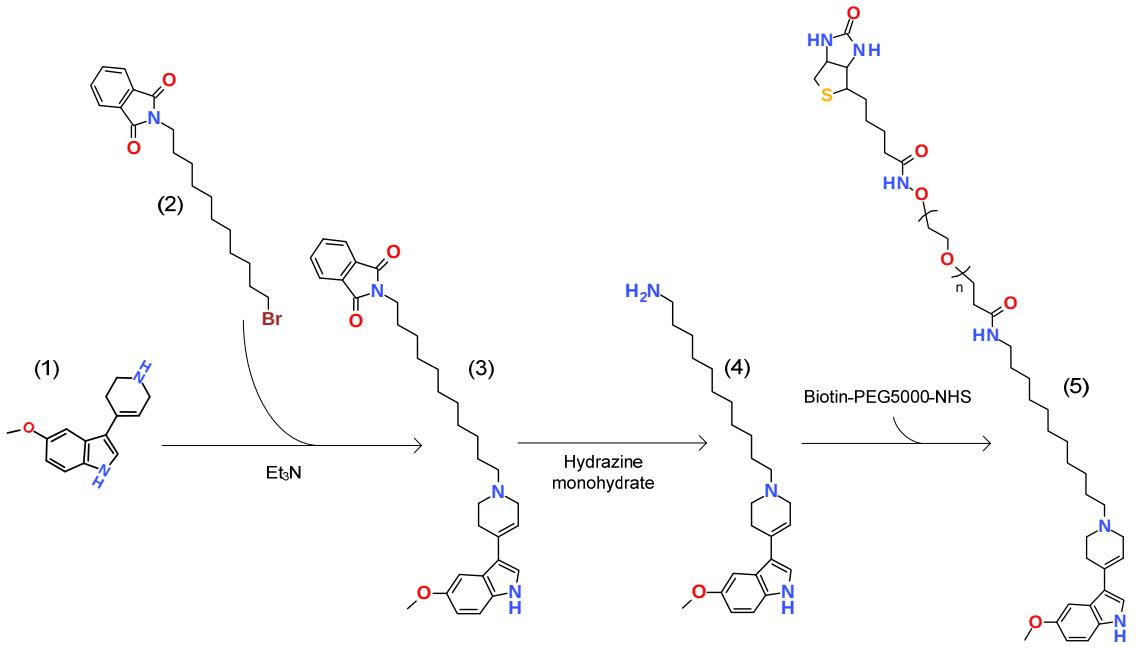

Figure A.1 Schematic of IDT318 synthesis

A.3.2 hSERT-expressing oocyte prepapation

Xenopus oocytes and hSERT cRNA were prepared and isolated as previously described.[12, 22] In brief, stage V-VI oocytes were harvested from *Xenopus laevis* (Nasco,

Medesto, CA). After harvesting, the follicle cell layer was removed by incubation with 2 mg/ml collagenase in Ringer's buffer (in mM, 96 NaCl, 2 KCl, 5 $MgCl_2$, 5 HEPES, pH 7.4) for an hour. cRNA injections were performed on the day of harvest. hSERT cRNA was transcribed from NotI (New England BioLabs, Beverly, MA)-digested cDNA in pOTV vector (a gift of Dr. Mark Sonders, Columbia University) using Ambion mMessage Machine T7 kit (Ambion, Austin, TX). The cRNA concentrations were confirmed by UV spectroscopy and gel electrophoresis. Each oocyte was injected with 3 ng cRNA and incubated at 18 C° for 3-6 days in Ringer's buffer supplemented with 550 μM/ml sodium pyruvate, 100 μg/ml streptomycin, 50 μg/ml tetracycline, and 5 % dialyzed horse serum. Healthy oocytes for subsequent electrophysiological and fluorescence assays were selected by visual inspection.

A.3.3 Quantum dot-hSERT labeling and displacement in oocytes

For two-step QDot-SERT labeling, oocytes were first incubated with 1 μM biotinylated ligand in PBS for 60 minutes prior to 5 minutes incubation of 2.5 nM SA-QDot (Qdot® 655 streptavidin conjugate, Invitrogen, Carlsbad, CA).

The pre-incubation affinity assay was demonstrated using paroxetine and 5-HT as testing drugs. In pre-incubation affinity assay, oocytes were first incubated with testing drug (1 μM for paroxetine; 1 mM for 5-HT) in PBS for 60 minutes, followed by a ligand/drug mixture incubation (1 μM/1μM for paroxetine; 1 μM/1 mM for 5-HT) in PBS for another 60 minutes, and then finally incubated with 2.5 nM SA-QDot for 5 minutes. After QDot labeling, single oocytes were transferred to 8-well Lab-Tek chamber slides (NUNC, Roskilde, Denmark) and imaged in PBS. Excess ligand, drug, and QDot were removed by two washes with PBS at each step.

For time course displacement assay, selected single hSERT expressing oocyte was transferred to one well of Lab-Tek 8-well chamber slide after processing two-step QDot-SERT labeling, each well contain either 0 μM (control), 10 μM or 20 μM of paroxetine in 400 μL PBS. A time series of fluorescent images was immediately acquired at a 1 minute interval over a 30 minute period.

A.3.4 Microscopy

Confocal images were obtained on a Zeiss LSM 510META confocal imaging system (Carl Zeiss Microimaging, Inc., Thornwood, NY). Images were collected using a Zeiss Plan-Apochromat 5×/0.16 numerical aperture (NA) objective lens and excited by an argon laser at 458 nm with 25% transmission rate and pinhole was set to 2 Airy units. All images were 512×512 pixels in size and had an 8-bit pixel depth. For single ligand labeling experiments, fluorescence signal was collected on photomultiplier-tube (PMT) detector after passing through a 650 nm cutoff filter to ensure the transmission of only the Qdot 655 signal.

Wide-field fluorescent images were acquired using a Zeiss Axiovert 200 M inverted fluorescence microscope equipped with a Photometrics Cool-Snap™ HQ2 electrically cooled CCD camera (Intelligent Imaging Innovations, Denver, CO), a Zeiss Plan-Neofluar 20×/0.4 numerical aperture (NA) objective lens and QDot655 filter set (XF 1002 filter, Omega Optical, Brattleboro, VT). Exposure time was set at 200 ms for all fluorescent imaging. Image acquisition and analysis was processed using Metamorph® 7 imaging software (Molecular Devices Corp.; Downingtown, PA).

A.3.5 Two-electrode voltage-clamp electrophysiological analysis

Whole-cell currents were measured with two electrode voltage clamp techniques using a GeneClamp 500 (Molecular Devices, Palo Alto, CA). Microelectrodes were pulled using a programmable puller (Model P-87, Sutter Instrument, Novato, CA) and filled with 3 M KCl (0.5-5 MΩ resistance). A 16-bit A/D converter (Digidata 1322A, Molecular Devices) interfaced to a PC computer running Clampex 9 software (Molecular Devices) was used to control membrane voltage and to acquire data. To induce hSERT-associated current, serotonin was dissolved (typically 10 μM) in a buffer solution (in mM, 120 NaCl, 5.4 potassium gluconate, 1.2 calcium gluconate, 7.2 HEPES, pH 7.4) and applied to oocytes using a gravity-flow perfusion system (4-5 ml/min flow rate). Serotonin-induced current is defined by subtraction of current in the presence of serotonin from current in the absence of serotonin. For recordings, data were low-pass filtered at 10 Hz and digitized at 20 Hz. Analyses were performed using Origin 7 (Origin Lab, Northampton, MA).

A.3.6 Data Analysis

For displacement assays, each time-series of wide-field fluorescence images was analyzed using Metamorph's active region measurement program. Briefly, an initial active region was selected from the membrane halo region of the fluorescent image, and this same region was applied to each fluorescence image for subsequent time flame. The correlation of background signal was performed by subtracting the result from the background image on a pixel-by-pixel basis. Background signal of the CCD detector was measured by taking the fluorescence image under the same experimental setup without sample loading. Data were measured as relative fluorescent units (RFUs) and normalized to the following equation:

$$normalized\ response = \frac{F_t}{F_0} \qquad [1]$$

, where F_t is the fluorescent signal generated in the presence of paroxetine at time t; F_0 is the initial fluorescent intensity generated in the absence of paroxetine.

Data were evaluated by fitting to either a linear or single exponential equation for control experiment and Paroxetine displacing experiment, respectively. For the control experiment, each time course data points were fit into a linear curve regression equation:

$$\frac{F_t}{F_0} = \frac{F_\infty}{F_0} + A \cdot t \qquad [2]$$

, where F_t is the fluorescent signal generated in the presence of paroxetine at time *t*; F_0 is the initial fluorescent intensity generated in the absence of paroxetine, F_∞ is the fluorescent intensity at infinite time, and *A* represents amplitude. For the paroxetine displacing experiment, the time courses were fit into a single-exponential equation:

$$\frac{F_t}{F_0} = \frac{F_\infty}{F_0} + B \cdot e^{-k_{app} \cdot t} \qquad [3]$$

, where F_t is the fluorescent signal generated in the presence of paroxetine at time *t*; F_0, the initial fluorescent intensity generated in the absence of paroxetine; F_∞, the fluorescent intensity at infinite time; k_{app}, the apparent rate constant; *B*, the amplitude. All the fitting curves were generated by using Sigmaplot™ software (Version 11.2, Systat Software Inc., San Jose, CA).

Measurements of each reaction kinetics for QDot-based displacement assays were performed by taking the natural logarithm of each time courses fluorescent data point generated from the paroxetine displacing experiments and then plotted as a function of time. First-order dissociation was evaluated by fitting the 0-10minute data points to the linear curve regression using Sigmaplot software.

Note that the SA-QDots we used in this study have potentially 4-10 streptavidins/QDot, suggesting a possible 16-40 binding sites/QDot.[23] A recent study reported that this particular kind of SA-QDots has ~5 biotin binding sites/QDot.[24] As can be seen in Fig. 3B, the dissociation of QDot-ligand from hSERT proteins can be categorized into roughly two stages where the first 10 minutes seems significantly faster. Further analysis in Fig. 3C indicated that a plot of $ln(F_t/F_0)$ as a function of time at the initial 10 minutes appear to be linear, a character of first-order dissociation, suggesting the binding valency is monovalent. As illustrated in the figure 5, we recognize that it is possible that the displacement in our platform may be indicative of a two-stage dissociation process in which the initial monovalent dissociation is followed by a multivalent dissociation. A solution to resolve this issue is to introduce the monovalent streptavidin conjugated QDots developed by Ting and coworkers.[23]

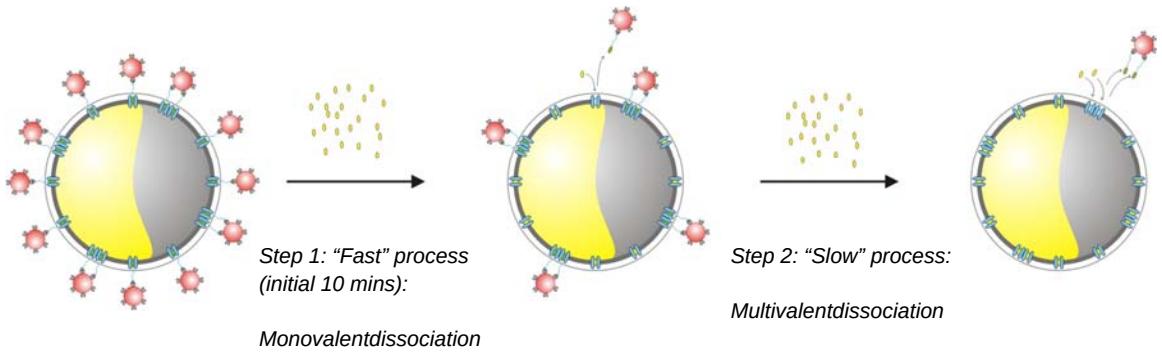

Figure A.2 Schematic of putative two-stage ligand-SERT dissociation mechanism of QDot-labeled ligand-SERT complexes in the oocyte expression system

A.4 Results

Figure A.3 illustrates two modes by which ligand-conjugated QDot displacement can occur. The first mode is by preventing the ligand re-association with the primary (orthosteric) binding site (left); and the second mode is through an allosteric mechanism that shifts the primary binding site conformation, dissociating the ligand (right).

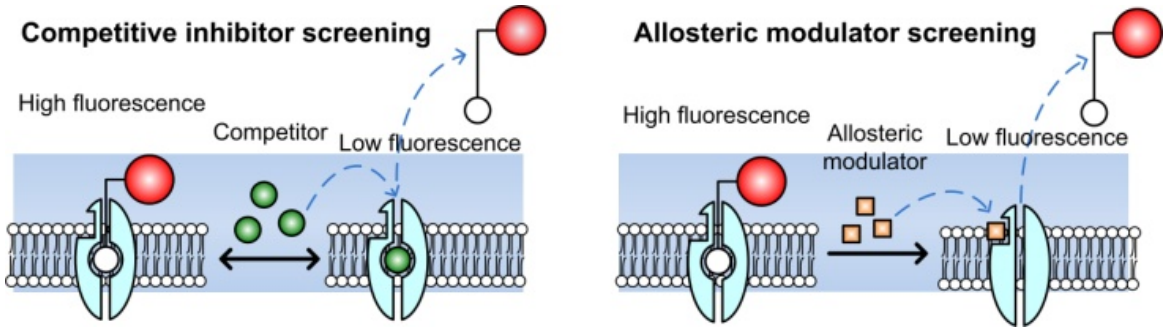

Figure A.3 Fluorescence displacement assay based on ligand-conjugated QDots for antidepressant drug discovery. Target proteins (transporters or receptors) bind to the QDot-tagged ligands, forming complexes that increase fluorescent signal along the membrane. When exposed to a potential drug which competes with the binding (left) or induces a conformational change in the binding site (right), the QDot-tagged ligands are displaced resulting in a decrease in fluorescence intensity. The blue shadow area indicates the imaging focal plane while processing the assay.

The structure of the IDT318 ligand used in this study is depicted in Figure A.4A. The synthesis details have been previously described.[20, 21] As indicated, IDT318 ligand is composed of four components. Ligand design was based on comprehensive screening of trypamine derivatives.[25] 5-methoxy-3-(1,2,5,6-tetrahydro-4-pyridinyl)-1H-indole (RU24969), which retains the tryptamine moiety for a putative common 5-HT binding site and features enhanced selectivity for human serotonin transporter (hSERT),[25] is readily adapted as a tethered ligand for hSERT binding[26] (component I). The alkyl spacer serves to enhance the ligand binding through the interaction of the hydrophobic residues in the transmembrane domains of membrane channels or transporters (component II, see also Figure A.5B). The polyethylene glycol (PEG) chain is used to increase water

solubility of the ligand and decrease steric hindrance from the bulky QDot (component III). The biotin group (component IV) allows for specific binding to the streptavidin-conjugated QDot (SA-QDot). In addition, only surface pegylated, streptavidin conjugated QDots were used for theirultra-low nonspecific binding property.[27, 28]

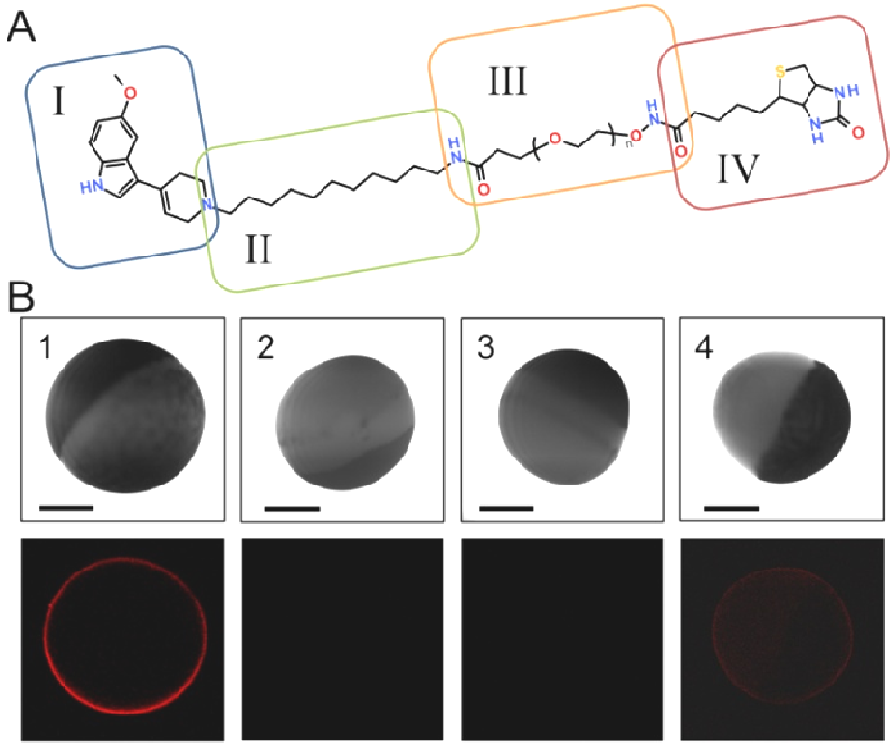

Figure A.4 Target-selective QDot-SERT labeling via IDT318. (A) The structure of IDT318 ligand used in the study (see text for details of each component) (B) Column 1: Incubation of hSERT oocyte with 1 μM IDT318 ligand prior to 2.5 nM SA-QDot treatment. The observed QDot fluorescence forms a sharp halo correlating to the membrane of hSERT expressing oocyte. Column 2: Control experiment where the buffer-injected oocyte was treated under the same conditions as in column 1. Column 3: hSERT expressing oocyte was incubated with paroxetine (1 μM), subsequently exposed to the ligand/paroxetine mixture (1 μM/1 μM) prior to 2.5 nM SA-QDot treatment. Column 4: hSERT expressing oocyte was pre-incubated with 5-HT (1 mM), subsequently exposed to the ligand/5-HT mixture (1 μM /1 mM) prior to 2.5 nM SA-QDot treatment. The halo was dimmer but not completely blocked, indicating a competitive binding mechanism. Upper panel: DIC image; Lower panel: fluorescent image. Scale bar = 0.5 mm. The results are representative micrographs from at least 3 independent experiments.

To visualize the hSERT distribution in our oocyte model, a two-step labeling approach was implemented in which a hSERT-expressing oocyte was incubated with IDT318 followed by incubation with SA-QDots. As shown in Figure A.4B (Column 1), the QDot fluorescence forms a sharp halo correlating to the membrane of the hSERT expressing oocyte, whereas incubation with non-expressing control oocyte shows no sign of labeling (Column 2). Ligand binding specificity was demonstrated using a QDot-based pre-incubation affinity assay where the hSERT-expressing oocyte is pre-incubated with paroxetine prior to the two-step QDot labeling. As can be seen in Column 3, paroxetine effectively blocked the QDot labeling, demonstrating the binding specificity of IDT318 to hSERT. In comparison, preincubation of a hSERT-expressing oocyte with 0.1 mM 5-HT prior to the two-step QDot labeling only shows reduced QDot fluorescence intensity (Column 4). This reduced QDot labeling could be the result of incomplete saturation of hSERT binding with 5-HT; however, this is unlikely since the 5-HT concentration was 120 times greater than the reported K_i value against hSERT.[25] A more likely explanation is the reversible binding mode, in which IDT318 competes with 5-HT for the primary binding site. This rationale is also consistent with our previous finding indicating that tryptamine analogs including RU24969 shares, a common substrate binding site at hSERT.[25] Importantly, the influence of IDT318 on hSERT activity was further characterized with an oocyte electrophysiological assay (Figure A.5A), indicating the role of IDT318 as a hSERT antagonist.

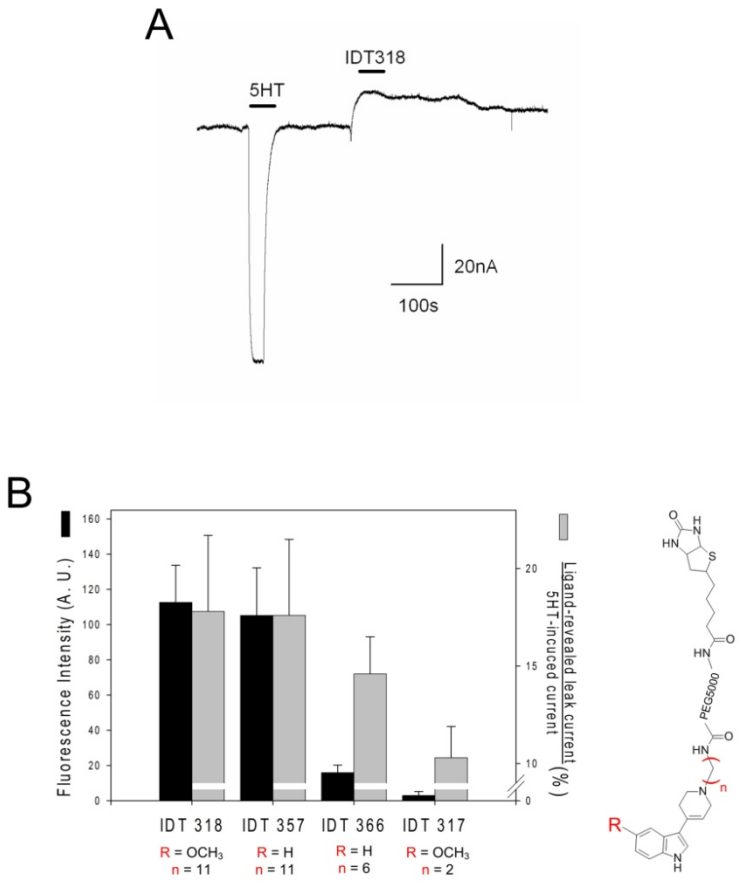

Figure A.5 (A) Current response induced by IDT318 ligand incubation. Figure shown here is a representative recording from a single hSERT expressing oocyte voltage-clamped at -60 mV. The leakage current profile after incubating with IDT318 displays a typical SERT antagonist behavior.[29] (5HT: 5-Hydroxytryptamine, serotonin) (B) Comparison of current responses with QD labeling results for the indication of alkyl space participated in ligand binding. We recently published the current responses of the IDT318 and its structure-related ligands (left scale) using hSERT expression oocytes. Here we compared the current responses with QD labeling results (right scale). As can be seen, results generated by both methods show a similar trend as the length of alkyl spacer increases. However, the QD labeling result shows higher sensitivity as evident by a smaller standard deviation. (Fluorescent results: n = 6 oocytes/group; Current results: n = 4 oocytes/group)

The potential utility of our labeling model for SSRI screening was explored utilizing paroxetine. In order for the drug candidate to rapidly displace the fluorophore-tagged ligand at a reasonable drug concentration, a ligand with an affinity in the μM

range is required.[30] As indicated in Figure A.6, the IDT318 shows the desired μM affinity. In our displacement assay, a 30 minute time-course imaging at 1 minute intervals was carried out immediately after paroxetine incubation. QDotfluorescence intensity was measured and normalized to F_t / F_0, where F_0 is the initial fluorescent signal and theF_t is the fluorescent signal at time *t*. Representative time-lapse fluorescent images and fluorescence intensity traces are shown in Figure A.7A and A.7B, respectively. Time- and concentration-dependent fluorescenceintensity reduction is apparent in the presence of paroxetine. In contrast, when using 5-HT as the displacing drug, the dramatic QDot fluorescent reduction as seen with paroxetine treatment vanished (Figure A.8). Note that there was less than a 10 % reduction in fluorescence intensity observed after 30 minutes of buffer incubation (Figure A.7B), indicating that the effect of QDot quenching and spontaneous ligand dissociation minimally contributes to the results. Furthermore, the log plot of F_t / F_0 as a function of time is linear in the first 10 minutes, indicating first-order dissociation kinetics (Figure A.7C). Analysis of the 10 μM paroxetine displacement trace yields an apparent dissociation rate constant of k_{app} = (5.0 ± 0.4) $\times 10^{-4}$ s^{-1}. Doubling the paroxetine concentration results in a nearly proportional increase in k_{app} = (1.08 ± 0.05) $\times 10^{-3}$ s^{-1} (see methods for fitting details). Hence, this displacement platform exhibits necessary sensitivity for SSRI screening. Importantly, the dissociation kinetics shown in FigureA.7C indicate that the time-series displacement can be performed in less than 10 minutes. From a technological perspective, the throughput of our QDot-based displacement assays can be increased more than 100 fold if used with a commercially available automated multiwell plate high throughput screening imaging system.

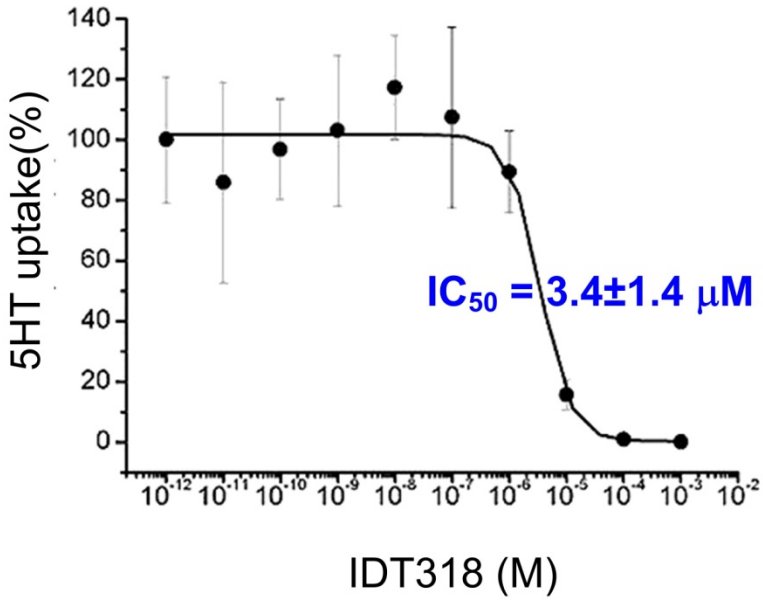

Figure A.6 IC_{50} measurement of IDT318 ligand. The ability of IDT318 to inhibit the uptake of serotonin was measured by incubating hSERT expressing oocytes in the presence of 50 nM tritiated serotonin and increasing concentrations of IDT318. The accumulated radioactivity was plotted against concentration of IDT318. The IC_{50} of IDT318 was found to be 3.4 ± 1.4 μM (mean ± SD).

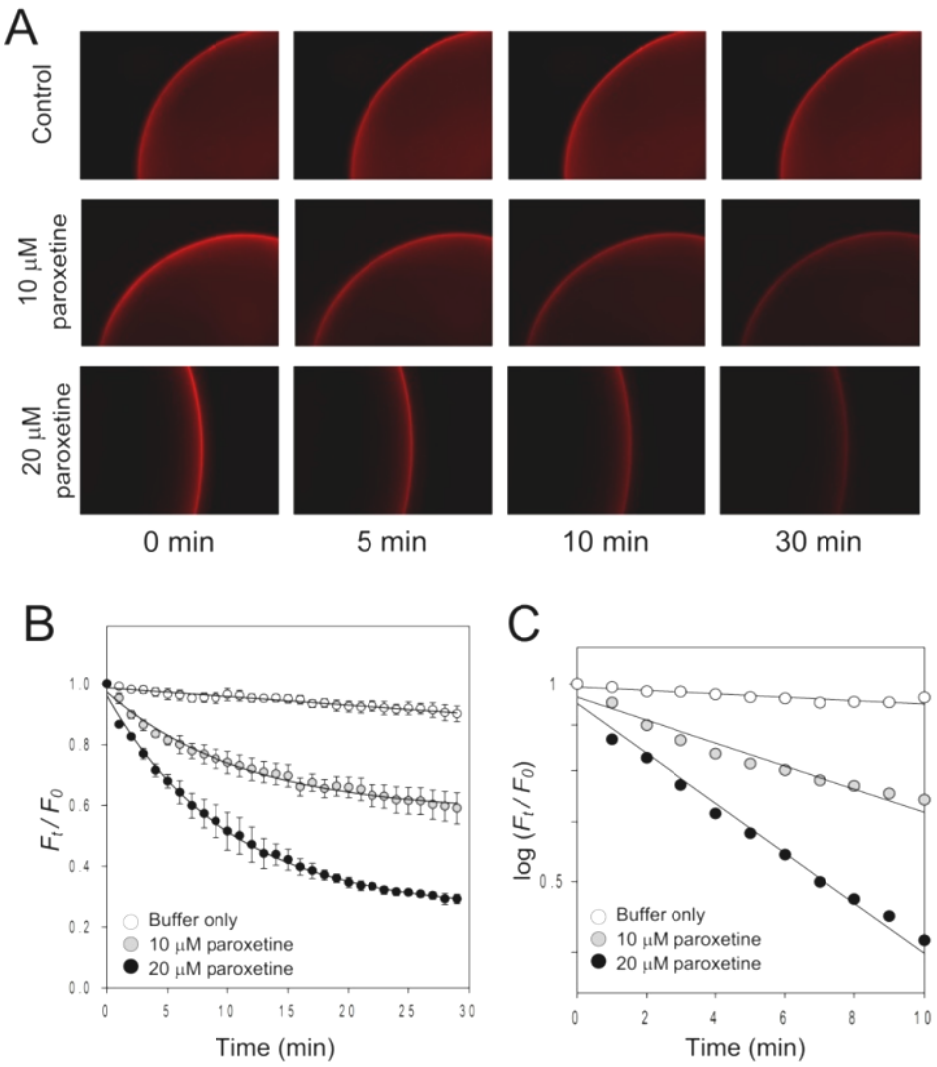

Figure A.7 Displacement analysis of the QDot-ligand labeled hSERT with paroxetine. Representative time-lapse Qdot fluorescent images (A), time-dependent relative fluorescent intensity plot (B), and kinetic analysis (C) show the effect of paroxetine on ligand-SERT displacement in the presence of PBS buffer (control), 10 μM, and 20 μM paroxetine. Solid lines in (B) reflect best fits (see section A3.6 for detail). A log scale plot of the displacement curves is fit to a linear function (C), indicating first-order dissociation kinetics. Each data point in (B) and (C) represents the mean of three independent measurements. Data points in (B) are given as mean ± SD. Results in A are representative micrographs from at least 3 independent experiments.

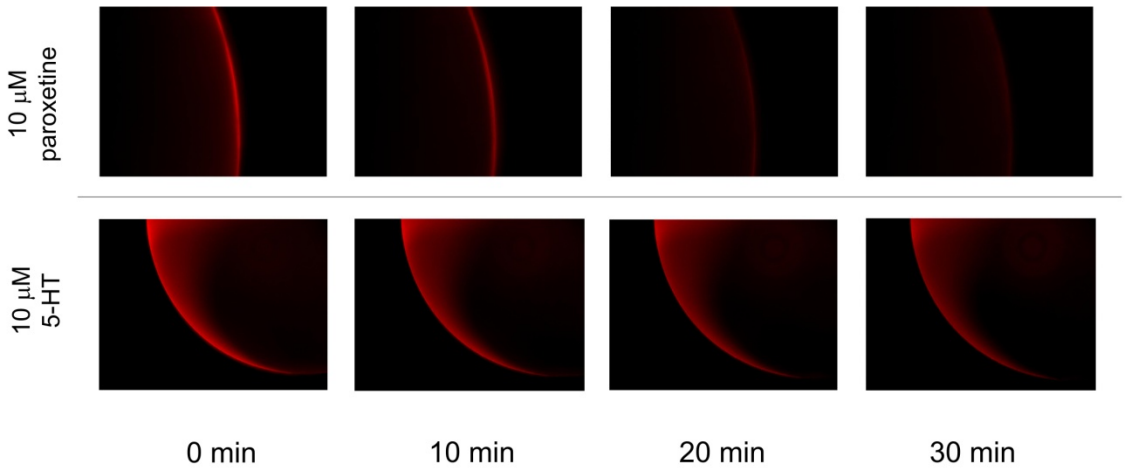

Figure A.8 Displacement of the IDT318 conjugated QD with 10 μM paroxetine and 5-HT. Results are representative micrographs from at least 3 independent experiments.

A.5 Discussion

The ability of paroxetine to displace IDT318 at SERT is most likely to be a non-competitive, allosteric modeof interaction of the antidepressant with the transporter, as opposed to a simple competition for an orthosteric binding site.[11, 31]Recently, it was shown that mutations at the major antidepressant binding site of SERT do not impact paroxetine,also suggesting a non-competitive mode of interaction.[26]Additionally, non-competitive dissociation of ligands from binding sites is expected to follow first-order dissociation kinetics, as in the case of *S*-citalopram,[32, 33]an SSRI frequently proposed to interact with SERT *via* an allosteric mechanism.

In conclusion, we have demostrated a fluorescence displacement assay for antidepressant drug discovery based on ligand conjugated QDots. Furthermore, our method is the first target-selective drug discovery platform that utilizes fluorescent QDots. This system may aid in mapping allosteric mechanisms of SERT modulation and potentially form the basis for a multi-target drug discovery platform employing ligand-conjugated QDots that selectively bind to other pharmacologically relevant proteins, such as dopamine transporter[19] and norepinephrine transporter. Ultimately, this platform may provide more insight into the effects of different structural features on the binding kinetics of any ligand-protein interaction and therefore serve as a generalized approach for the development of drugs beyond antidepressants.

A.6 References

(1) Nestler, E. J.; Barrot, M.; DiLeone, R. J.; Eisch, A. J.; Gold, S. J.; Monteggia, L. M., Neurobiology of depression. *Neuron* **2002,***34*, 13-25.

(2) Duric, V.; Banasr, M.; Licznerski, P.; Schmidt, H. D.; Stockmeier, C. A.; Simen, A. A.; Newton, S. S.; Duman, R. S., A negative regulator of MAP kinase causes depressive behavior. *Nat. Med.* **2010,***16*, 1328-32.

(3) Henry, L. K.; DeFelice, L. J.; Blakely, R. D., Getting the message across: a recent transporter structure shows the way. *Neuron* **2006,***49*, 791-6.

(4) Ramamoorthy, S.; Blakely, R. D., Phosphorylation and sequestration of serotonin transporters differentially modulated by psychostimulants. *Science* **1999,***285*, 763-6.

(5) Carneiro, A. M.; Airey, D. C.; Thompson, B.; Zhu, C. B.; Lu, L.; Chesler, E. J.; Erikson, K. M.; Blakely, R. D., Functional coding variation in recombinant inbred mouse lines reveals multiple serotonin transporter-associated phenotypes. *Proc. Natl. Acad. Sci. U.S.A.* **2009,***106*, 2047-52.

(6) Kroenke, K.; West, S. L.; Swindle, R.; Gilsenan, A.; Eckert, G. J.; Dolor, R.; Stang, P.; Zhou, X. H.; Hays, R.; Weinberger, M., Similar effectiveness of paroxetine, fluoxetine, and sertraline in primary care - A randomized trial. *JAMA-J. Am. Med. Assoc.* **2001,***286*, 2947-2955.

(7) Milian, M. J., Multi-target strategies for the improved treatment of depressive states: Conceptual foundations and neuronal substrates, drug discovery and therapeutic application. *Pharmacol. Ther.* **2006,***110*, 135-370.

(8) Dolder, C.; Nelson, M.; Stump, A., Pharmacological and clinical profile of newer antidepressants: implications for the treatment of elderly patients. *Drugs Aging* **2010,***27*, 625-40.

(9) Starr, K. R.; Price, G. W.; Watson, J. M.; Atkinson, P. J.; Arban, R.; Melotto, S.; Dawson, L. A.; Hagan, J. J.; Upton, N.; Duxon, M. S., SB-649915-B, a novel 5-HT1A/B autoreceptor antagonist and serotonin reuptake inhibitor, is anxiolytic and displays fast onset activity in the rat high light social interaction test. *Neuropsychopharmacology* **2007,***32*, 2163-72.

(10) Sanchez, C., Allosteric modulation of monoamine transporters - new drug targets in depression. *Drug Discov. Today: Ther. Strategies* **2006,***3*, 483-488.

(11) Akunne, H. C.; de Costa, B. R.; Jacobson, A. E.; Rice, K. C.; Rothman, R. B., [3H] cocaine labels a binding site associated with the serotonin transporter in guinea pig brain: allosteric modulation by paroxetine. *Neurochem. Res.* **1992,***17*, 1275-83.

(12) Ramsey, I. S.; DeFelice, L. J., Serotonin transporter function and pharmacology are sensitive to expression level: evidence for an endogenous regulatory factor. *J. Biol. Chem.* **2002,***277*, 14475-82.

(13) Medintz, I. L.; Uyeda, H. T.; Goldman, E. R.; Mattoussi, H., Quantum dot bioconjugates for imaging, labelling and sensing. *Nat. Mater.* **2005,***4*, 435-46.

(14) Gao, X.; Yang, L.; Petros, J. A.; Marshall, F. F.; Simons, J. W.; Nie, S., In vivo molecular and cellular imaging with quantum dots. *Curr. Opin. Biotechnol.* **2005,***16*, 63-72.

(15) Alivisatos, P., The use of nanocrystals in biological detection. *Nat. Biotechnol.* **2004,***22*, 47-52.

(16) Rosenthal, S. J.; Chang, J. C.; Kovtun, O.; McBride, J. R.; Tomlinson, I. D., Biocompatible quantum dots for biological applications. *Chem. Biol.* **2011,***18*, 10-24.

(17) Rosenthal, S. J.; Tomlinson, I.; Adkins, E. M.; Schroeter, S.; Adams, S.; Swafford, L.; McBride, J.; Wang, Y.; DeFelice, L. J.; Blakely, R. D., Targeting cell surface receptors with ligand-conjugated nanocrystals. *J. Am. Chem. Soc.* **2002,***124*, 4586-94.
(18) Gussin, H. A.; Tomlinson, I. D.; Little, D. M.; Warnement, M. R.; Qian, H. H.; Rosenthal, S. J.; Pepperberg, D. R., Binding of muscimol-conjugated quantum dots to GABA(c) receptors. *J. Am. Chem. Soc.* **2006,***128*, 15701-15713.
(19) Kovtun, O.; Tomlinson, I. D.; Sakrikar, D. S.; Chang, J. C.; Blakely, R. D.; Rosenthal, S. J., Visualization of the cocaine-sensitive dopamine transporter with ligand-conjugated quantum dots. *ACS Chem. Neurosci.* **2011,***2*, 370-378.
(20) Tomlinson, I. D.; Iwamoto, H.; Blakely, R. D.; Rosenthal, S. J., Biotin tethered homotryptamine derivatives: high affinity probes of the human serotonin transporter (hSERT). *Bioorg. Med. Chem. Lett.* **2011,***21*, 1678-1682.
(21) Warnement, M. R.; Tomlinson, I. D.; Chang, J. C.; Schreuder, M. A.; Luckabaugh, C. M.; Rosenthal, S. J., Controlling the Reactivity of Ampiphilic Quantum Dots in Biological Assays through Hydrophobic Assembly of Custom PEG Derivatives. *Bioconjug. Chem.* **2008,***19*, 1404-1413.
(22) Iwamoto, H.; Blakely, R. D.; De Felice, L. J., Na+, Cl-, and pH dependence of the human choline transporter (hCHT) in Xenopus oocytes: The proton inactivation hypothesis of hCHT in synaptic vesicles. *J. Neurosci.* **2006,***26*, 9851-9859.
(23) Howarth, M.; Liu, W.; Puthenveetil, S.; Zheng, Y.; Marshall, L. F.; Schmidt, M. M.; Wittrup, K. D.; Bawendi, M. G.; Ting, A. Y., Monovalent, reduced-size quantum dots for imaging receptors on living cells. *Nat. Methods* **2008,***5*, 397-399.
(24) Mittal, R.; Bruchez, M. P., Biotin-4-fluorescein based fluorescence quenching assay for determination of biotin binding capacity of streptavidin conjugated quantum dots. *Bioconjug. Chem.* **2011,***22*, 362-8.
(25) Adkins, E. M.; Barker, E. L.; Blakely, R. D., Interactions of tryptamine derivatives with serotonin transporter species variants implicate transmembrane domain I in substrate recognition. *Mol. Pharmacol.* **2001,***59*, 514-523.
(26) Thompson, B. J.; Jessen, T.; Henry, L. K.; Field, J. R.; Gamble, K. L.; Gresch, P. J.; Carneiro, A. M.; Horton, R. E.; Chisnell, P. J.; Belova, Y.; McMahon, D. G.; Daws, L. C.; Blakely, R. D., Transgenic elimination of high-affinity antidepressant and cocaine sensitivity in the presynaptic serotonin transporter. *Proc. Natl. Acad. Sci. U.S.A.* **2011,***108*, 3785-90.
(27) Bentzen, E. L.; Tomlinson, I. D.; Mason, J.; Gresch, P.; Warnement, M. R.; Wright, D.; Sanders-Bush, E.; Blakely, R.; Rosenthal, S. J., Surface modification to reduce nonspecific binding of quantum dots in live cell assays. *Bioconjug. Chem.* **2005,***16*, 1488-94.
(28) Chattopadhyay, P. K.; Price, D. A.; Harper, T. F.; Betts, M. R.; Yu, J.; Gostick, E.; Perfetto, S. P.; Goepfert, P.; Koup, R. A.; De Rosa, S. C.; Bruchez, M. P.; Roederer, M., Quantum dot semiconductor nanocrystals for immunophenotyping by polychromatic flow cytometry. *Nat. Med.* **2006,***12*, 972-7.
(29) Mager, S.; Min, C.; Henry, D. J.; Chavkintt, C.; Hoffman, B. J.; Davidson, N.; Lester, H. A., Conducting states of a mammalian serotonin transporter. *Neuron* **1994,***12*, 845-859.
(30) Zhang, S.; Chen, L.; Kumar, S.; Wu, L.; Lawrence, D. S.; Zhang, Z. Y., An affinity-based fluorescence polarization assay for protein tyrosine phosphatases. *Methods* **2007,***42*, 261-267.
(31) Henry, L. K.; Meiler, J.; Blakely, R. D., Bound to be different: neurotransmitter transporters meet their bacterial cousins. *Mol. Interv.* **2007,***7*, 306-9.

(32) Sánchez, C.; Bøgesø, K. P.; Ebert, B.; Reines, E. H.; Braestrup, C., Escitalopram versus citalopram: the surprising role of the <i>R</i>-enantiomer. *Psychopharmacology* **2004,***174*, 163-176.
(33) Chen, F.; Larsen, M. B.; Neubauer, H. A.; Sanchez, C.; Plenge, P.; Wiborg, O., Characterization of an allosteric citalopram-binding site at the serotonin transporter. *J. Neurochem.* **2005,***92*, 21-8.